IChF
Institute of Physical Chemistry PAS

PhD Dissertation

Catalytic hydrogenation for technological applications and environmental protection

Emil Kowalewski

INSTITUTE OF PHYSICAL CHEMISTRY
POLISH ACADEMY OF SCIENCES

DOCTORAL THESIS

Catalytic hydrogenation for technological applications and environmental protection

Author:

Emil Kowalewski

Supervisor:

Anna Śrębowata, PhD DSc, Prof. IPC PAS

A thesis submitted in fulfilment of the requirements for the degree of Doctor of Philosophy
under

International Doctoral Studies
of the Institute of Physical Chemistry,
Polish Academy of Sciences
Kasprzaka 44/52
01-224 Warsaw, Poland

Warsaw, July, 2021

Per aspera ad astra

Pracę dedykuję moim Najbliższym

Mojej Pani Promotor
dr hab. Annie Śrębowatej, profesor IChF PAN
składam serdeczne podziękowania
za ogromny trud włożony w mój naukowy rozwój
oraz troskliwą opiekę w trakcie powstawania niniejszej pracy

Wszystkim, z którymi miałem przyjemność współpracować
dziękuję za pomoc udzieloną w trakcie prowadzonych badań
oraz miłą atmosferę w pracy

Abstract

Catalytic hydrogenation is one of the most essential processes for modern civilization. It is used in multiple manufacturing operations but also in environmental protection. The presented studies concern the application of catalytic hydrogenation in water purification from one of the most frequently detected chloroorganic contaminants (trichloroethylene and diclofenac) and in the selective transformation of nitrocyclohexane. The conducted research follows the international trend of increasing the economic efficiency of applied catalysts and making catalytic processes more environmentally friendly.

The general goal of the presented research was to develop efficient and stable catalysts for both hydrogenation processes. The consecutive chapters in this doctoral dissertation present the catalysts developing process, including modification of their morphology, as well as optimization of catalytic performance at various conditions in batch and flow reactors.

The application of various synthesis methods (incipient wetness impregnation, wet impregnation, ion-exchange, nanoparticles grafting, co-precipitation) in combination with alteration of pretreatment conditions allowed obtaining catalysts with extraordinary performance:

- 2 wt.% Ni(Cl)/CNR115/2173/26.54, which allowed for water purification from trichloroethylene for 25 h without any signs of deactivation,
- 2 wt.% Pd/SiO_2(bim), which allowed for water purification from diclofenac for 15 h without any signs of deactivation,
- a series of CuZnAl hydrotalcite derived materials, which selectively hydrogenate nitrocyclohexane into various value-added products under mild conditions.

A thorough analysis of catalysts structures by numerous characterization techniques allowed drawing general conclusions concerning the impact of catalyst morphology on its activity, selectivity and stability in tested conditions.

Streszczenie

Współcześnie katalityczne uwodornienie jest jedną z najważniejszych reakcji chemicznych. Reakcja ta jest wykorzystywana zarówno w nowoczesnych procesach przemysłowych, jak i w ochronie środowiska. Wyniki zaprezentowane w niniejszej pracy pokazują zastosowanie katalitycznego uwodornienia w oczyszczaniu wody z najczęściej wykrywanych zanieczyszczeń chloroorganicznych (trichloroetylenu oraz diklofenaku). Dodatkowo, wskazują na wysoką użyteczność selektywnego katalitycznego uwodornienia nitrocykloheksanu. Przeprowadzone badania wpisują się w międzynarodowe trendy, mając na celu poprawienie balansu ekonomicznego wykorzystywanych katalizatorów oraz uczynienie procesów katalitycznych bardziej przyjaznych środowisku.

Ogólnym celem przeprowadzonych badań było wytworzenie katalizatorów, które będą aktywne w obydwu wyżej wspomnianych reakcjach. Kolejne rozdziały pracy opisują procesy syntezy katalizatorów, uwzględniając modyfikację jego morfologii oraz testy katalityczne w różnych warunkach.

Zastosowanie różnorodnych metod syntezy (impregnacji kapilarnej, impregnacji mokrej, wymiany jonowej, szczepienia nanocząstek, współstrącania) w połączeniu z modyfikacją warunków traktowania wstępnego układów katalitycznych pozwoliło otrzymać niezwykle wydajne katalizatory:

- 2 wt.% Ni(Cl)/CNR115/2173/26.54, który jest w stanie oczyszczać wodę z trichloroetylenu przez 25 h bez jakichkolwiek oznak deaktywacji,
- 2 wt.% Pd/SiO_2(bim), , który jest w stanie oczyszczać wodę z diklofenaku przez 10 h bez jakichkolwiek oznak dezaktywacji,
- serię katalizatorów CuZnAl, które w łagodnych warunkach w selektywny sposób uwodarniają nitrocykloheksan do związków o wartości dodanej.

Szczegółowa analiza właściwości układów katalitycznych umożliwiła wyznaczenie ogólnych zależności pomiędzy strukturą katalizatora a jego aktywnością katalityczną w testowanych warunkach.

Contents

List of abbreviations

Abbreviation	Meaning
HDC	hydrodechlorination
TCE	trichloroethylene, 1,1,2-trichloroethene
DCF	diclofenac, [2-(2,6-Dichloroanilino)phenyl]acetic acid
NC	nitrocyclohexane
TCE	Thermal Conductivity Detector
ECD	Electron Capture Detector
TPR	Temperature-Programmed Reduction
TPHD	Temperature-Programmed Hydride Decomposition
CO_2-TPD	Temperature-Programmed Desorption of CO_2
NH_3-TPD	Temperature-Programmed Desorption of NH_3
H_2-TPD	Temperature-Programmed Desorption of H_2
TGA	Thermogravimetric Analysis
XRD	X-ray Diffraction
XPS	X-ray Photoelectron Spectroscopy
XAS	X-ray Absorption Spectroscopy
TEM	Transmission Electron Microscopy

1. Introduction

Hydrogenation reactions are undoubtedly one of the most important processes for the modern chemical industry [1,2]. Thanks to this simple reaction, in which molecular hydrogen reacts with another compound, tons of chemicals, pharmaceuticals and fuels are produced every year. The hydrogenation process's efficiency strongly depends upon the presence of a catalyst, which was discovered by Paul Sabatier and Jean-Baptiste Senderens in 1897 [3]. Over the last few decades, multiple hydrogenation catalysts have been designed, tested and developed [4–7]. Despite their high efficiency, most of them are based on precious transition metals, which contradicts Sustainable Development Goals and process economy [2]. In the last few years, a lot of research groups have been making efforts to develop active catalysts but based on low-cost transition metals [8]. These studies contribute to significant changes in chemical manufacture by making the hydrogenation processes more profitable and less harmful to the environment. The results described in this dissertation are in line with this global trend.

Catalytic hydrogenation is not only a manufacturing tool but also an excellent solution for environmental problems. The enormous experience gained during the development of industrial catalysts could be used to design catalytic materials for environmental protection. Therefore, every year more and more scientists are involved in the application of catalytic hydrogenation in this crucial field.

2. Literature background

2.1. Catalytic hydrogenation in the face of environmental challenges

Continuous development contributes to a significant improvement in the quality of human life. However, it also intensifies the progressive degradation of the environment, especially in the case of uncontrolled and unlimited progress. In the last few years, Sustainable Development Goals have been played a crucial role in modern industry. Nevertheless, many years of raging production, careless usage and reckless chemical disposal resulted in enormous environmental pollution, which strongly affects the current state of air, soil and water.

Drinking water is one of the most important resources of humankind. It is the basis of life. Therefore, access to high-quality drinking water is a fundamental human right. Nonetheless, the finest drinking water resources are diminishing every year due to the pollution caused by physical, biological, radical and chemical wastes. Among them, chemical contaminants are one of the most common in the natural environment [9]. Unfortunately, most of them are detrimental to aerial, terrestrial and aquatic living creatures. Examples of such chemicals can be chloroorganic compounds.

2.1.1 Chloroorganic water contaminants

Chloroorganic compounds are one of the most popular types of chemical water pollutants in the environment. Their widespread occurrence in water is the result of high popularity associated with their unique properties. Among them can be found: insecticides like hexachlorocyclohexane (lindane), dichlorodiphenyltrichloroethane (DDT) and heptachlor; pharmaceuticals like triclosan, chloramphenicol, diclofenac and sertraline but also very popular solvent and metal degreaser – 1,1,2-trichloroethene.

In my PhD research, I focused on two of them: trichloroethylene (TCE) and diclofenac (DCF). One of the most frequently detected substances in the natural environment.

1,1,2-trichloroethene

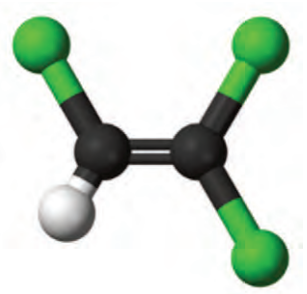

Figure 1. Model of 1,1,2-trichloroethene (TCE); • - Cl, • - C, • - H.

1,1,2-trichloroethene (known as: TCE, trichloroethylene, tri; **Figure 1**) is a colourless volatile, non-flammable liquid with a chloroform-like sweet smell. It is very well miscible with many non-polar organic solvents (e.g. ethanol) and has excellent solvency properties for numerous natural and synthetic chemicals. On the other hand, trichloroethylene is poorly soluble in water. Due to higher than water density, it tends to aggregate at the bottom of water reservoirs [10], where it can stay unchanged for decades.

TCE was firstly synthesised by Fisher in 1864 by the reduction of hexachloroethane with hydrogen. Commercial production started in 1920 in Germany and then in 1925 in the USA [6]. Initially, the industrial production was based on the two-step process, in which acetylene was chlorinated to 1,1,2,2-tetrachloroethane, and then trichloroethylene was produced by dehydrohalogenation of the intermediate product. Nowadays TCE manufacturing process involves the chlorination of ethylene over ferric chloride catalyst [7].

Thanks to the unique properties, TCE has found numerous applications in various fields. It is best known for its use as a cleaner and degreaser for metal

elements. Nevertheless, in the past, it was also used as an aesthetic before medical procedures, solvent in food processing and as a dry-cleaning agent.

Initially the harmfulness of trichloroethylene was unknown. This state has changed with the growing popularity and broader application. A thorough analysis of the effects induced by short-term and prolonged exposure indicates cancerogenic properties, regardless of the route of exposure. In addition to cancer-inducing effects, TCE also revealed toxicity to the central nervous system, liver, kidneys, immune system and male reproductive system [10].

The discovery of TCE toxicity resulted in the imposition of restrictions on its production and use. Despite this, it still has many applications, such as: a component in the production of fluorinated compounds (polymers, refrigerants, cooling agents), an extraction solvent for asphalt testing, a metal and electronic cleaner/degreaser and a special solvent in the cleaning of membranes in battery separators [11].

The demand for trichloroethylene grew until 1970, when annual production, only in the USA, reached 277 000 tons [10]. However, due to the discovered toxicity and imposed restrictions, its annual production decreased systematically and in 2015 was equal to 77 986 tonnes in the USA [12]. Nevertheless, IHS Markit, in their report from August 2020 - C2 Chlorinated Solvents, estimated total global consumption of trichloroethylene for 450 000 tons in 2020 with growing tendency [13].

Despite the limits set on trichloroethylene production and application, it remains one of the most commonly detected pollutants. According to the EPA Toxic Release Inventory (TRI), only in 2017 in the USA, approximately 1 000 tonnes was released into the environment. Taking into account the constant release of TCE and its persistence in groundwater, it is one of the most severe environmental contamination. Especially when its harmful effect on living organisms would be considered.

Diclofenac

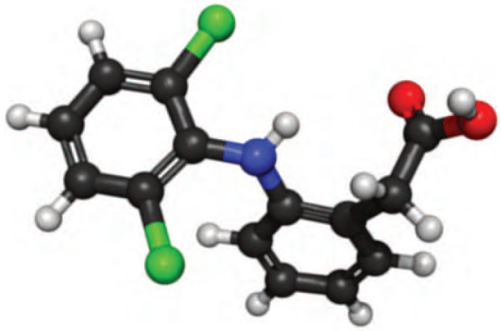

Figure 2. Model of diclofenac (DCF); • - Cl, • - C, • - H, • - N, • - O.

[2-(2,6-Dichloroanilino)phenyl]acetic acid, known also as diclofenac (**Figure 2**), is a popular non-steroidal analgesic anti-inflammatory drug. It is a relatively new compound designed and first synthesised in the '70s of XX century by Alfred Sallmann and Rudolf Pfister as a novel drug with high activity and outstanding tolerability [14]. In 2021 it was 72th on the list of the most prescribed drugs in the USA, with over 11 million prescriptions [15]. Considering that there is a lot of diclofenac containing non-prescription medicines on the market, the scale of annual usage is almost inestimable.

Most of the diclofenac is administered orally. Only 6 % is used in the form of ointment [16]. It should be stressed here that only 6 – 7 % of applied ointment is absorbed through the skin, while the rest remains on the surface, from where it is usually washed with water [17]. DCF introduced into the body is majorly excreted in the urine in its original form or in the form of its metabolites. Approximately 75 % of consumed diclofenac entering the water cycle [18]. As a result of the facts mentioned above, diclofenac is one of the most frequently detected pharmaceuticals in water [19].

Even at very low concentration, the constant presence of DCF in water may result in detrimental consequences for aquatic and terrestrial organisms [20–22]. It can cause oxidative stress, disturb metabolic processes in different groups of organisms and even contributes to DNA damage. Moreover, it promotes histopathological changes in various organs

and accumulates in different tissues. The diclofenac's negative influence on the liver, kidney and gills was observed for the rainbow trout. It also contributed to the extinction of enormous amounts of wild vultures across the Indian subcontinent. Due to these destructive effects, it has been listed as a monitored micropollutant by the European Union since 2015 [23].

Unfortunately, like other chloroorganic compounds, diclofenac shows long-term persistence, low biodegradability, high bio-accumulative potential and significant toxicity [24,25]. It is relatively stable in wastewater treatment processes and is barely removal upon conventional treatment [26].

2.1.2. Methods of water purification from chloroorganic water contaminants

Generally, the sources of contamination by chloroorganic compounds are numerous and not always very obvious. In the view of organochlorides widespread existence in water and their detrimental effects on living organisms, multiple purification techniques have been developed to remove and decompose these pollutants. However, due to the enormous diversity of organochlorines group, effective purification requires a multi-track approach. Therefore, before applying a specific remediation technique, multiple physicochemical properties (e.g. volatility, solubility, reactivity) have to be considered.

The universal method of water purification does not exist. Each technique has advantages and disadvantages and shows different efficiency in removing chloroorganic contaminants from water. In general, they could be classified as: non-destructive and destructive.

2.1.2.1 Non-destructive methods

The water purification process using non-destructive methods is based on the separation of contaminants from the treated water. This process does not destroy the chemical substance. Hence, further steps are required for the disposal of polluted gas or regeneration of adsorbent (e.g. usage of trapping agents, thermal incineration of sorbent). Nevertheless, unlike the other purification techniques, non-destructive methods offer the possibility to recover the chemicals for further use. Some of the most used non-destructive methods are: stripping and adsorption.

Stripping

A stripping method is based on the physical separation process, in which the stream of gas (air-stripping) or vapour (steam-stripping) removes pollutant from a liquid stream of water. This technique can be effectively applied only to the volatile compounds, with relatively high vapour pressure and low solubility in water (e.g. 1,1,2-trichloroethene (TCE)). The efficiency of the stripping depends on the flow rate of water and a kind of stripping agent. In the case of a low water flow rate and sufficient steam supply, the combination of steam-stripping and direct recycling of the contaminants by condensation is a cost-effective process. On the other hand, a high water flow rate without adequate steam source demands air-stripping usage to balance the process's economy [27]. Additionally, the initial concentration of pollution plays a crucial role, and stripping is not applicable at low concentrations [28].

Nevertheless, compared to other water purification methods, stripping has almost universal applicability for removing chloroorganic volatile compounds, and hence it is not selective for specific chemical substances.

Adsorption

Adsorption by definition is a process of the adhesion of a gaseous or liquid matter to another material's surface. It is a part of the most water purification

installations, as it can be used to remove almost all hazardous inorganic and organic pollutants [29]. It is a relatively cheap purification method with a cost range of 50 – 150 USD per million litres [30].

Like for other purification processes, the efficiency of adsorption strongly depends on several parameters. Presence of suspended particles and oils in water affects this process badly. Hence, pre-filtration is required. The concentration of contaminants, temperature, pH, contact time and particle size of adsorbent can also influence water treatment effectiveness [30].

Because adsorption is based on the adsorbent materials' surface, it requires a well-developed specific surface area. [31]. Moreover, sorption material should have enhanced porosity, defects in the structure, active sites, functional groups and stability (chemical, thermal and mechanical) [29]. On the other hand, the cost balance of the process requires inexpensive adsorbents [31]. There are several basic types of them: carbon nanomaterials (e.g. carbon nanotubes), gels (e.g. hydrogels), layered nanomaterials (e.g. nanoclays), polymer-based materials (e.g. conjugated polymers), nanoparticles (e.g. mixed oxide nanoparticles) and conventional materials (e.g. activated carbon, molecular sieves, zeolites) [29,32–35].

The high versatility of the adsorption process is tantamount to a lack of selectivity towards water contaminants. More significant disadvantages of this technique include the need for adsorbent regeneration after each cycle and the necessity to manage exhausted adsorbents. However, this method is the most commonly used process in water treatment plants despite the above mentioned difficulties.

2.1.2.2 Destructive methods

Destructive methods of water purification change properties of a contaminant in chemical or biological reactions. Due to the chemical nature of the reactions, they can be divided into oxidising and reducing

techniques. Nevertheless, it is essential to ensure that the chosen approach leads to less harmful or harmless products. The selected destructive methods are briefly characterized below.

Oxidation methods:

Oxidation aims at the mineralisation of the contaminant into carbon dioxide, water and other inorganic compounds, which can be problematic in the case of chloroorganic pollutants. Hence, strong oxidising agents are recommended for the high overall efficiency of the water purification process. An example of such an oxidant could be hydroxyl radical, used in all of the Advanced Oxidation Processes (AOPs). Unfortunately, highly active radicals are not selective, resulting in the formation of unwanted and more toxic by-products [36].

Ozonation

Water remediation by ozonation is a complex process which could occur in two different ways: by direct reaction with dissolved ozone (O_3) or by oxidation with formed hydroxyl radicals (·OH) [37]. In fact, ozone is not stable in water and decomposes through a complex reaction path that depends on the matrix composition [38]. Hence, water remediation by ozonation is the combination of the direct and indirect pathway.

Direct ozonation dominates under acidic conditions (**Reaction 1**).

$$3O_3 + OH^- + H^+ \rightarrow 2OH + 4O_2 \qquad \textbf{Reaction 1}$$

The indirect route takes control at higher pH (> 9) [37]. The ozone decomposition rate increases with pH (**Reaction 2**), which induces other reactions related to indirect oxidation (**Reaction 3 - 7**). Additionally, in alkali conditions, a fast side-reaction should be considered (**Reaction 8**) [37].

$$O_3 + OH^- \rightarrow O_2 + HO_2^- \qquad \textbf{Reaction 2}$$

$$O_3 + HO_2^- \rightarrow HO_2 + O_3^- \qquad \textbf{Reaction 3}$$

$$HO_2 \rightarrow H^+ + O_2^-$$ **Reaction 4**

$$O_2^- + O_3 \rightarrow O_2 + O_3^-$$ **Reaction 5**

$$O_3^- + H^+ \rightarrow HO_3$$ **Reaction 6**

$$HO_3 \rightarrow OH\cdot + O_2$$ **Reaction 7**

$$HO + O_3 \rightarrow HO_2\cdot + O_2$$ **Reaction 8**

Ozonation can be used for removal of diclofenac and trichloroethylene from water [39,40]. Even though direct ozonation of diclofenac results in fast decomposition, the reaction by-products are ozone resistant, which means that the mineralisation rate of DCF is relatively low [41]. In the case of trichloroethylene, ozonation in combination with stripping allows reaching limits of the European Union for drinking water (10 μg/L) only if the initial concentration of TCE is below 80 μg/L. For higher concentrations – the final amount of TCE is far from the limits [42]. Moreover, it should be noticed here that more harmful products are formed [39,42]. In the case of diclofenac, they areoxalaldehyde and N-(2,6-dichlorophenyl)-2-oxoacetamide, which are harmful to aquatic organisms [39]; and for trichloroethylene – trichloroacetic acid with cancerogenic properties [42].

To summarise, ozonation has several advantages. Ozone purifies water in a rapid and effective way, it does not require the addition of chemicals into water, and it eliminates itself by decomposition.

On the other hand, it should be remembered that ozone is very reactive and may react with the matrix, which will result in the formation of more harmful compounds. Moreover, the required equipment is relatively expensive, and the method is high energy demand. Additionally, each O_3 molecule has to be transferred from the gas into the liquid phase, which involves the problem of mass transfer [37]. All of these factors should be seriously considered before the ozonation purification process.

Photocatalytic oxidation

The process of water purification by photocatalytic oxidation involves the presence of a photocatalyst, and the most commonly used is titanium dioxide (TiO_2). The photocatalyst, as a semiconductive material, absorbs radiation with energy above its bandgap, which results in the formation of hollow-electron pairs (h^+/e^-) (Reaction 9) [43].

$$TiO_2 + h\nu \rightarrow TiO_2\,(e^-) + TiO_2\,(h^+) \qquad \textbf{Reaction 9}$$

The positive holes tend to react with H_2O or adsorbed HO^- species, which causes the formation ·OH radicals (**Reaction 10 - 11**). On the other hand, the electrons can transform adsorbed O_2 molecules into $\cdot O_2^-$ radicals (**Reaction 12**) [43].

$$TiO_2\,(h^+) + H_2O \rightarrow TiO_2 + \cdot OH + H^+ \qquad \textbf{Reaction 10}$$

$$TiO_2\,(h^+) + HO^- \rightarrow TiO_2 + \cdot OH \qquad \textbf{Reaction 11}$$

$$TiO_2\,(e^-) + O_2 \rightarrow TiO_2 + \cdot O_2^- \qquad \textbf{Reaction 12}$$

The electrons transfer could directly oxidise the contaminants adsorbed on the surface of the photocatalyst. Moreover, in the case of redox species adsorbed on the photocatalyst's surface, there is a possibility of co-occurrence reactions: oxidation and reduction. The electrons support the reduction process, while the holes – the oxidation process [37].

The photocatalytic oxidation can be used for purification of water from various chloroorganic contaminants, also trichloroethylene and diclofenac [44–49]. TiO_2-SnO_2 catalyst (0.8 g/L) allowed for removing 90 % of diclofenac (initial concentration - 20 mg/L) after 5 hours of UV irradiation. However, after each cycle, the catalyst's efficiency dropped, and the final conversion after the fourth cycle was equal to 55 % [44]. Different ZnO catalysts (modified by F, C, N and S) used for water contaminated by DCF let to obtain around 90 % degradation after 4 hours of UV irradiation, with the initial concentration

in the range 10 – 20 μg/L [46]. In the case of trichloroethylene, TiO_2 catalyst (0.7 g/L) remove 45 % of TCE (35 μg/L) at 45 mm water depth after 3 h of irradiation [47]. These results may be considered as satisfying in terms of contaminants conversion. However, similarly to the other oxidation techniques, the reaction products were equally or more toxic than original contaminants [50–52].

The photocatalytic oxidation has several advantages like the possibility of using sunlight as a source of irradiation. The reaction could be conducted under atmospheric pressure at room temperature, and the required catalyst cost is relatively low. On the other hand, this method has significant disadvantages, such as enormous problems with providing uniform radiation on the catalyst surface in large scale processes [37]. However, as with the other oxidation methods, the possibility of the formation of more harmful products is a significant drawback of this method [50–52].

Fenton oxidation

In this process hydroxyl radical is generated from the Fenton's reagent – a mixture of H_2O_2 and ferrous iron (typically $FeSO_4$). Radicals are generated according to **Reaction 13**. [53]. Nevertheless, the such active reactants' presence results in subsequent reactions, like the regeneration of Fe^{2+} from Fe^{3+} (**Reaction 14**).

$$Fe^{2+} + H_2O_2 \rightarrow Fe^{3+} + \cdot OH + HO^- \qquad \textbf{Reaction 13}$$

$$Fe^{3+} + HO_2\cdot \rightarrow Fe^{2+} + H^+ + O_2 \qquad \textbf{Reaction 14}$$

Fenton oxidation is highly effective remediation technique. However, its efficiency strongly depends on several factors: pH, temperature and reagents concentration. Water treatment should be conducted in the pH range 3-5, because higher pH values induce precipitation of the $Fe(OH)_3$ and increase decomposition of the H_2O_2. Similar problems are observable at temperatures higher than 313 K. Crucial for this process hydroxyl radicals are not formed

without iron ions. Nevertheless, increasing iron concentration increases the efficiency of the oxidation process only to some level. A higher concentration of H_2O_2 positively affects the purification process, but at the same time, H_2O_2 also scavenge ·OH radicals [37] All of these aspects strongly affect the remediation process and should be taken into account at the planning level, which complicates the water purification.

Similarly to other oxidation techniques, Fenton oxidation could be applied with success to trichloroethylene and diclofenac removal [54–59]. However, classic homogeneous Fenton oxidation needed to be modified to achieve satisfying results. Usage of alternative pyrite-Fenton processes with H_2O_2 improves the reaction's efficiency compared to the classic homogeneous Fenton system [57,60,61]. Effect of this remediation technique could be satisfying. Nevertheless, despite the immense applicability of the Fenton oxidation and several advantages, this method has also significant disadvantages:

- enormous amounts of iron salts are necessary, which increase the cost of the procedure,
- the European Union expect a very low concentration of iron in the water – further water treatment is required,
- this process is typically coagulation-flocculation which results in huge amounts of metal sludge waste.

Oxidation methods proved their efficiency in the removal of chloroorganic contaminants from water. Each technique is applicable but has some limitations, which could be compensated by combining different ways. Many studies related combined systems usage consist of ozonation, photocatalytic oxidation and Fenton oxidation in their original and modified versions [36,37,62–68]. Unfortunately, the need to combine methods significantly complicates the process of water purification.

The main obstacle in the implementation of the oxidation processes at the full-scale, especially Advanced Oxidation Processes, is the high operational cost related to required chemicals and high energy demand. Besides, the possibility of the formation of more toxic products is the substantial drawback of these methods.

Reductive methods:

The chemical nature of the chloroorganic compounds, determined by chlorine's electronegative character, suggests that reductive dechlorination is preferable from the thermodynamical point of view. Moreover, the reduction reaction products (e.g. chlorine ions and non-chlorinated hydrocarbons) are less toxic or non-toxic at all.

Zero-valent metal reduction

The zero-valent metal reduction is the process, in which the reduction of chloroorganic contaminant is coupled with the oxidation of a metal, the most commonly used is iron (ZVI – zero-valent iron) [69]. The basic reaction mechanism involves the direct transfer of the electron from zero-valent metal into adsorbed chlorinated organic compound (**Reaction 15**) [70]. Simultaneously, metallic iron in aqueous phase reduces water (**Reaction 16**). Both reactions suggest reductive dechlorination mechanisms, in which contamination is reduced by Fe^{2+} (**Reaction 17**) or by H_2, in the presence of metal with hydrogenolytic properties (e.g. Pd) (**Reaction 18**) [71].

$$Fe^0 + RCl + H^+ \rightarrow Fe^{2+} + RH + Cl^- \qquad \textbf{Reaction 15}$$

$$Fe^0 + 2H_2O \rightarrow Fe^{2+} + 2OH^- + H_2 \qquad \textbf{Reaction 16}$$

$$2Fe^{2+} + RCl + H^+ \rightarrow 2Fe^{3+} + RH + Cl^- \qquad \textbf{Reaction 17}$$

$$RCl + H_2 \text{ (hydrogenation catalyst)} \rightarrow H^+ + Cl^- \qquad \textbf{Reaction 18}$$

ZVI reduction is an inexpensive, non-toxic and effective method of water purification from chloroorganic contaminants. It is reflected in the huge interest of research groups from all over the world [70–78]. Nevertheless, like other treatment techniques, the zero-valent metal reduction has its problems and limitations. It is more efficient than biodegradation, but still it takes days to perform this process with a high chloroorganic contaminant removal ratio [73]. Purification effectiveness strongly depends on the electron transfer efficiency [74], and the degradation of the pollutant is much stronger in the presence of metallic form [69]. Hence, all of the processes that block metal surface are not desired (e.g. corrosion, passivation). There are several ways to modify and protect the surface, like doping with other metal (e.g. Pd) [72,75], coating (e.g. with polymers or CMC) [72,76], the formation of emulsified ZVI [77] or adsorption on the support material (e.g. carbon, silica) [78]. The process of reduction is also temperature sensitive. The reaction rate is four times lower at 283 K than at 298 K [69], which could be a problem since groundwater temperature varies in the range 282 – 288 K. Another obstacle is the composition of treatment water, some of the non-reducible anions (e.g. PO_4^{3-}, SO_4^{2-}, Cl^-) may influence the process efficiency [74].

All of these factors determine the usability of zero-valent metal reduction in the water remediation from chloroorganic contaminants. Taking into account its advantages and limitations, it can be applied in specific environmental conditions.

Electrochemical reduction

Electrochemical reduction is the process, in which the transformation of chloroorganic contaminant is performed by direct or indirect reduction and dechlorination at the cathode surface. The direct reduction is going through the electron tunnelling between a chemisorbed complex and the cathode material [79]. The indirect pathway occurs

via the hydrodechlorination reaction due to water electrolysis. Hydrogen adsorbs at the cathode surface (M) by electrochemical adsorption (Volmer reaction – **Reaction 19**). Then, adsorbed hydrogen (H_a) can undergo chemical desorption by Heyrovsky reaction (**Reaction 20**) or chemical desorption by Tafel reaction (**Reaction 21**) to form H_2. Alternatively, it can interact with adsorbed chloroorganic contaminant (**Reaction 22**) [80].

$$H_3O^+ + (M) + e^- \rightarrow (M)H_a + H_2O \qquad \textbf{Reaction 19}$$

$$H_3O^+ + (M)H_a + e^- \rightarrow (M) + H_2 \qquad \textbf{Reaction 20}$$

$$(M)H_a + (M)H_a \rightarrow H_2 + 2(M) \qquad \textbf{Reaction 21}$$

$$2(M)H_a + RCl \rightarrow RH + H^+ + Cl^- \qquad \textbf{Reaction 22}$$

The hydrodechlorination (HDC) is affected by electron transfer, mass transfer, chemical reactions and surface reactions [81,82]. The cathode material is crucial for the efficiency of the HDC process. It should have a sufficiently strong bond with H_a to allow the proton-electron transfer, but also weak enough to provide the possibility of bond breaking and the release of the products [83]. If the binding energy between hydrogen and metal is too high, adsorption is slow and overall activity is also low. On the other hand, low binding energy reduces the desorption rate. The elements like Pd, Pt, Ag and other noble metals showed excellent efficiency in the removal of chloroorganic contaminants from water by electrochemical reduction. Their high activity is related to the fact that hydrogen adsorption free energy is close to zero [83].

Comparison of different cathode materials (Fe, Cu, Ni, Al, C) showed the superiority of the Ni cathode in the removal of TCE from water (the initial concentration – 5.3 mg/L). The electrodes activity was in follow order: Fe – Al < Cu < C < Ni. The Ni foam's obtained conversion was equal to 68 % after 180 minutes of the process, and it was improved to 78 % after Pd coating. Additionally, the efficiency of all electrodes was improved by the coating operation, especially for Fe cathode – from 43 % to 99 % [80].

In the same research, the impact of nitrates in the water matrix was evaluated, which is important due to their common groundwater presence at high levels. The comparison of the highest conversion – 99 % in the absence of nitrates with the value obtained for 100 mg/L of nitrates – 41 %, showed a huge influence on the reduction process [80].

Regardless of the high efficiency of electrochemical reduction in water purification for most of the chloroorganic contaminants, this method has some significant issues. It requires a high amount of energy due to low current efficiency. Additionally, electrodes are quite expensive and unstable. Hence, like for other purification techniques, all of the conditions should be taken into account before applying electrochemical purification of water.

Catalytic hydrodechlorination (HDC)

Catalytic hydrodechlorination is the process, in which the C-Cl bond undergo hydrogenolysis in the presence of the catalyst, usually in the form of metal nanoparticles supported on, or incorporated in another material. During the catalytic reaction, one or more of chlorine atoms are replaced by hydrogen, which results in the formation of hydrochloric acid and less-or non-chlorinated compounds (**Reaction 23**) [84].

$$R\text{-}Cl + H_2 \xrightarrow{\text{catalyst}} R\text{-}H + HCl \qquad \textbf{Reaction 23}$$

The process of catalytic hydrodechlorination of the organochlorides discussed in this doctoral dissertation (trichloroethylene and diclofenac) occurs in accordance with the presented schemes (**Scheme 1** and **Scheme 2**). In both cases, the formed products revealed significantly lower toxicity than the original chemical compounds.

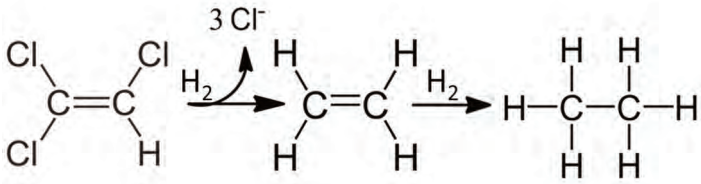

Scheme 1. Reaction pathway for HDC of TCE in the aqueous phase.

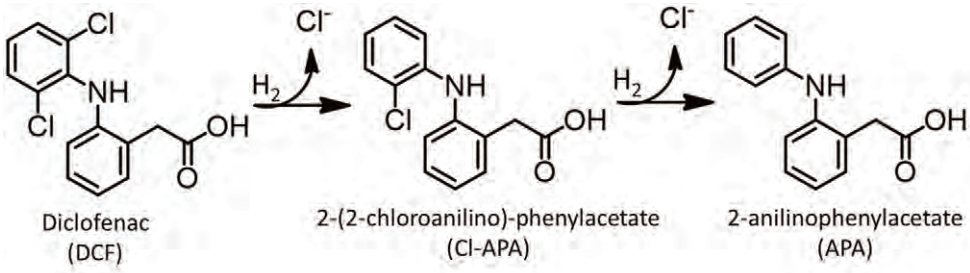

Scheme 2. Reaction pathway for HDC of diclofenac in the aqueous phase [26].

In the past, the process of catalytic hydrodechlorination was the primary treatment method of liquid organic wastes containing chlorinated hydrocarbons [85]. However, before the discovery of the common and dangerous presence of chloroorganic compounds in water, no one tried to use this reaction in the direct purification of wastewater or groundwater. Only in 1992, Kovenklioglu et al. [85] proved that a variety of these chemicals could be treated directly in the aqueous solution with a reasonable efficiency. Since that time, the interest in the usage of hydrodechlorination process has been raised significantly, and now it is considered as one of the most promising methods for removal of chlorocarbons from water [86].

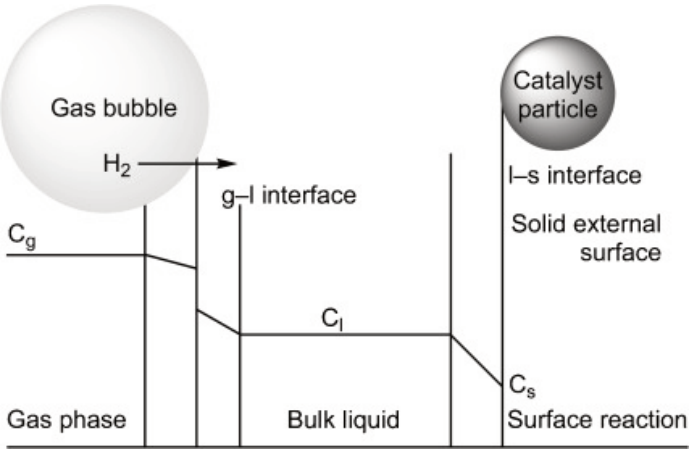

Figure 3. Scheme of H_2 transfer to the catalyst surface, with the possible effects on its concentration in each phase [84].

Aqueous phase hydrodechlorination of chloroorganic contaminants can be performed with hydrogen transfer agents, e.g. alcohols [87], organic acids [88] and organic/inorganic salts [89]. However, the majority of the research has involved molecular hydrogen, which means that this process is carried out in a three-phase catalytic system [84,90,91]. Hence, the overall activity is controlled by series of sequential mass-transfer and reaction steps, which are illustrated in **Figure 3** [84]. At the beginning of the process, the H_2 has to be diffused through the gas and liquid film at the gas-liquid interface. Next, both H_2 and organochloride have to be transferred to the liquid-solid interface, which is the crucial step for further reaction. The possible diffusional constraints within pores may significantly affect the whole process. Finally, after the adsorption of theses substrates on the catalytic surface – the HDC can happen, which is followed by desorption of the formed products and their reverse transfer into the reaction mixture.

The mass-transfer limitations can directly affect the effectiveness of water treatment, but also may hinder the research on the catalytic performance. When the diffusion rate of any substrate is lower than the reaction rate, the obtained result reflects this parameter. Hence, like in other catalytic

processes, one of the most crucial things is to ensure the reaction conditions under which the kinetics of the reaction will be studied. The elimination of the diffusional issues can be achieved by providing a sufficiently large interface available for the substrates transfer. In practice, this is accomplished with the vigorous stirring [92] or by changing the reaction method [93].

Beside the mass-transfer limitations, there are other essential factors which determine the effectiveness of HDC process

- a type and a form of metal active phase (e.g. size and distribution of metal nanoparticles, doping with other metals) [94–96],
- properties of the material, which is used for incorporation of metal nanoparticles or as their support (e.g. porosity, specific surface area, acidity, chemical stability) [97–99],
- properties of the solution in which reaction is conducted (e.g. pH, temperature, presence of other ions) [26,100,101].

A comprehensive and insightful analysis involving the impact of these factors is necessary for the synthesis of active and stable hydrodechlorination catalysts.

Similar to catalytic hydrogenation, the HDC process requires metal with high activity towards dissociative adsorption of molecular hydrogen. Pd nanoparticles are well-known from the formation of reactive atomic hydrogen on their surface, but also for facilitating the cleavage of the C-Cl bond [102–104]. Hence, most of the studies on the water purification from any chloroorganic compound are focused on palladium catalysts [81,105]. However, due to the high cost of noble metals, the possibility to use low-cost transition metals with the preservation of high activity has been studied for years. One of the most promising results were obtained for nickel, copper, cobalt, iron and multi-component catalysts [106–109]. If the activity

of these catalysts is not satisfactory enough, they could be doped with noble metals in order to increase performance to the desired value [110,111].

Not only the kind of the used metal but also its morphology plays a crucial role in the catalytic performance. Among studies on the influence of the active phase structure, the most attention is paid to the size and dispersion of metal nanoparticles. Despite the importance of these properties, careful analysis of the literature data showed conflicting evidence for the superiority of both smaller and larger nanoparticles. The smaller ones are more active than larger, but on the other hand, larger nanoparticles are more resistant to deactivation in the liquid phase hydrodechlorination [112,113]. Simultaneously, larger species showed a higher tendency to leaching, which lowered the overall efficiency [114]. These information suggest the importance of both types. Hence, Wu et al. [115] made an attempt to determine their contribution towards the catalytic hydrodechlorination. The researchers proposed that the activation of H_2 occurs with higher efficiency on larger nanoparticles, but at the same time, there are less cationic species on their surface (responsible for the C-Cl bond activation [115]). Therefore, a well-design catalyst should balance nanoparticles size and their dispersion to achieve the desired activity.

Most of the research on catalytic water purification uses metal nanoparticles supported on or incorporated into another material. It is well established that their properties strongly influence the above-mentioned parameters, and as a result – the catalyst's overall activity. An enormous number of various materials have been tested in this reaction. Among them: activated carbon, silica, alumina and zeolites have received significant attention [116–120].

Due to the extremely high specific surface area and large porosity, activated carbons (ACs) are especially interesting. They are resistant to the corrosive conditions of the hydrodechlorination reaction but also non-toxic to the environment. Their production is relatively inexpensive, and it can be done with the usage of renewable raw materials (e.g. coconut shells, soybean hulls, nutshells) [121]. Moreover, the production process

facilitates modification of the carbon's final properties [122–125]. Although, the application of the ACs as support materials for catalysts is very common, there are many articles with conflicting data, which contribute to the elective interpretation of the catalytic results [126,127]. For instance, in accordance with Munoz et al.[126], higher overall efficiency in the hydrodechlorination process is observed for materials with high specific surface area and low ordered structure of carbon support. On the other hand, further studies by Baeza et al. [127] revealed higher activity of the Pd nanoparticles supported on highly ordered or even graphitised carbon. Hence, there is a strong need to investigate this topic more thoroughly to draw more general conclusions.

The starting reaction conditions are critical to the initial reaction rate, but also for the overall efficiency of the water treatment process. The catalytic hydrodechlorination performed in the aqueous phase produces hydrochloric acid, which significantly lowers the pH of the solution, but it is also the most widely accepted cause of the deactivation of the catalyst [128–130]. The most reasonable and sensible solution to this problem seemed to be the introduction of the pH modifiers [131–133]. A series of experiments performed by de Pedro et al. [133] in various solutions showed that the best results could be obtained by increasing the pH of reaction medium up to 8.5-9 with the addition of NaOH (0.77 mM). More acidic reaction conditions support the catalyst deactivation, on the other hand, a higher concentration of OH^- results in the blockage of metal active sites [133].

The water purification tests are usually conducted in the deionised water contaminated by specific chloroorganic compound. However, as it was demonstrated by Xia et al. [134], the presence of other ions in the reaction mixture should be taken under consideration. For example, a high concentration of basic metal ions and alkali earth metals (Na^+, K^+, Mg^{2+}, Ca^{2+}) does not affect hydrodechlorination reaction. On the other hand, metal ions, such as Ni^{2+}, Pb^{2+}, Cu^{2+} and Fe^{2+} may decrease the overall activity or even contribute to the complete deactivation of the catalyst [134].

Hence, the influence of the present ions should be well-studied before the transition to large-scale experiments.

Most of the catalytic hydrodechlorination research are conducted in batch reactors, despite the benefits from process adaptability and scalability provided by flow reactors. There are several works on the catalytic HDC in the liquid flow conditions [101,116,135–137], mostly related to 4-chlorophenol. The direct comparison between batch and flow conditions in the removal of 2,4-dichlorophenol showed higher HDC rate in the continuous flow operation [93]. Additionally, switch from batch to continuous flow should decrease catalyst deactivation and increase its lifetime, as an effect of more efficient removal of HDC products. Moreover, a switch from batch to flow conditions is one of the most mentioned priorities for the modern chemical industry. Hence, the use of the flow catalysis should also be taken into account in environmental protection.

Aqueous phase hydrodechlorination of trichloroethylene

The excellent Pd catalytic performance in the aqueous phase hydrodechlorination of trichloroethylene was firstly observed by Kovenklioglu et al. [85] at the beginning of 1990s. Series of Pd catalysts revealed high efficiency in the direct removal of TCE and other organochlorides like chloroform, trichlorobenzene and dichloromethane [85]. For example, the usage of 1.25 g of 5 wt.% Pd/C in the shaker type reactor allowed for complete degradation of trichloroethylene in 3 h process conducted at room temperature and slightly elevated pressure (initial concentration of TCE = 125 μL L^{-1}). Additionally, Kovenklioglu et al. [85] considered the vital role of the support material. The straight comparison between activity values determined by substrate uptake and by the formation of the chloride ion exposed significant differences at the beginning of the HCD process. It was explained by the rapid adsorption of organochlorine, which accumulates

on the support surface. Moreover, the catalysts with higher specific surface area showed greater overall efficiency [85].

Hence, the investigation of the support material effect seems to be crucial for the activity of Pd nanoparticles. Other studies showed that various modifications could significantly increase their effectiveness in this process. For instance, Zhang et al. [138] stabilised Pd nanoparticles by carboxymethyl cellulose and immobilised them on the alumina support. These operations gave greater particles dispersion than observed for the typical Pd/alumina catalyst. In effect, trichloroethylene was removed in a very effective way. The purification process, at room temperature and under atmospheric pressure, was completed in 30 minutes with by 1.0 g of the 0.33 wt.% Pd/alumina catalyst [138].

Even better results in terms of Pd:TCE ratio was obtained by Meduri et al. [95]. Application of 20 mg of 5 wt.% Pd supported on granular activated carbon completely removed TCE from the reaction mixture in 5 minutes at room temperature and under atmospheric pressure, where the initial concentration of TCE was equal to 0.87 μL L^{-1} [95].

In contradiction to traditional support materials, Ozkan's group from the Ohio State University synthesised a series of catalysts with Pd nanoparticles deposited inside the swollen matrix of Swellable Organically-modified Silica (SOMS) [139–141]. Nanoparticles located on the interior surface, available only by swelling, were much more resistant to the inhibition. The comparison of 1 wt.% Pd/SOMS and 1 wt.% Pd/Al_2O_3 showed the superiority of the latter in terms of the rapid degradation of trichloroethylene. However, Pd/SOMS revealed resistance to complete deactivation, and hence the HDC could be conducted for a long time under the same reaction conditions [139].

Another approach was presented by Śrębowata et al. [99]. The researchers, encouraged by great catalytic performance provided by Pd-loaded zeolites in the gas-phase HDC, decided to use these materials in the aqueous phase experiments. Pd nanoparticles were deposited on microporous ZSM-5 and

its hierarchical mesostructured analogue – obtained as a result of the desilication process. The catalytic tests revealed the superiority of the desilicated material. It turned out that this type of structure contributes to the formation of uniformly dispersed species with a large amount of Pd^0, which favoured the hydrodechlorination of trichloroethylene in the aqueous phase [99].

The unusual activity of the Pd nanoparticles allows them to be used in the hydrodechlorination reaction with the alternative sources of hydrogen, like formic acid, metal hydrides and isopropyl alcohol [88,90]. Both Yu et al. [88] and Diaz et al. [90] proved that thanks to the lower activation energy of the formic acid decomposition (49.7 kJ mol^{-1}) than the TCE degradation (62.4 kJ mol^{-1}), the HDC reaction is favoured at room temperature. Due to the low solubility of the H_2 in water, hydrodechlorination with formic acid as a source of hydrogen seems to be an interesting alternative. However, achieving high activity requires careful selection of the support material in order to take control of the competitive adsorption of substrates [90].

The extraordinary catalytic activity of palladium nanoparticles in the hydrodechlorination process is contradicted by relatively fast deactivation. The poisoning effect is caused by the protons and chloride ions, which are the main products of the HDC process. The appearance of these ions also contributes to the leaching of the metal active phase [101].

It is well established and widely accepted that the reduced form of Pd is the active form in this reaction. Released protons can promote oxidation of the Pd^0 into Pd^{2+}, which reduces the overall efficiency of the process, but this reaction is not favourable from the thermodynamic point of view. Unfortunately, the presence of chloride ions stabilises the formation of Pd^{2+} complexes, such as $PdCl_3^-$ and $PdCl_4^{2-}$, which are stable at pH values lower than 7 [142]. The negative effect of these ions could be countered

by the addition of a strong base, like NaOH. Sodium hydroxide neutralises protons, but at the same time, stabilises Pd^{2+} by the formation of the hydroxides [101]. On the other hand, the addition of external alkalinity (like Na_2CO_3) neutralises formed protons without Pd^{2+} stabilisation effect. Hence, this compound seems to be a better neutralising agent, which also consists of naturally occurred ions.

The concentration of protons and chloride ions in the vicinity of the active phase could be moderated by the acidity of the support material and pH of the reaction mixture. Nevertheless, pH values lower than 3 contributes to the metal active phase leaching [141]. Fortunately, apart from the deactivation caused by leaching effect, the activity of the Pd catalyst can be recovered by washing the catalyst with distilled water.

All of the research related to the catalytic hydrodechlorination of trichloroethylene in water by Pd catalysts are in agreement on one point – the main products of the reaction are non-chlorinated and non-toxic compounds, what is extremely important from the environmental point of view.

Despite the clear advantage of noble metals, there is also a strong need to develop catalysts based on low-cost transition elements (e.g. Ni). In the first attempt to introduce non-noble metals into TCE HDC in the aqueous phase, Śrębowata et al. [143] tested a series of 2 wt.% Ni catalysts doped with Pd. These materials were synthesised by the co-impregnation method with the mesoporous activated carbons as support materials. Catalytic experiments were performed at room temperature, under atmospheric pressure, and without additional solvents with the TCE concentration equal to 5.7 μL L^{-1}. Small addition of Pd (0.19 wt.%) significantly improved activity of the Ni/C catalyst, 95 % of TCE was removed in 150 minutes [143]. Further research with comparable 2 wt.% Ni catalysts, but obtained by soft-templating synthesis procedure on mesoporous carbon, showed that similar activity could be achieved by the usage of the monometallic catalyst [144].

Nonetheless, similar to the Pd catalysts – all of the obtained products are non-chlorinated and less toxic than trichloroethylene.

Aqueous phase hydrodechlorination of diclofenac

Due to the fact that the problem of water contamination by micro-pollutants is relatively new, all of the studies on catalytic hydrodechlorination of diclofenac in the aqueous phase are focused on the Pd catalysts. Interestingly, in the first reported article by De Corte et al. [145], monometallic bio-Pd, produced by the metal respiring bacterium *Shewanella oneidensis* in the presence of H_2, turned out to be inactive in this process. The same behaviour was observed for cell-associated bio-Au nanoparticles. Only the formation of bimetallic Au core with the Pd shell allowed to obtained satisfactory results – 78 % dehalogenation after 24 h (20 mg L^{-1}) [145]. These values are not very spectacular. However, biosynthesis of nanoparticles by bacteria, which also serves as a support material, makes this method extremely interesting in terms of cost balance, safety and ecological impact. The experiments performed by the same research group with the effluents of hospital wastewater treatment plants [146], showed that the same nanoparticles are less active in the environmental conditions, but still able to remove diclofenac from water – 44 % after 24 h (6.4 μg L^{-1}).

The catalytic performance of Au-Pd core-shell nanocomposites was further explored by Wang et al. [147]. Also in this case, monometallic Au and Pd were almost inactive in the removal of diclofenac from water. Surprisingly, nearly 90 % of the initial concentration (30 mg L^{-1}) was dechlorinated in 6.5 h by the mixture of both nanoparticles. However, this is far from the results achieved for the Au-Pd core-shell nanocomposites – 100 % conversion in 4.5 h [147], which drastically surpassed the results previously obtained by de Corte [145]. Further studies on the influence of Au-Pd composition showed that their concentration should be balanced to achieve the best results [147]. Higher Au content promotes activity, but at the same

time, too much gold might be the reason for the formation of thinner or even incomplete Pd shell, which in the result decreases efficiency [147].

Recent studies performed at Beijing Normal University showed that different preparation methods of bio-Pd might affect its activity [148]. The researchers used in the synthesis procedure a unique form of microbial aggregates with three-dimensional heterogeneous structure – Anaerobic Granular Sludge (AGS). Bio-Pd nanoparticles were formed by AGS, and hence incorporated in its structure. The combination of microbial metabolic function of AGS with catalytic properties of Pd allowed for complete removal of diclofenac within 90 minutes (DCF initial concentration – 20 mg L^{-1}).

The more traditional approach to the synthesis of the catalysts was presented by Wu et al. [149], which synthesised a series of Pd nanoparticles supported on different materials Al_2O_3, SiO_2, CeO_2 and activated carbon (AC). These catalysts were prepared by the deposition-precipitation method with target metal loading equal to 2 wt.%. All of the experiments were performed in the batch reactor, at room temperature, under atmospheric pressure with established initial pH equal to 9. The reaction mixture consisted of water, NaOH and diclofenac (240 μM) was purged continuously with hydrogen. Interestingly, in these conditions, Pd/SiO_2 revealed almost negligible activity. On the other hand, Pd/CeO_2 showed excellent efficiency – complete removal of diclofenac from the reaction mixture in 50 minutes. In this case, higher activity was explained by higher Pd dispersion and more cationised Pd species [149]. Nevertheless, it should be noticed that the addition of base into reaction mixture results in higher HDC rate [150].

Hence, the results obtained by Nieto-Sandoval et al. [26] without base addition, for the commercially available 1 wt.% Pd/Al_2O_3 are quite impressive. The complete removal of DCF from the reaction mixture was achieved in 20 min (0.5 g L^{-1} Pd/Al_2O_3, 68 μM DCF, 25 °C, 1 atm).

More recent studies of Nieto-Sandoval group are focused on the applicability of the Pd/Al_2O_3 in more natural aqueous matrices:

mineral water, surface water and tap water [120]. It was proved that complete degradation of diclofenac (3 mg L^{-1}) could be achieved in 1 h with the Pd/Al_2O_3 (0.25 g L^{-1}). The application of higher catalyst concentration (1 g L^{-1}) allowed for even faster water purification (under 15 min). Additionally, all of the experiments showed that co-existence of other substances in the solution does not affect HDC rate. It should be emphasised that in each case, the products of the diclofenac catalytic HDC were less-toxic or non-toxic at all. It makes catalytic hydrodechlorination an extremely attractive way of water purification from micropollutants, like diclofenac.

In summary, catalytic hydrodechlorination in the aqueous phase is an extremely attractive method of water purification from chloroorganic contaminants. It can be conducted at room temperature and under atmospheric pressure. This operation procedure requires a small amount of relatively low-cost equipment, but even in the case of expensive noble metal catalysts – extraordinary activity compensates their high cost. Furthermore, there is also a possibility to use active catalysts based on low-cost transition metals. Nevertheless, the most important is the fact, that in contradiction to other purification techniques, the products of the catalytic HDC are non-toxic and environmentally friendly.

2.2. Catalytic hydrogenation for industrial applications – nitrocyclohexane hydrogenation

The chemical industry, as a leading provider of materials for other industrial branches, is crucial to the global economy. Therefore, even a slight change in the chemical process may have a tremendous impact on many areas related to human activity. Hence, there is a strong need to search for novel, environmental-friendly and inexpensive methods of synthesis, or modification of currently used ones. For instance, switch from batch to flow is one

of the most often mentioned priority for sustainable manufacture in the fine chemical sector [151].

A significant increase in interest in the flow chemistry has been observed since the 2000s [152]. Most of the previously conducted research were focused on batch processes [153]. Kirschning et al. [154] suggested that the reason for that state of affairs in the past was related to the lack of flow equipment for laboratory-scale research. However, the systems for three-phase catalytic hydrogenation, for example developed by Kobayashi et al. [155], had opened entirely new perspectives for flow reaction studies.

The growing interest in flow syntheses is related to several different attributes of continuous processes, which make this way of conducting reactions extremely attractive in comparison to other methods [153]. Starting from the efficiency expressed in throughput per unit time and per unit volume, which dominates the efficiency achieved in batch reactors [156–159]. Excellent performance is due to elimination and easier control over the limitations characteristic for multi-phase reactions, e.g. requirement of large interfacial area. In batch reactors, vigorous stirring is needed to keep proper contact between reactants to achieve desired activity as well as the transfer of the products into the reaction mixture. At the same time, a solid catalyst is usually crushed during the mixing process, which causes issues with catalyst recovery and isolation of the reaction products. On the other hand, precise control over reactants concentration and their stoichiometry, contact time, pressure and temperature in a smaller reaction vessel, provided by flow processes, significantly reduce above problems [159]. Moreover, all of these features prevent side reactions and hence the formation of undesired products [160].

Additionally, operating at flow conditions makes working with hazardous reactants at elevated pressure and temperature safer, due to the enhanced reaction control. Reaction systems equipped with efficient heat receivers cause exothermic processes less risky as well as more efficacious [161]. The shorter

residence time of dangerous compounds in the reaction vessel prevents their accumulation and reduces potential detrimental effects [162,163].

Among the many advantages of flow chemistry, easy scale-up, and process intensification are the most interesting from the industrial point of view [156,164,165]. Furthermore, a simple modification of the reaction conditions supports the procedure of the process optimisation, which can be performed even by automatic systems [166,167].

Nevertheless, the transition from batch to flow operation conditions is not the ultimate goal for all industrial syntheses, especially in the case of well-established manufacture processes. The possibility and profitability of such transformations have been the subject of much research in the past two decades [168–172]. Some researchers approached this issue in a very comprehensive and universal manner. For instance, Calabrese and Pissavini [173] suggested a screening algorithm for batch reactions to determine the] feasibility of transition processes. Similar work was performed by Teoh et al. [174] by proposing practical assessment technology for converting fine chemicals production from batch to continuous. Hence, to eliminate expensive in time and money procedure, starting research on new synthesis pathway with the continuous flow reactors seems to be a very reasonable idea.

A perfect example of such an approach could be the use of nitrocyclohexane hydrogenation in liquid flow conditions. This reaction has been performed in batch reactors since the 1940s [175], and it has enormous and unfortunately still untapped application potential. The lack of laboratory-scale continuous flow equipment seems to be a reasonable explanation for the underestimation of this reaction [154]. Despite the simplicity of nitrocyclohexane (NC), the process of its hydrogenation could be very challenging due to follow-up hydrogenation and competing reactions, which are presented in the **Scheme 3**. Hence, easy control of reaction conditions and the usage of an appropriate catalyst are essential to achieve

desired activity and selectivity to specific products. Among them are cyclohexanone oxime, cyclohexanone, cyclohexylamine, cyclohexanol and dicyclohexylamine. Each one of these compounds found application in modern industry.

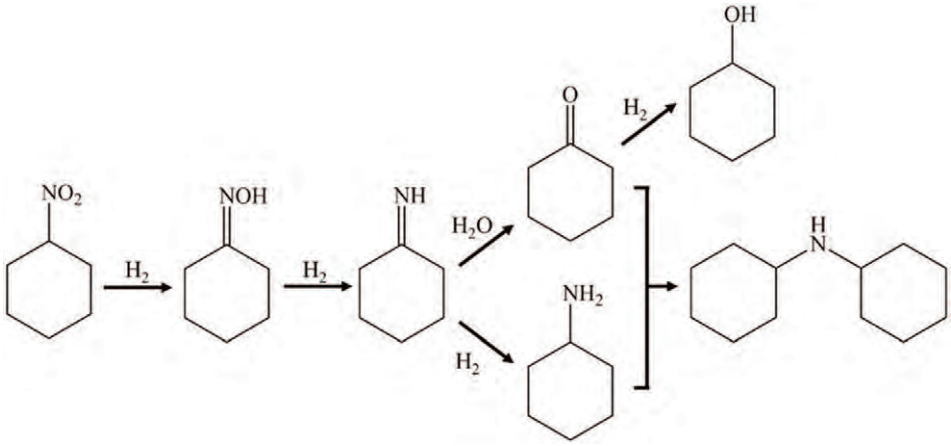

Scheme 3. Mechanism of nitrocyclohexane hydrogenation proposed by Wang et al. [176]

Cyclohexylamine – is colourless aliphatic amine compound in liquid form, which is miscible with water. It is used as a versatile intermediate in the production of: herbicides, insecticides, artificial sweeteners (sodium/calcium cyclamate), corrosion inhibitors, rubber vulcanising additives, plasticisers and a lot more [177,178]. Industrial production of cyclohexylamine is realised by amination of cyclohexanone over Group VIII metal-containing catalyst [179], or by catalytic hydrogenation of aniline over Ni or Cu catalyst [180]. However, these processes require high temperature and pressure, excess of hydrogen and a large amount of ammonia to prevent side reactions, which is the cause of the waste formation.

Dicyclohexylamine – is a colourless liquid secondary amine, sparingly soluble in water. It is used as a valuable chemical intermediate in the production of rubber vulcanisation accelerators, textiles, commercial insecticides, varnishes and corrosion inhibitors [181]. Currently, it is produced by catalytic hydrogenation of aniline at elevated pressure and temperature over

Ru/Pd catalyst [182]. This process leads to the formation of the cyclohexylamine/dicyclohexylamine mixture, which is hard to separate [181].

Cyclohexanol – is a secondary alcohol. This colourless substance creates crystalline needles with a camphor-like odour. Mild oxidation or catalytic dehydrogenation leads to cyclohexanone, whereas stronger oxidation gives adipic acid [183]. Cyclohexanol is an essential intermediate in the production of Nylon-6, but also with cyclohexanone is a part of KA oil (ketone-alcohol oil) – necessary for the production of adipic acid. Most of cyclohexanol is produced by liquid phase air oxidation of cyclohexane [183,184], which gives cyclohexanone/cyclohexanol mixture. The ratio between these compounds could be modified by changing the production parameters or application of the specific metal catalyst. Presence of anhydrous boric acid in the process leads to a higher yield of cyclohexanol, thanks to trapping of intermediate product [183]. Another synthesis procedure involves hydrogenation of phenol over metal catalysts, e.g. Raney Nickel catalyst at specific conditions gives 99.9% of selectivity to cyclohexanol [185].

Cyclohexanone – is a cyclic ketone in the form of colourless liquid with acetone-like odour. It can be hydrogenated to cyclohexanol, but also at more reductive conditions, it could be transformed into cyclohexane [183]. In combination with cyclohexanol could be used in the synthesis of adipic acid [183]. It is also used for syntheses of pharmaceuticals, plasticisers, herbicides and growth regulators for plants. However, the most important application, from the industrial point of view, is the synthesis of cyclohexanone oxime in the reaction with hydroxylamine. Cyclohexanone is synthesised similarly to the cyclohexanol, mainly by the liquid phase air oxidation of cyclohexane [183]. Addition of chromium (III) to the air oxidiser promotes the formation of the cyclohexane [186].

Cyclohexanone oxime – is solid colourless compound. The main application of the cyclohexanone oxime is the role of intermediate in the enormous

industry of Nylon-6 production. It is transformed into ε-caprolactam via Beckman rearrangement. The industrial method of cyclohexanone synthesis involves the condensation reaction between cyclohexanone and hydroxylamine [187]. However, this process demands significant excess of ammonia to displaced the equilibrium and hence a significant amount of ammonia sulphate waste is generated in this process [176].

As it was shown above, the production of these compounds is carried out with various technological processes with their advantages and disadvantages. The biggest problem for most of them is the generation of waste, which affects the cost-effectiveness, but also has a negative impact on the environment. Hence, the possibility to synthesise each one of them in one reaction makes catalytic hydrogenation of nitrocyclohexane extremely interesting.

Despite the enormous versatility of nitrocyclohexane hydrogenation, a thorough literature investigation showed only limited data related tothis process, and most of these research were focused on the batch conditions at elevated pressure and temperature [175,188–193]. Nevertheless, these studies can serve as a guide for further experiments carried out in flow reactors.

First attempt to use nitrocyclohexane hydrogenation to obtain value-added products in the heterogeneous process was performed by Grundmann et al. at the beginning of 1950s [175]. These results proved that, depending on the used catalyst, it is possible to synthesise various useful chemical compounds. All of the experiments were conducted in 250 cm^3 shaking autoclave with 15 g of the catalyst and 50 cm^3 of nitrocyclohexane dissolved in methanol. This reaction solvent was determined in the independent tests. Well known and commercially available hydrogenation catalysts, like Raney-Ni, transformed NC into cyclohexylamine at 313 K and 30 bar. Similar selectivity was observed for Cu containing catalysts in reactions performed at a significantly higher temperature and pressure, 413 K and 100 bar.

Transition to the multi-component systems changed selectivity to cyclohexanone oxime, 26% in the case of Cu-Zn-Mn-Cr-O catalyst [175]. However, harsh conditions were the main drawback for these materials. In order to achieve higher selectivity to cyclohexanone oxime, the researchers moved to the silver-containing catalysts. The usage of complex Ag-Zn-Cr-O material produced cyclohexanone oxime with 64% selectivity at 368 K and 50 bar. Additionally, in these studies, Grundman et al. [175] also analysed the influence of the support, which was recognised as insignificant for catalysts selectivity. In the light of recent studies, the used conditions were relatively high, and some of the observations do not correspond to the current knowledge. Nevertheless, these results were very important foundation for research on this topic.

Du Pont performed a further investigation on nitrocyclohexane hydrogenation with Pd catalyst at the beginning of 1960s [194,195]. The experiments conducted under 35 bar and 413 K with palladium supported on acetylene-black gave selectivity mainly to cyclohexylamine (63%). The other products were cyclohexanone oxime (24%) and cyclohexanone (13%). The introduction of lead to the reaction system completely changed proportions between products. Interestingly, different results were induced by the mere presence of Pb, irrespectively to the method of introduction. For instance, the hydrogenation catalyst may be treated with elemental lead, a catalyst may be supported on a lead-containing material, or the reaction medium may be enriched with the lead compound. Even the reactor lined with lead gave different selectivity than pure Pd catalyst, the best results, in terms of selectivity to cyclohexanone oxime, were obtained in the presence of lead oxide at 35 bar and 433 K – 80 % selectivity. All of these results were quite promising and hence were patented by Du Pont [194,195]. It should be noted here that the requirement to use Pb-containing compounds entails enormous environmental costs. This could be a possible reason why this process was not implemented on an industrial scale.

More recent studies on the nitrocyclohexane hydrogenation have changed the strategy of designing catalysts and usually used milder reaction conditions. Serna et al. [188] tested various catalytic materials in the experiments performed in ethanol, and in the temperature and pressure range of 373 - 413 K and 4 - 15 bar. Typical hydrogenation catalyst – 5 wt.% Pd/C was used as a reference sample. Only 15 mg of it converted NC into cyclohexylamine with 85% selectivity (97% conversion) in the process conducted for 195 min under 15 bar and 413 K. However, the main goal of this research was to investigate the catalytic properties of catalysts with low Pt loading [188]. For instance, under the same reaction conditions, 100 mg of 0.2 wt.% Pt/C produced mainly cyclohexylamine (70%, conversion – 85%). On the other hand, Pt nanoparticles supported on the TiO_2 contributed to the formation of different products, with emphasis on dicyclohexylamine (41%, conversion – 97%). Additional modification of this catalyst by high-temperature treatment in H_2 flow (723 K, 50 ml/min) resulted in the formation of TiO_2 decorates on the platinum surface. It was followed by addition of Na – the inhibitor of the hydrolysis of the intermediates. These operations gave the active catalyst (95% conversion), which steered the reaction into the creation of cyclohexanone oxime – 85% selectivity in the process conducted for 880 minutes under 4 bar and 383 K. All of these results indicated the need to reduce hydrogenolysis properties of the metal nanoparticles to obtain products of partial hydrogenation of nitrocyclohexane.

Serna et al. [188] found Au/Al_2O_3 catalyst to be inactive in this process, which was verified by Shimizu et al. In their research [189], they were focused on the Au clusters supported on various metal oxides (Al_2O_3, SiO_2, MgO and TiO_2) [189]. Surprisingly, such catalysts turned out to be active and selective in nitrocyclohexane hydrogenation in the experiments performed at 373 K and 6 bar with ethanol as a solvent. For instance, 1.5 wt.% Au/TiO_2 was selective to cyclohexylamine, cyclohexanone and cyclohexyl-cyclohexylidene at the beginning of the process conducted for 12 h (unfortunately specific

values were not provided). However, with prolonged reaction time, these products decomposed to undetectable compounds. On the other hand, 1 wt.% Au/Al_2O_3 gave selectivity to cyclohexanone oxime (83%) and cyclohexanone (7%) at 100% conversion. Moreover, in other studies, the researchers discovered various correlations between morphology and catalytic parameters, like the influence of the average particles size. Independently from the support material, smaller Au nanoparticles gave higher conversion. For example, in the case of previously mentioned 1 wt.% Au/Al_2O_3, increasing the size of nanoparticles from 2 nm to 6 nm resulted in a significant drop in conversion (from 100% to 4.5%) and changed selectivity to cyclohexanone oxime (from 83% to 0%) in the processes conducted for 6 h at 373 K. Beside the influence of the particles size, the properties of the support materials also have a huge impact on catalytic behaviour of gold. Basic metal oxides (MgO), but also the one with more acidic character (SiO_2) gave worse results than the amphoteric Al_2O_3. Acid-base pair sites seems to be crucial for this reaction. Based on these observations, Shimizu et al. [189] proposed cooperative mechanism, in which dissociative adsorption of H_2 at the gold-support interface produces $H^{\delta-}$ on the low coordinated Au and $H^{\delta+}$ on the support. Both groups are transferred to the polar nitro group, which is preferably adsorbed on $Al^{\delta+}$– $O^{\delta-}$ site [189]. This phenomenon could be the explanation of higher activity of the gold nanoparticles supported on Al_2O_3. Hence, the impact of a rection pressure and the temperature was investigated for the best catalyst – 1 wt.% Au/Al_2O_3 with 2.5 nm nanoparticles. Its activity increased with the pressure incrementation up to 6 bar, to achieve 100% conversion and 83% selectivity to cyclohexanone oxime. Above this pressure, the selectivity to oxime decreased and the formation of cyclohexanone was observed up to maximum at 11 bar. After exceeding this value, cyclohexyl-cyclohexylidene amine and dicyclohexylamine appeared among reaction products. The same compounds were observed for the temperatures above 373 K. In this temperature catalyst achieved its maximum activity and selectivity to cyclohexanone oxime (83%) and

cyclohexanone (7%). Serna et al. [188] proved, that the combination of specific morphology parameters and reaction conditions makes gold catalysts active and selective in nitrocyclohexanone hydrogenation.

The group of professor Liu from Xiangtan University came back to Pd catalysts, and thoroughly investigated the catalytic performance of palladium nanoparticles supported on various carbon materials [190,191,196,197]. In general, all of these catalysts showed high activity and selectivity to cyclohexanone oxime in the processes performed in the temperature and pressure range of 313 – 353 K and 2 – 3 bar, respectively. Unlike the other studies, ethylenediamine was chosen as the reaction solvent. The researchers established the optimal temperature for this process – 323 K, but also the minimal time required to achieve satisfactory conversion – 85 % after 2 h. The initial experiments were performed with palladium nanoparticles supported on microporous activated carbon and carbon nanotubes, marked respectively as 5 wt.% Pd/C, 5 wt.% Pd/CNTs [190]. These tests, conducted in optimal temperature and under 2 bar, showed the superiority of the Pd/CNTs in terms of selectivity to cyclohexanone oxime - 85.9 % after 6 h, in comparison to 55.1 % obtained after 3 h by Pd/C. Pd/CNTs domination was explained by smaller Pd nanoparticles size and the positive influence of CNTs support [190].

Despite the satisfying results, Liu et al. [196] decided to investigate more carbon derivative materials. Hence, a series of Pd catalysts (5 wt.%) supported on activated carbons made from lignin, coal and coconut shell (LAC, CAC and CSAC), but also on carbon nanotubes: single-wall, double-wall and multi-wall (SWCNTs, DWCNTs, MWCNTs) were synthesised [196]. Due to previously performed experiments [190] it was not very surprising that all of these catalysts were active in the nitrocyclohexane hydrogenation conducted in batch mode under 3 bar and 323 K. However, the usage of carbon materials with different properties allowed to establish, that the structure of the support is crucial to catalyst selectivity. The reactants sizes are comparable with the micropores

dimension. Hence, the microporous structure is unfavourable for its adsorption and diffusion [196]. The comparison between materials with the lowest and highest pore size, Pd/CAC – 0.95 nm and Pd/SWCNTs – 2.73 nm, showed similar conversion for both catalysts ~ 100%. However, Pd/CAC gave 55 % selectivity to cyclohexanone oxime, and PD/SWCNTs – 94.6 %.

In overall, the carbon nanotubes revealed better catalytic performance, but there were also differences among them. Various structure of CNTs affected the reduction state of palladium. The Pd^+ content increased in the following order: Pd/DWCNTs → Pd/MWCNTs → Pd/SWCNTs. Simultaneously, the selectivity to cyclohexanone oxime also increased for these materials in the same order 83.5% → 87.9% → 94.6%. Therefore, it could be concluded that Pd^+ favours the formation of cyclohexanone oxime.

The studies performed in 2015 [197] aimed at the optimisation of the synthesis procedure to achieve higher Pd^+ content for Pd/SWCNTs catalysts. The researchers checked various preparation methods: wet impregnation in water, wet impregnation in methanol, ion exchange and chemical reduction, but also different pretreatment conditions. Among obtained catalysts, the ones gained by the wet impregnation in water showed the best catalytic performance. With the increasing reduction temperature of Pd precursor (523 K → 623 K → 723 K) the selectivity to cyclohexanone oxime also increased (85.9 % → 93.5 % → 96.4 %). It was related to the Pd^+ content which incremented, with the temperature of reduction, in the following order 33.0 % → 33.8 % → 38.7 %.

Unfortunately, the preparation of carbon nanotubes on a large scale is extremely complicated and expensive [191]. Hence, Yan et al. [191] attempted to achieve better results with palladium nanoparticles supported on mesoporous activated carbons. The researchers tested different materials synthesised by soft templating, hard templating and hydrothermal synthesis from various raw materials. The best results were obtained for Pd (5 wt.%) supported on mesoporous carbon obtained by hard template method from mesoporous silica [198]. In the case of this catalyst, the selectivity

to cyclohexanone oxime was equal to 82.8 % in the experiments performed for 6 h at 323 K and 3 bar. However, its catalytic performance was affected by small surface area and pore volume, and hence the final conversion was only 71.4 %. Nevertheless, due to the cost of activated carbons, it can be an interesting alternative for carbon nanotubes.

In the end, all of the results obtained by the group of professor Liu led to the conclusion that smaller Pd nanoparticles with higher dispersion and greater Pd^{+} content (which are supported on carbon materials with adequate pore size) favour the formation of cyclohexanone oxime with high activity [190,191,196,197].

Despite the attempt performed by Liao et al. [190] with the Ni catalyst, hydrogenation of nitrocyclohexane were performed with noble metals. It did not change until 2017, in which Zhang et al. [192] tested with success low-cost transition metals. Among them were Cu, Ni, Fe and Co supported on silica dioxide with target metal loading – 15 wt.%. All of the experiments were performed for 3 h at 373 K and under 10 bar in ethylenediamine. Dependent on the used metal nanoparticles, the catalysts were selective to different reaction products: Co – cyclohexanone (88%) and cyclohexanone oxime (12%), Fe - cyclohexanone (75%) and cyclohexanone oxime (25%), Ni – cyclohexanone oxime (59%), cyclohexanone (21%) and cyclohexylamine (20%), Cu – cyclohexanone oxime (92%), cyclohexanone (5%) and cyclohexylamine (3%). Because Zhang et al. [192] were focused on the selectivity to cyclohexanone oxime, the copper catalyst was selected for further studies. Modification of various factors, such as support material, synthesis method and metal loading led to catalyst with 92% selectivity to cyclohexanone oxime in combination with 74% conversion. The process of characterisation of these catalysts revealed the coexistence of metallic Cu and Cu_2O. The ratio between these two species seems to be crucial for catalytic performance. Zhang et al. [192] postulated that Cu^0 species dissociate H_2 and Cu^{2+} sites function as electrophilic sites to polarise nitro group.

Additionally, the researchers also discovered that with the increase of the pressure from 10 to 40 bar, the time needed to obtain the same conversion shortened proportionally from 4 to 1 h, which can be crucial for designing process on the industrial scale.

In general, apart from the used catalyst, the combination of time, temperature and pressure is crucial to the catalytic performance in the hydrogenation of nitrocyclohexane in batch reactors. In order to obtain products of partial hydrogenation, the reaction has to be conducted at lower temperature and pressure. Higher values favour the formation of cyclohexanone, cyclohexanol, cyclohexylamine and dicyclohexylamine. A similar situation is observed for the reaction time, which also affects the selectivity of the catalysts. Prolonged time supports further hydrogenation and even the decomposition of the products into undetectable compounds. For the above reasons, easy control of the reaction conditions provided by flow reactors appears to be very attractive.

Nevertheless, all of the articles mentioned above were focused on the catalytic hydrogenation of nitrocyclohexane in batch conditions. Thorough literature investigation revealed only one paper related to the usage of gas flow conditions in this reaction. Inspired by the studies performed by Serna et al. [188], Wang and coworkers [199] proved that gold catalysts could be as active in flow as in batch conditions. Series of Au catalysts were prepared by the deposition-precipitation method with various metal oxides: 0.8 wt.% Au/ZrO_2, 1.2 wt.% Au/TiO_2, 1.1 wt.% Au/Al_2O_3 and 3.0 wt.% Au/CeO_2. Different support materials affected nanoparticles size and their distribution, a decrease in the mean values was observed in the following order: Au/ZrO_2 (7.0 nm) → Au/TiO_2(4.7 nm) → Au/Al_2O_3 (4.3 nm) → Au/CeO_2 (3 nm). Similar to the previous studies [188], Wang et al. [199] observed a strong correlation between Au nanoparticles size and the overall activity of the catalyst, smaller particles are better in the activation of H_2

which is a crucial step in the hydrogenation of nitrocyclohexane. These properties were reflected in the catalytic performance. In the experiments performed at 353 K each one of these catalysts was selective to different products: Au/ZrO_2 – cyclohexanone (54%), cyclohexylamine (28%) and cyclohexanone oxime (18%), Au/CeO_2 – cyclohexanone (98%), cyclohexylamine (2%), Au/TiO_2 – cyclohexanone (40%), cyclohexylamine (34%), dicyclohexylamine (20%) and cyclohexanone oxime (6%), Au/Al_2O_3 - cyclohexanone oxime (80%), cyclohexylamine (18%) and cyclohexanone (2%). In general, selectivity to cyclohexanone oxime is sensitive to surface hydrogen. The formation of cyclohexanone and cyclohexylamine are favoured at low and high coverage, respectively.

Based on the presented results, seemingly simple catalytic hydrogenation of nitrocyclohexane can be very challenging due to the enormous amount of crucial factors. However, the possibility to obtain numerous valuable compounds from the same substrate seems to be an exciting topic for further research. Hence, more advanced studies on the influence of metal active phase, support materials and reaction conditions should be carried out in the future. Noteworthy is the lack of reactions carried out in flow reactors in the liquid phase. These reactors were used with success with the hydrogenation of other nitro compounds [200–204]. Hence, the hydrogenation of nitrocyclohexane in liquid flow conditions should be a priority for further research on this topic.

3. Aim of the studies

Catalytic hydrogenation is one of the most essential processes for modern civilization. It is used in multiple manufacturing processes but also as a solution for many environmental problems. The majority of hydrogenation reactions proved to be sensitive to various factors, for example, the catalyst structure and reaction conditions. In order to develop more and more effective catalysts, it is extremely important to conduct further and more detailed research on parameters crucial for catalytic hydrogenation processes. Even changing the way of conducting the reaction could be critical for the final effects. For example, switch from batch to flow operation conditions is one of the most frequently mentioned priorities for sustainable development.

Hence, the aim of this work was to:

- develop the application procedure of the flow conditions into catalytic hydrodechlorination of trichloroethylene and diclofenac in the aqueous phase,
- investigate and determine general relations between catalyst activity and its structure (average nanoparticle size and particle size distribution, type of support materials, structure ordering of the support material, etc.),
- develop efficient catalysts for batch and flow water purification from one of the most frequently detected chloroorganic contaminants: trichloroethylene and diclofenac,
- introduce liquid flow operation mode into nitrocyclohexane hydrogenation process,
- develop an effective catalyst based on low-cost transition metals for catalytic hydrogenation of nitrocyclohexane and determine the direction for further own research in this field.

4. Experimental

Catalysts tested in this research were partially synthesised at IPC PAS, and partially obtained within the cooperation with Warsaw University of Technology, Sorbonne Université in Paris, and Centre for Research and Education of Unipetrol in Litvinov.

Unless explicitly stated, it should be assumed that a mentioned catalyst was synthesised at IPC PAS, mainly by incipient wetness impregnation (description of the general procedure for this method is in **Chapter 4.1.1.**). In the case of the catalysts synthesised by other research units, descriptions of the syntheses are placed in adequate paragraphs.

4.1. Catalyst synthesis

All of the catalysts synthesised at IPC PAS by incipient wetness impregnation are marked in this chapter in accordance with the below pattern:

X wt.% M(P)/Support

, where:

X % - weight percentage of metal active phase,

M – metal active phase (e.g. Ni, Pd),

P – metal precursor (e.g. N – metal nitrate, Cl – metal chloride),

Support – support material (e.g. C – activated carbon, SiO_2 – silica dioxide, Al_2O_3 – aluminium oxide).

However, in the Results and Discussion section, the abbreviated names of the catalysts are used to keep the text's clarity. All of the shortened names emphasize the differences between the tested materials, while shortening the common structural elements. The lists of full and abbreviated names can be found in the subsections concerning the synthesis of an adequate catalyst.

4.1.1. Incipient wetness impregnation

Incipient wetness impregnation was chosen as a primary synthesis method due to high repeatability and easy control over the treatment parameters. This was particularly important due to the fact that applied conditions could affect the metal-support catalysts final morphology.

Preparation procedure started from dissolving of the appropriate metal salt in distilled water. Metal precursor amount was calculated by target metal loading, and the volume of the solution was equal to the pore volume of chosen support material (with 10 % excess).

Example results of the calculations for the Ni catalyst are provided below:

Information:

Support material: activated carbon, V_{pore} = 1.00 cm^3/g

Metal precursor: $Ni(NO_3)_2 * 6\ H_2O$ (M_{salt} – 290.8 g/mol)

Target metal loading: 2 wt.%

Results of the calculations

Mass of the support material – 0.98 g

Mass of the metal active phase – 0.02 g

Mass of the metal precursor – 0.0991 g

Volume of precursor solution – 0.98 cm^3

Obtained catalyst: **2 wt.% Ni(N)/C**

The metal precursor solution in distilled water was added to the previously prepared support material and vigorously stirred for a few minutes. In the next step, the catalyst precursor was placed in the rotary beaker device (equipped with the source of infrared light), which provides constant proper mixing and preliminary drying for the next 24 h (**Figure 4**).

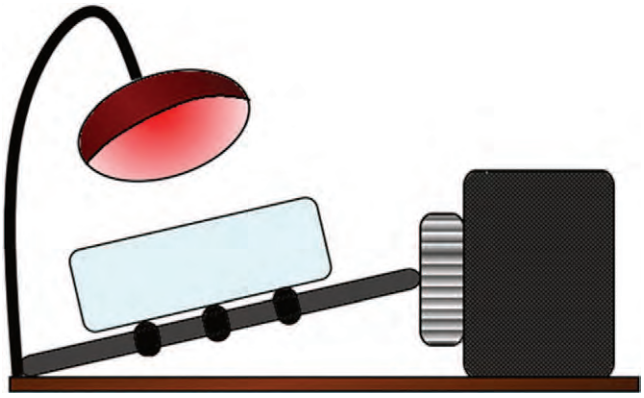

Figure 4. Rotary beaker for catalysts synthesis.

Afterwards, depending on the used support material and target catalyst morphology, the obtained material was calcined in air flow and/or reduced in the stream of 10 % H_2/Ar at elevated temperature (determined by temperature-programmed reduction (**Chapter 4.3**)).

4.1.2. Synthesis of the carbon-supported catalysts

Preparation of the carbon support materials

All of the works related to the preparation of the carbon materials were performed by the group of Professor Wioletta Raróg-Pilecka from Warsaw University of Technology. All of these materials were an essential part of the presented research.

The application of various modification methods of the parent carbon material (CNR115, Norit B.V. Company) allowed for obtaining carbon materials with different properties, discussed in details in **Chapter 5.1.1**.

Commercially available active carbon with an amorphous structure (Norit CNR115) was used as a starting material for the synthesis of various carbon supports. The modification of CNR115 was performed by a two-step procedure. In the first step, carbon material was heated in Ar flow at 2173 K for 2 h, which resulted in the formation of the turbostratic structure. However, simultaneously significantly decreased specific surface area and

removed porosity of the material. Hence, in the next step, this material was treated in the H_2O/Ar stream at 1129 K, which resulted in the mass loss and recreation of the porosity. The obtained carbon materials are enlisted in **Table 1**. They are marked in accordance to the pattern CNRI15/X/Y, where X – the temperature of treatment in Ar stream (2173 K), Y – percent mass loss after treatment in the stream of H_2O/Ar at 1129 K.

Table 1. Obtained carbon materials.

Carbon material
CNRI15
CNRI15/2173
CNRI15/2173/0.62
CNRI15/2173/26.54

Synthesis of the carbon-supported catalysts

Syntheses of the carbon-supported materials were performed by incipient wetness impregnation with various carbon materials (**Table 1**). The obtained catalysts are presented below (with specified treatment procedure) (**Table 2**).

Materials used for the syntheses: Chempur analytical grade $Ni(NO_3)_2$*$6H_2O$, Chempur analytical grade $NiCl_2$*$6H_2O$, Sigma-Aldrich ≥ 99.9 % $PdCl_2$.

Table 2. Catalysts synthesised by incipient wetness impregnation at IPC PAS.

Catalyst
Reduction: *heat up to 1173 K in 10 % H_2/Ar (temperature ramp – 10 K/min)*
2 wt.% Ni(N)/CNRI15/2173/26.54-H – Ni(N)/C-H
2 wt.% Ni(Cl)/CNRI15/2173/26.54-H – Ni(Cl)/C-H

Reduction: *3 h at 673 K in 10 % H_2/Ar (temperature ramp – 10 K/min)*
2 wt.% Ni(Cl)/CNR115/2173/26.54-M – Ni(Cl)/C-L
2 wt.% Ni(N)/CNR115/2173/26.54-M – Ni(Cl)/C-L
2 wt.% Ni(Cl)/CNR115 – Ni/CNR1115
2 wt.% Ni(Cl)/CNR115/2173 – Ni/CNR115/2173
2 wt.% Ni(Cl)/CNR115/2173/0.62 – Ni/CNR115/2173/0.62
2 wt.% Ni(Cl)/CNR115/2173/26.54 – Ni/CNR115/2173/26.54
Reduction: *2 h at 673 K in 10 % H_2/Ar (temperature ramp – 10 K/min*)
1.57 wt.% Pd(Cl)/CNR115/2173/26.54 – Pd/C

4.1.3 Synthesis of Pd-loaded BEA zeolites

Synthesis of Pd-loaded BEA zeolite materials were performed at Sorbonne Université in Paris in the group of Professor Stanisław Dźwigaj. Detailed description could be found in the publication by Kamińska et al. [205].

A commercially available zeolite material – TEABEA (Si/Al = 3, RIPP China) was divided into two portions. The first one was dealuminated with 13 mol/l solution of HNO_3 for 4 h at 343 K (Si/Al = 1300). This material was marked as SiBEA. The second portion was firstly calcined in air at 823 K for 15 h under static conditions, and then twice treated with 0.1 mol/l NH_3NO_3 (400 ml) at 343 K for 3 h. After filtration and washing procedure, it was dried at 363 K and calcined at 773 K for 3 h to remove NH_3. The obtained material was marked as HAlBEA.

Pd-loaded zeolites were prepared by impregnation of zeolites by the aqueous solution of $PdCl_2$ (Sigma-Aldrich ≥ 99 %) under ambient conditions. Obtained catalysts precursors were calcined in the air flow at 773 K for 3 h and reduced at 873 K in the stream of 10 % H_2/Ar for 3 h.

Synthesised catalysts are collected below:

- 1 wt.% Pd(Cl)@SiBEA – Pd@SiBEA
- 1 wt.% Pd(Cl)@HAlBEA – Pd@HAlBEA

4.1.4. Synthesis of the alumina-supported materials

A commercially available chlorine-free γ-alumina (Puralox SCCa series, Sasol) was used as a support material in the synthesis of Pd supported catalyst. The alumina-supported catalyst was prepared by incipient wetness impregnation with the aqueous solution of $Pd(NO_3)_2 * 2 H_2O$ (Sigma-Aldrich analytical grade). The precursor of the catalyst was calcined in the stream of air at 773 K for 3 h and then reduced in the flow of 10 % H_2/Ar for 3 h at 673 K.

Obtained catalyst:

- 1 wt.% Pd(N)/γ-Al_2O_3 – Pd/Al_2O_3

4.1.5. Synthesis of the silica-supported materials

A series of Pd/SiO_2 catalysts was synthesised in cooperation with doctor Magdalena Bonarowska from IPC PAS. Commercially available Davison 62 SiO_2 (75 - 210 mesh), which was pre-calcined in the stream of air at 723 K for 4 h, was used as a support material. The use of various synthesis methods and the modification of pretreatment conditions allowed for obtaining catalysts with different morphology (various particle size and distribution). The obtained catalysts are collected in **Table 3**, with specified synthesis procedure and pretreatment conditions.

Table 3. Silica supported Pd catalysts synthesised in IPC PAS.

Catalyst / Synthesis method and pretreatment conditions
1.1 wt.% Pd/SiO_2 – Pd/SiO_2(s)
Synthesis: Ion-exchange of the hydroxyl group of silica for $[Pd(NH_3)_4](NO_3)_2$
Calcination: 723 K for 3 h in air stream (temperature ramp – 2 K/min)
Reduction: 673 K in 10 % H_2/Ar stream for 3 h
2.0 wt.% Pd/SiO_2 – Pd/SiO_2(bg)
Synthesis: Incipient wetness impregnation with the aqueous solution of $(CH_3COO)_2Pd$.
Calcination: 723 K for 3 h in air stream (temperature ramp – 2 K/min)
Reduction: 673 K in 10 % H_2/Ar stream for 3 h
2.0 wt.% Pd/SiO_2 – Pd/SiO_2(bim)
Synthesis: Incipient wetness impregnation with the aqueous solution of $PdCl_2$.
Calcination: 723 K for 3 h in air stream (temperature ramp – 2 K/min)
Reduction: 673 K in 10 % H_2/Ar stream for 3 h

4.1.6. Synthesis of the Pd grafted on the polymeric resin

Metal nanoparticles supported on a polymeric resin was prepared by the grafting method. A commercially available polyethylene glycol-based polymer terminated with a primary amine group was used as catalyst matrix – Tentagel-S-NH_2 (Rapp Polymere GmbH).

The catalyst synthesis involves a two-step procedure performed in one pot. In the first step, Pd nanoparticles were formed in ethanol solution from Pd (II) acetylacetonate (Sigma-Aldrich 99 %) by chemical reduction with $NaBH_4$, in the presence of an excess of trioctylphosphine (TOPO, capping

agent). The reducing agent added dropwise to the constantly stirred solution caused a colour change (from orange to black), which indicated the formation of Pd nanoparticles.

In the next step, metal nanoparticles were immobilised on the polymeric matrix. The polymeric resin was added to the nanoparticles containing solution and stirred for 36 h (1000 rpm) under Ar atmosphere, at room temperature. Then, the obtained material was washed several times with ethanol, filtered and dried for 3 h at 373 K.

The obtained catalyst was marked as:
2.2 wt.% Pd(acc)/$TSNH_2$ – $PdTSNH_2$

4.1.7. Synthesis of the CuZnAl hydrotalcite based materials

Synthesis of the hydrotalcite based CuZnAl materials were performed at the Centre for Research and Education of Unipertrol.

Parent CuZnAl hydrotalcite materials, with different metal composition, were synthesised by co-precipitation method in a glass reactor, equipped with a shaft stirrer, a pH meter, a thermocouple and two piston pumps. The solution of metal nitrates in distilled water (1 mol/l) was inserted simultaneously into the reactor with alkali solution (K_2CO_3 and KOH in distilled water), pH stabilised at 9.5. The co-precipitation process was carried out at 333 K with intensive stirring. Hydrotalcites were aged for one hour after the precipitation process and then separated from the reaction mixture and washed with distilled water.

Before further measurements, the hydrotalcites were calcined at 773 K, which resulted in the formation of mixed oxides materials. The reduction procedure was performed at 673 K for 3 h in the stream of 10 % H_2/Ar.

The obtained catalysts are collected below:

- CuZnAl(0.5-1-1)
- CuZnAl(1-1-1)

The numbers in parentheses indicate molar ratio between elements.

4.2. Glass gas flow system for temperature treatment of catalysts precursors

The majority of the tested materials required temperature treatment before characterization measurements and catalytic tests (drying, calcination, activation). All of these operations were performed on a specially designed at IPC PAS gas-flow system. The glass installation provides an inert environment for the catalysts treatment processes, ensuring adequate conditions for catalysts modification. This system, presented in **Figure 5**, consists of: independent gas lines (H_2, Ar, 10 % H_2/Ar and O_2) controlled with mass-flow controllers and equipped with impurities traps, quartz reactor with quartz frit, furnace with temperature controller, thermal-conductivity detector (TCD) and computer for data collection.

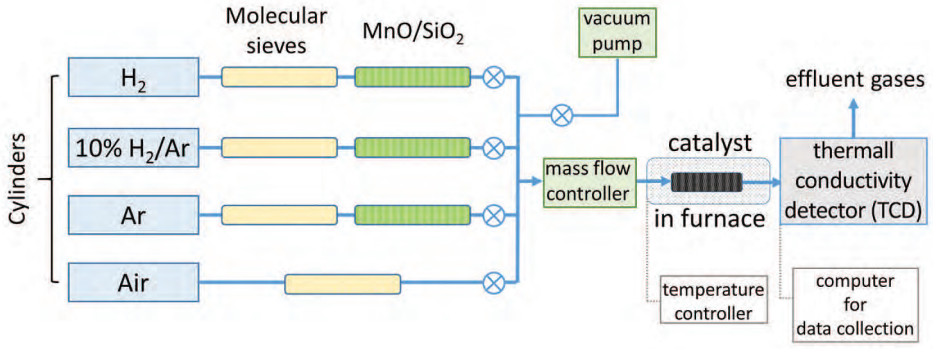

Figure 5. Glass gas-flow system designed for catalysts treatment.

4.3 Characterisation techniques

Analysis of the surface parameters

Analysis of the specific surface area and porosity of the catalytic materials was performed with ASAP 2020 from Micromeritics. Catalysts parameters were determined by BET(Brunauer-Emmet-Teller), t-plot, BJH (Barret-Joyner-Halenda) and HK (Horwath-Kawazoe) methods with a nitrogen molecule as an adsorbate. Before measurements, each sample was evacuated at elevated temperature (adjusted for a specific sample) to clean its surface. Adsorption isotherms were determined at 77 K.

Thermogravimetric analysis

Thermogravimetric analyses (TGA) were performed in TGA Discovery series (TA Instrument) equipped with mass spectrometer (Pfeifer Vacuum). In each case, approximately 15 mg of the sample was placed in the open alumina crucible and heated from 313 K to 1173 K (ramp 10 K/min) in the flow of nitrogen (20 ml/min).

Temperature-programmed reduction

Experiments of the temperature-programmed reduction (TPR) were performed in the glass gas-flow system (described in **Chapter 4.2.**) or with analogous glass gas-flow system equipped with mass spectrometer (Amatek Dymaxion Dycor with quadrupole detector). A sample of the catalytic material was placed in the quartz reactor, which could be heated up to 1200 K with a selected temperature increase (typically 10 K/min). All of the measurements were performed in the stream of 10 % H_2/Ar.

Chemisorption

Chemisorption measurements were performed by the conventional static method with ASAP 2020 from Micromeritics. Samples of the catalytic materials were first reduced in the glass gas-flow system described in **Chapter 4.2**. Then, the reduction procedure was repeated in ASAP 2020 just before

measurement. Reductions conditions were determined by temperature-programmed reduction. The probe molecule (H_2, CO, CO_2) and its stoichiometry was chosen depending on the tested catalyst.

H_2 temperature-programmed desorption (H_2-TPD)

H_2 temperature-programmed desorption measurements were performed in glass gas-flow system described in **Chapter 4.2**. Freshly reduced catalysts were cooled down to 313 K and then saturated in 10 % H_2/He mixture for 1 h. This step was followed by purging with Ar for 30 min to remove any physically adsorbed hydrogen molecules. H_2-TPD experiments were performed by heating to 673 K under Ar flow at temperature ramp rate – 20 K/min.

NH_3 and CO_2 temperature-programmed desorption (NH_3-TPD and CO_2-TPD)

NH_3 and CO_2 temperature-programmed desorption were performed in quartz tube reactor connected to a quadrupole mass spectrometer (HPR 60, Hiden). Before each measurement, the pre-reduced catalyst (50 mg) was treated with helium at 773 K for 1 h to remove adsorbed impurities. In the next step, the sample was subjected to 50 ml/min flow of 5 % CO_2-He or 5 % NH_3-He mixture for 30 min, and then purged with He for 30 min to remove all physically adsorbed molecules. TPD experiments were performed up to 773 K with 10 K/min temperature ramp in 50 ml/min He. NH_3 and CO_2 peaks were quantitively calibrated by injecting NH_3 and CO_2 pulses.

X-ray Diffraction (XRD)

Powder XRD measurements were performed employing Bragg-Brentano configuration. The XRD profiles were recorded with PANalytical Empyrean diffraction platform, powered at 40 kV x 40 mA, equipped with a vertical goniometer, with theta-theta geometry using Ni filtered Cu Kα radiation. Powder samples were used for measurement. The diffraction intensities were collected in the range 2θ = 5 - 95°, with 0.008° step (counting time 6 s per step).

X-ray Photoelectron Spectroscopy (XPS)

XPS measurements for specific samples were performed on one of the following devices:

- 1.57 wt.%. Pd(Cl)/CNRI15/1900/26.54 – VG Scientific photoelectron spectrometer ESCALAB-210 with X-ray source operating at the voltage of 14.5 kV and the current of 25 mA (Al Kα radiation –1486.6 eV). The survey spectra were recorded in range 0 – 1350 eV (with 0.4 eV step); high resolution spectra with 0.1 eV step, 100 ms dwell time and 25 eV pass energy. Fitting of the curves was performed with ADVANTAGE software (Thermo Electron), the background was fitted by using the nonlinear Shirley model. Measured transmission function and Scofield sensitivity factors were used for quantification.
- $PdTSNH_2$ – PHI 5000 VersaProbe (ULVAC-PHI) with X-ray source operating at voltage of 15 kV, 25 W and 100 μm spot size (Al Kα radiation – 1486.6 eV).
- CuZnAl – PHI 5000 VersaProbe (ULVAC-PHI) with X-ray source operating at the voltage of 15 kV, 25 W and 10 μm spot size (Al Kα radiation – 1486.6 eV). HR XPS spectra were recorded with the hemispherical analyser with 0.1 eV step at pass energy of 23.5. Evaluation of the XPS data was performed by CasaXPS. Shirley background and Gaussian peak shape with 30 % Lorentzian character was used for deconvolution of HR XPS spectra. XPS experiments for CuZnAl catalysts were performed twice – precisely for the same spot of the sample, before and after *in situ* reduction at 673 K for 30 minutes in the flow of H_2.

X-ray Absorption Spectroscopy (XAS)

Absorption spectra for selected samples were performed on in-air X-ray absorption spectroscopy setup (XAS) arranged in von Hamos geometry (**Figure 6**). An X-ray source, XOS X-Beam Superflux PF X-ray tube, is equipped

with focusing optics and operates at the voltage of 40 kV and the current of 0.9 mA.

The generated polychromatic X-ray beam, with 3° divergence, was diffracted by Si(440) crystal (cylindrically bent with 25 cm radius) at Bragg angle of 50.8° and registered by Andor Newton camera sealed with 250 μm-thick Be window. The catalyst sample was positioned in the beam focal spot with a nominal size of 100 μm.

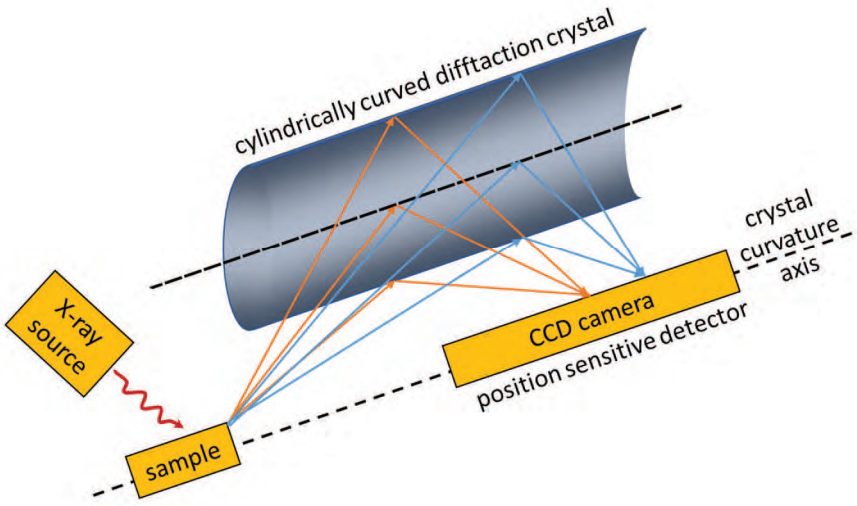

Figure 6. Illustration of von Hamos geometry.

Transmission-electron microscopy (TEM)

TEM measurements were performed on the Titan G2 60-300 kV (FEI, Japan) equipped with field emission gun (FEG), monochromator, the objective lens system, a three condenser lens system, image correction (Cs-corrector), an EDS spectrometer with Si(Li) detector and a HAADF detector. Measurements were performed at accelerating voltage equal to 300 kV. The catalysts samples were dispersed in pure alcohol by an ultrasonic cleaner, and then a drop of the suspension was placed on carbon films on copper grids.

All of the measurements were performed by Grzegorz Słowik at Maria Skłodowska Uniwersity in Lublin or by Krzysztof Matus at Silesian University of Technology in Gliwice.

4.3 Catalytic experiments:

4.3.1 Catalytic hydrogenation in the batch reactor

Sorption experiments and catalytic tests were performed in a batch reactor equipped with a magnetic stirring bar, a pH meter and a temperature controller (**Figure 7**). Processes in batch operation mode were performed under atmospheric pressure at 303 K. In the first step of the process, 350 ml of Millipore water was saturated with hydrogen for 30 minutes, and then chloroorganic compound was added to the reaction mixture (TCE – trichloroethylene or DCF – diclofenac). After the time needed to obtain homogeneity (30 minutes) – a reference sample was taken. The catalytic reaction started with the introduction of the catalyst (typically 0.1 g). The samples were collected at 2, 5, 10, 15, 20, 40, 60, 90, 120 and 150 min of the process.

Figure 7. Batch reactor used for sorption experiments and catalytic hydrodechlorination of chloroorganic contaminants in water.

4.3.2. Catalytic hydrogenation in the continuous flow reactor

Continuous flow catalytic hydrogenation processes were conducted in commercially available microreactor HCube Pro™ (**Figure 8**), which provides the possibility to change reaction conditions in the range 1 – 100 bar, and 283 – 423 K. In this system, hydrogen is generated *in situ* via electrolysis of water with maximum efficiency – 60 ml/min. After the H_2 drying process, it is mixed with a reaction mixture before entering the catalyst bed. Selected catalyst is placed in CatCart stainless-steel tube closed with a set of filters. Prepared in advance reaction mixture flows through the catalyst with selected flow-rate (0.3 – 10 ml/min) provided by HPLC pump.

Depending on the performed catalytic process, the reaction mixture consists of:

- MiliPore Water + Diclofenac (Sigma Aldrich) or Trichloroethylene (Chempur) in the case of purification of water from chloroorganic compounds,

  or
- Ethanol (POCH, 99.8 %) + Nitrocyclohexane (TCI, >95%) in the case of nitrocyclohexane hydrogenation.

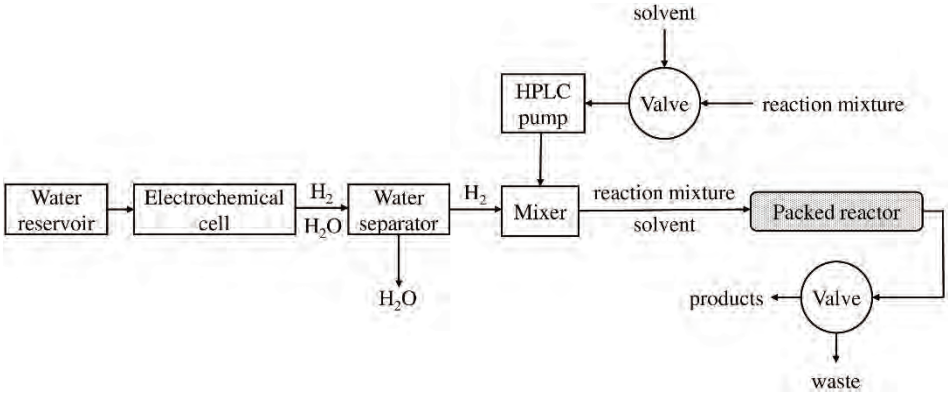

Figure 8. Scheme of the HCube Pro™ by Thales Nano.

4.3.4 Analysis of the reaction samples

Due to the different nature of the hydrogenated compounds and different chemical nature of taken samples, various and tailored analysis techniques were required.

Catalytic hydrodechlorination of trichloroethylene

Analysis of the water samples contaminated by trichloroethylene was performed by gas chromatograph (Bruker Scion 456) equipped with headspace analyser (SHS-40), BP-5 column (30 m x 0.25 mm x 0.25 μm) and Electron Capture Detector (ECD – with high sensitivity for chloroorganic compounds).

Catalytic hydrodechlorination of diclofenac

Analysis of the water samples was performed by Water Acquity UPLC system equipped with PDA eλ detector on a C18 column (120 Å; 2.1 x 50 mm). Isocratic method of analysis was used with a flow rate 0.3 ml/min of mobile phase (acetonitrile : 0. 1 % formic acid, 1 : 1) and detection at 254 and 270 nm.

Catalytic hydrogenation of nitrocyclohexane

Analysis of the samples from nitrocyclohexane hydrogenation was performed by gas chromatograph (Bruker Scion 456) equipped with an autosampler, BP1 column (60 m x 0.25 mm x 0.25 μm) and Flame Ionization Detector (FID).

5. Results and discussion

5.1. Catalytic hydrogenation for environmental protection

As shown in the Introduction, modern civilisation has to face growing water contamination by chloroorganic pollutants. Many techniques have been developed so far, but research groups from all over the world do not stop at searching for more effective ways of water purification [9,36,37]. Nevertheless, before the application of specific methods, several conditions have to be taken into account. However, the most crucial criterion is the lack of reaction products, which are equally or more dangerous to the living organisms than the original contamination. Catalytic hydrogenation of chloroorganic contaminants, usually named catalytic hydrodechlorination (HDC), fulfil this essential requirement.

Studies over the possibility of using catalytic HDC in the removal of chloroorganic contaminants from water have been conducted since the '90s [85]. However, most of them are focused on noble metal catalysts. There are only few articles related to the application of low-cost transition metals in this reaction [106,206–209], and even fewer studies use flow conditions in the water purification process [93,210,211]. Therefore, the presented in the below chapter results attempt to fill some gaps in the knowledge about catalytic hydrodechlorination, contributing to the design of more effective catalysts.

5.1.1 Adsorption tests of TCE on carbon materials in batch and flow mode

The catalyst support material's sorption properties may significantly influence catalytic performance, especially in the batch reactor with a limited contamination concentration. High sorption capacity may affect or even mask the metal nanoparticles' catalytic activity in specific situations. Consequently,

the catalyst's performance is a component of two factors: the presence of a metallic active phase and the adsorption affinity of the support for organic compounds, like TCE.

Various support materials show different sorption capacity toward water contaminants. Activated carbons definitely stand out among these materials in terms of specific surface area, porosity and efficiency in the purification process. Moreover, they proved to be stable under reaction conditions, and hence are common support material for hydrodechlorination catalysts, also in the case of the presented research.

For the purpose of the conducted research, carbon materials were prepared from the parent commercially available amorphous active carbon CNR115, which is produced from a renewable raw material source by Norit BV Company (detailed description in **Chapter 4.1.2**). Physisorption analysis and TEM performed at each stage of their biography demonstrated differences in the surface parameters and structure ordering between the obtained materials (**Table 4**, **Figure 9**). The amorphous structure of CNR115 is well visible in **Figure 9a**. On the other hand, parallel graphene layers in CNR115/2173 and CNR115/2173/26.54 can be distinguished in the structures presented in the **Figure 9b** and **9c**.

Table 4. Surface parameters of carbon materials obtained from CNR115.

Carbon	Specific surface area [$m^2 g^{-1}$]		Pore volume [$cm^3 g^{-1}$]	
	BET	micropores	micropores	mesopores
CNR115	1860	1640	0.9	0.2
CNR115/2173	1	-	-	0
CNR115/2173/0.62	820	710	0.4	0.1
CNR115/2173/26.54	1610	1440	0.8	0.2

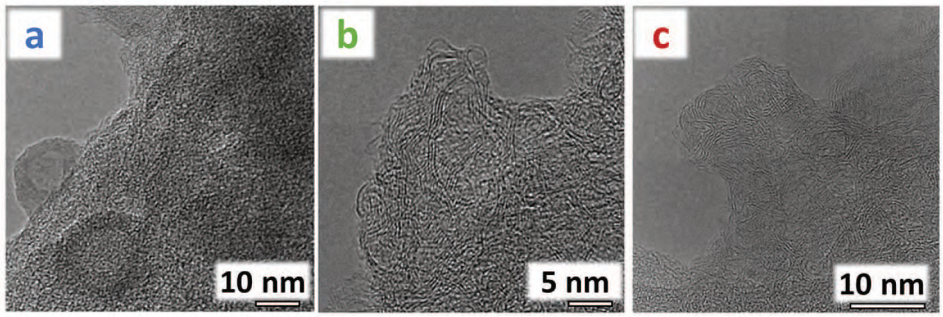

Figure 9.TEM images of a) CNR115, b)CNR115/2173 and c) CNR115/2173/26.54

In order to determine the sorption capacity of the selected support materials, a series of carbons was tested in TCE sorption experiments. According to the procedure used for further catalytic tests (**Chapter 4.3.1., Chapter 4.3.2.**), all of the measurements were performed in the reaction conditions (**Figure 10 and 11**).

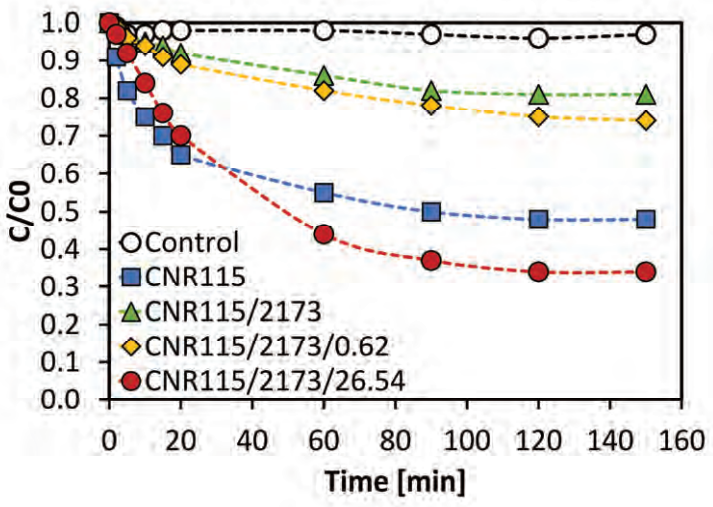

Figure 10. Evolution of TCE sorption with carbon materials in batch conditions: 303 K, 8 ppm TCE, 1 atm, 0.1 g of carbon material.

A control experiment showed that trichloroethylene did not decompose spontaneously under batch and flow reaction conditions (**Figure 10** and **11**). On the other hand, all of the carbon materials partially removed TCE from water without the formation of any reaction product.

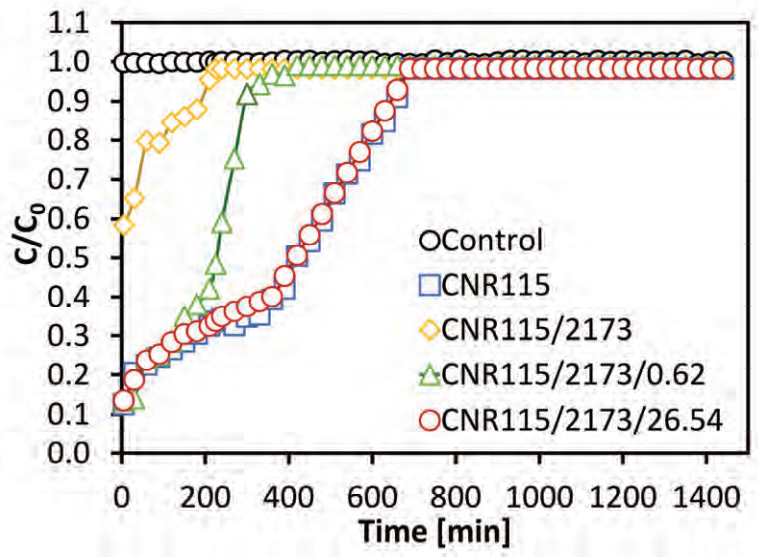

Figure 11. Evolution of TCE sorption with carbon materials in flow conditions: 303 K, 83 ppm TCE, 1 atm, 0.15 g of carbon material.

For both operation modes, the purification efficiency increased in order: CNR115/2173 → CNR115/2173/0.62 → CNR115 → CNR2173/2173/26.54, which correlates with the specific surface area and porosity of these materials (**Table 4**). Although, CNR115 showed higher surface parameters (1860 m^2/g, 1.1 cm^3/g), better sorption was obtained for CNR115/2173/26.54 (1610 m^2/g, 1 cm^3/g). It suggested the superiority of partially ordered turbostratic structure over the amorphous one in removing chloroorganic contaminants from water.

The turbostratic mesoporous active carbon with partially recovered specific surface area and porosity (CNR115/2173/26.54) was able to remove 65 % of the initial concentration of TCE in a batch reactor (**Figure 10**), and also to purify water to some extent in flow conditions (**Figure 11**). Due to the excellent sorption properties, CNR115/2173/26.54 was selected as a support material for the early stage of research over catalytic hydrodechlorination of chloroorganic contaminants in the aqueous phase.

5.1.2 Comparative study of Pd/C catalyst in the hydrodechlorination of trichloroethylene in batch and flow mode

Palladium catalysts proved to be very effective in various kinds of hydrogenation reactions, also in the hydrodechlorination of chloroorganic compounds [95,101,135,138,212]. Extraordinary performance in hydrogenolysis makes Pd catalysts excellent starting materials for further studies, in which the use of hydrogen will be an essential element. Hence, the involvement of palladium seemed to be a rational choice for research over catalytic HDC in the aqueous phase, at least for the initial steps. The most convenient and popular form of Pd catalyst for laboratory use is metal nanoparticles deposited on various support materials.

Therefore, taking into consideration the exceptional sorption properties of CNR115/2173/26.54 and high activity of Pd nanoparticles – 1.57 wt.% Pd(Cl)/CNR115/2173/26.54 (marked in this chapter as a "Pd/C") was synthesised by simple incipient wetness impregnation, with $PdCl_2$ as a metal precursor.

Typically, the transformation of Pd precursor into metal nanoparticles is observed at relatively low temperature, below 373 K. Nevertheless, temperature-programmed reduction (TPR) can confirm a full reduction of the metal precursor and allows to determine activation conditions (**Figure 12**).

The obtained profiles showed the process of precursor reduction and the simultaneous release of chemical species (**Figure 12**). The water release can be observed at a temperature below 373 K (m/z = 18), followed by the formation of hydrogen chloride (m/z = 36) with the peak maximum at 420 K. This maximum coincides with the negative peak minimum for hydrogen (m/z = 2), which indicates Pd^0 formation. The possible reasons for the shift

of this peak maximum towards higher temperatures (420 K), in comparison to values reported in the literature [213], are related to big Pd nanoparticles' presence or the influence of the ordered structure of the support material [214]. Since CO chemisorption, XRD and TEM (results presented below) confirmed the presence of uniformly dispersed 3 nm Pd nanoparticles in the freshly activated catalyst, the influence of turbostratic structure is the most probable explanation of this phenomenon.

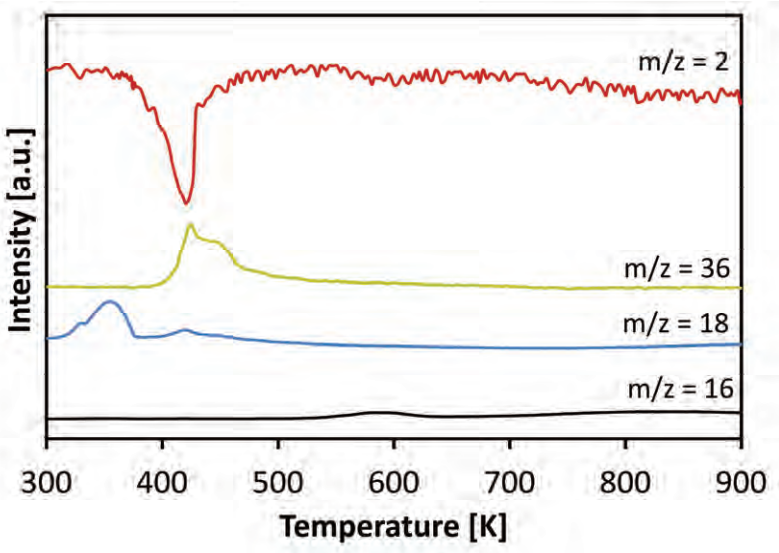

Figure 12. Temperature-programmed reduction of Pd/C.

Further investigation of the formed PdH with temperature-programmed hydride decomposition (TPHD) showed a relatively narrow peak with a maximum at 344 K (**Figure 13**). According to Bonarowska et al. [215], shape and intensity of TPHD peak or peaks are correlated with type of support material, metal-support interaction, metal nanoparticles size and Pd dispersion. Hence, the obtained result could be interpreted as the β-PdH decomposition from uniformly formed small palladium nanoparticles, which was also confirmed by XRD and TEM (3 nm).

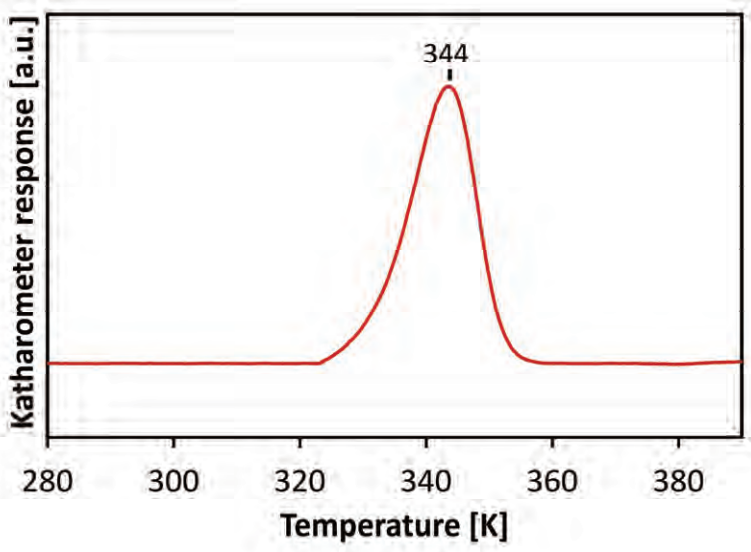

Figure 13. Temperature programmed hydride decomposition of Pd/C.

According to the procedure established on the TPR results, Pd/C catalyst was activated by heating at 673 K for 3 h in the stream of 10 % H_2/Ar directly before catalytic experiments and characterisation measurements.

Catalytic removal of TCE from water was carried out in batch and flow mode. Freshly reduced Pd/C catalyst (0.15 g) was initially used in the hydrodechlorination of TCE (8 ppm) in batch reactor at 303 K under atmospheric pressure (**Chapter 4.3.1.**). The extraordinary activity of Pd nanoparticles supported on turbostratic carbon resulted in the rapid removal of trichloroethylene from water (**Figure 14**). The purification process was finished until 60 minute. Hence, to investigate the full potential of the palladium catalyst, the concentration of organochloride contaminant was increased to 83 ppm, which exceeded 8000 times the norm for tap water (**Figure 15**).

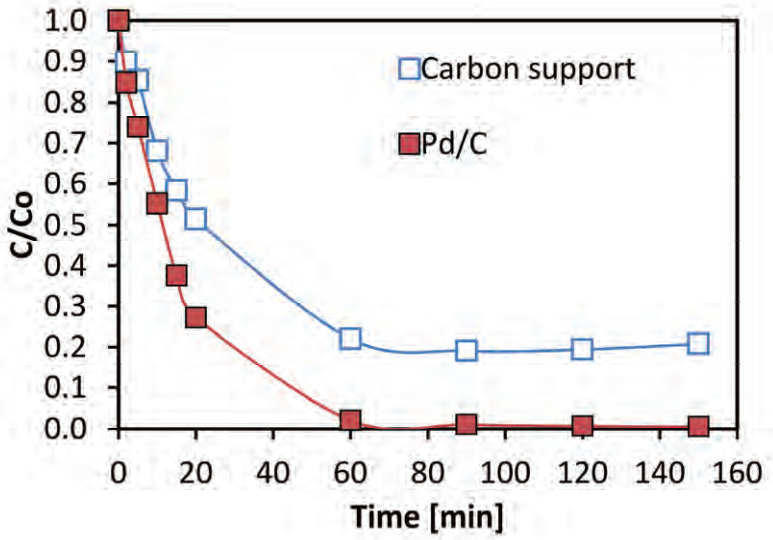

Figure 14. Removal of TCE from water by hydrodechlorination and sorption process in batch operation conditions, 303 K, 1 atm, 8 ppm TCE, 0.15 g of the catalyst or active carbon material.

The experiments with significantly higher trichloroethylene concentration seemingly showed the limits of Pd/C efficiency (**Figure 15**). However, the results of the additional experiments showed that technical issues may limit the activity of the palladium catalyst. Approximately 60 % and 90 % of the trichloroethylene was removed from the water, respectively by active carbon and the palladium catalyst, after 150 minutes of the purification process. However, it should be mentioned that in the case of carbon material, reaction products were not detected and pH value remained constant during the operation. Hence, plateau observed after 100 minute indicated the sorption equilibrium state. On the other hand, decreasing pH and the formation of C_2H_6 and C_2H_4 were observed for Pd/C. Moreover, more detailed analysis of the catalytic results and negligible changes in the pH after 100 minute of hydrodechlorination could suggest not sufficient amounts of hydrogen in the reaction mixture. This indicates the possible limitation of batch operation mode, in which solubility of hydrogen in water is the bottleneck of the process.

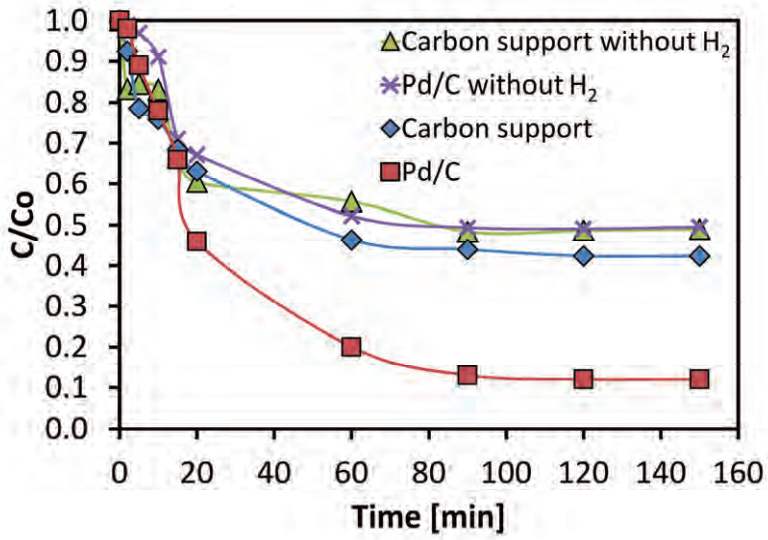

Figure 15. Removal of TCE from water by hydrodechlorination and sorption process in batch operation conditions, 303 K, 1 atm, 83 ppm TCE, 0.15 g of the catalyst or active carbon material.

Additional experiments performed for carbon material and palladium catalyst without hydrogen in the reaction mixture (**Figure 15**) showed almost the same curves for both materials. The sorption equilibrium was reached at the same time and at the same level of C/Co. This proves that regardless of the used material, the process without a hydrogen is limited to trichloroethylene sorption.

Catalytic hydrodechlorination of TCE in the aqueous phase is considered as pseudo-first order reaction. The calculated kinetic parameters for Pd/C take into account both the catalytic activity of Pd nanoparticles and extraordinary sorption properties of carbon material. The determined initial reaction rate (at 300 s) was equal to 1.98 mmol min^{-1} g_{Pd}^{-1}, reaction rate constant k = 0.027 s^{-1} and TOF = 0.01 s^{-1}. It is difficult to directly compare the obtained results with the published ones, due to the differences in the hydrodechlorination procedures. Nevertheless, given the lack of additional solvents in the reaction mixture, rapid removal of TCE and extremely high initial concentration

of a contaminant, catalytic performance of Pd/C should be considered as satisfying in a batch operation mode.

Most studies over the application of TCE hydrodechlorination in the aqueous phase focus on processes performed in batch conditions. Only a few scientific reports paid attention to flow reactors, despite the benefits, like easy process scalability [214]. Therefore, freshly reduced Pd/C was also used in the continuous-flow catalytic HDC (**Figure 16**). The application of this catalyst allowed for effective removal of TCE for over 25 h, without any sign of deactivation. On the other hand, the carbon material's sorption capacity was entirely exhausted by 400 minutes of the purification process. However, to evaluate the limits of Pd/C activity, the experiment with only 10 mg of the catalyst was performed (**Figure 17**). As it can be observed, only in this case, the conversion drop below 100 %, which proves very high catalytic activity and stability of palladium catalyst.

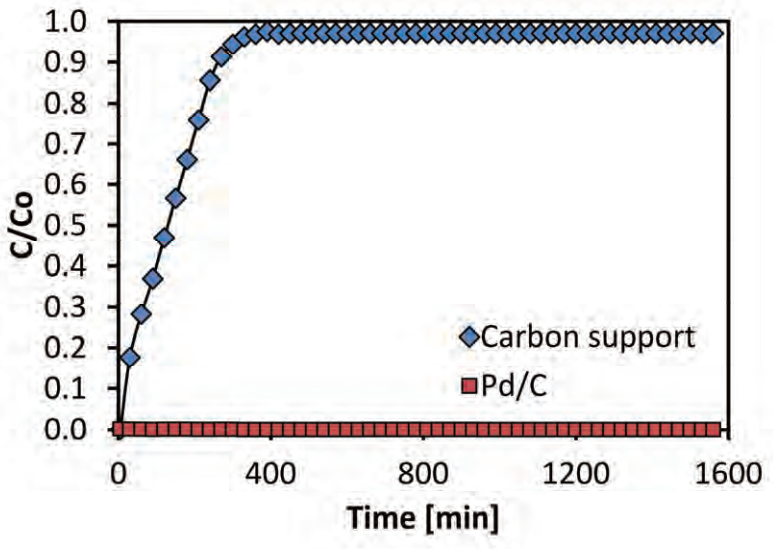

Figure 16. Removal of TCE from water by hydrodechlorination and sorption process in continuous-flow liquid-phase process, 303 K, 1 atm, 83 ppm TCE, 0.1 g of the catalyst or active carbon material.

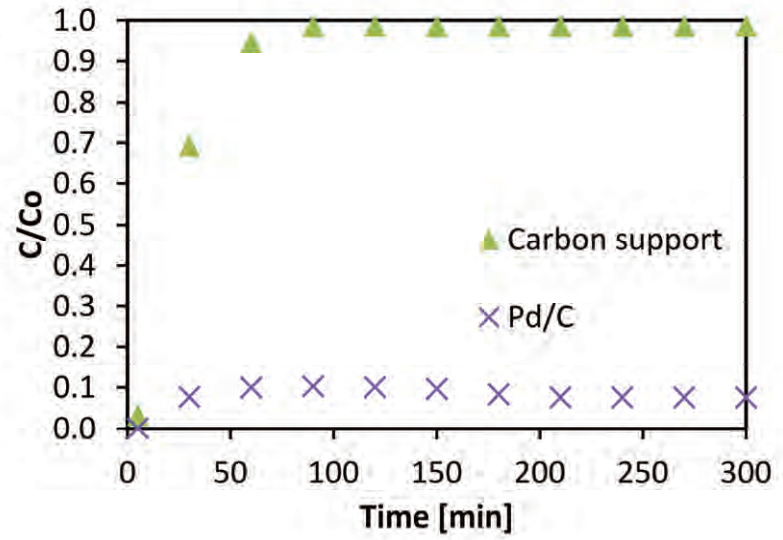

Figure 17. Removal of TCE from water by hydrodechlorination and sorption process in continuous-flow liquid-phase process, 303 K, 1 atm, 83 ppm TCE – 0.64 μmol/min, 0.01 g of the catalyst or active carbon material.

Despite the inability to directly compare the reactions carried out in batch and flow reactor, the results were satisfying in both cases. Although batch reactor allows removing higher amounts of TCE per unit of time, continuous flow operations offer a shorter transfer time between research and potential application.

The extraordinary Pd/C activity in the hydrodechlorination of TCE in the aqueous phase has to be considered in terms of this material's structural parameters. The obtained results agree with the previous observations, in which metal nanoparticles confined in the ordered mesoporous structure revealed satisfactory efficiency [144,216]. Moreover, turbostraticity and hydrophobicity of carbon support make Pd/C catalyst relatively resistant to ionic poisons, like chloride ions [210,212], which in consequence protect metal active phase and increase the overall process efficiency.

In order to investigate high stability and activity of the Pd/C, the catalyst was subjected to characterisation measurements, before and after the catalytic reaction.

The XRD results for Pd/C at different stages of its biography are presented in the **Figure 18**. The presence of turbostratic two dimensional ordering (first (0 0 2) peak with a maximum at ~24.2° and next (1 0 0) peak at ~43.5°) for fresh and spent Pd/C samples confirmed that the hydrodechlorination conditions did not affect the turbostratic structure of the support (marked with asterisks). The lack of clear and visible Pd(1 1 1) reflection indicates the presence of very small and well-dispersed Pd nanoparticles, both before and after the catalytic reaction.

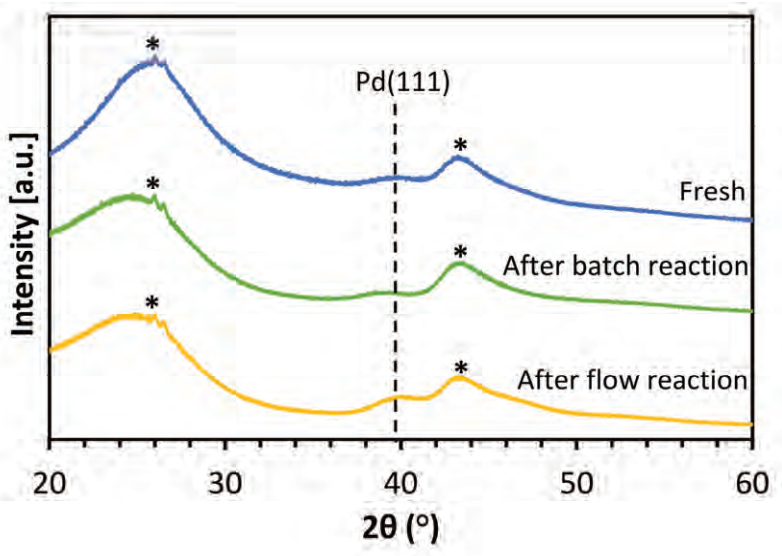

Figure 18. XRD profiles for Pd/C: activated and after batch and flow TCE hydrodechlorination.

Further analysis of the Pd/C surfaces by TEM measurements revealed redispersion of palladium nanoparticles during the catalytic reaction (**Figure 19**). Analysis of TEM images showed uniformly formed and well-dispersed 3.5 nm nanoparticles for fresh catalyst, and ~2 nm for the spent catalyst. Moreover, the differences between particles size were more visible

for the catalyst after the purification process. The observed decrease in the size of nanoparticles during hydrodechlorination was also previously observed by Ordóez et al. [217] for carbon supported Pd and Pt catalysts. The redispersion effect is the most often explained by the influence of HCl, which contributes to the formation of mobile metallic chlorides. These observations were in agreement with the XPS results for fresh and spent catalyst (**Figure 20**).

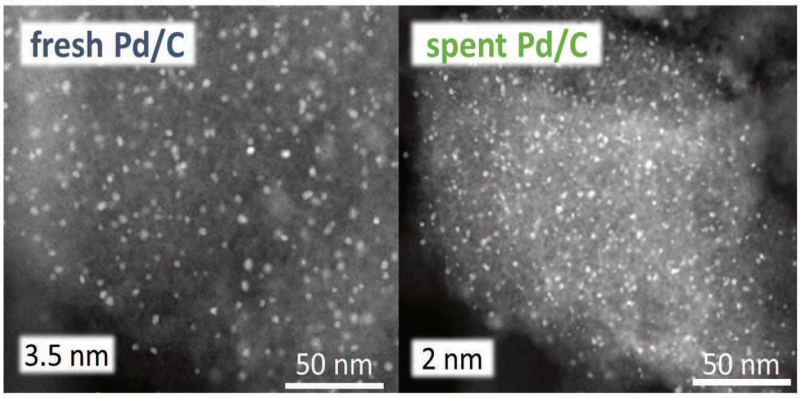

Figure 19. STEM images of fresh and spent Pd/C.

The XPS spectra for freshly reduced catalyst showed slightly shifted into higher binding energy dominant signal of 3d $Pd_{5/2}$ (located at 335.9 eV), which indicated metallic Pd in the form of small nanoparticles [217] (**Figure 20**). The same 3d $Pd_{5/2}$ signal for spent catalyst was located at 337.0 eV and was associated with the presence of Pd^{2+} ions, possibly in the form of $PdCl_2$ (confirmed by the presence of 2p Cl signal). All of these observations suggested the reaction mechanism, in which the palladium surface is chlorinated and subsequently cleaned by the hydrogen spillover, which contributes to the formation of HCl.

The obtained results confirmed the high activity of Pd nanoparticles in the hydrodechlorination of trichloroethylene in the aqueous phase, both in batch and flow conditions. Nevertheless, the overall activity and stability of the catalyst were strongly affected by the turbostratic and hydrophobic character of mesoporous activated carbon.

1.57 wt.% Pd(Cl)/CNR115/2173/26.54 catalyst may rapidly remove trichloroethylene from water in batch operation conditions, but also purify water for a long time in flow without any signs of deactivation.

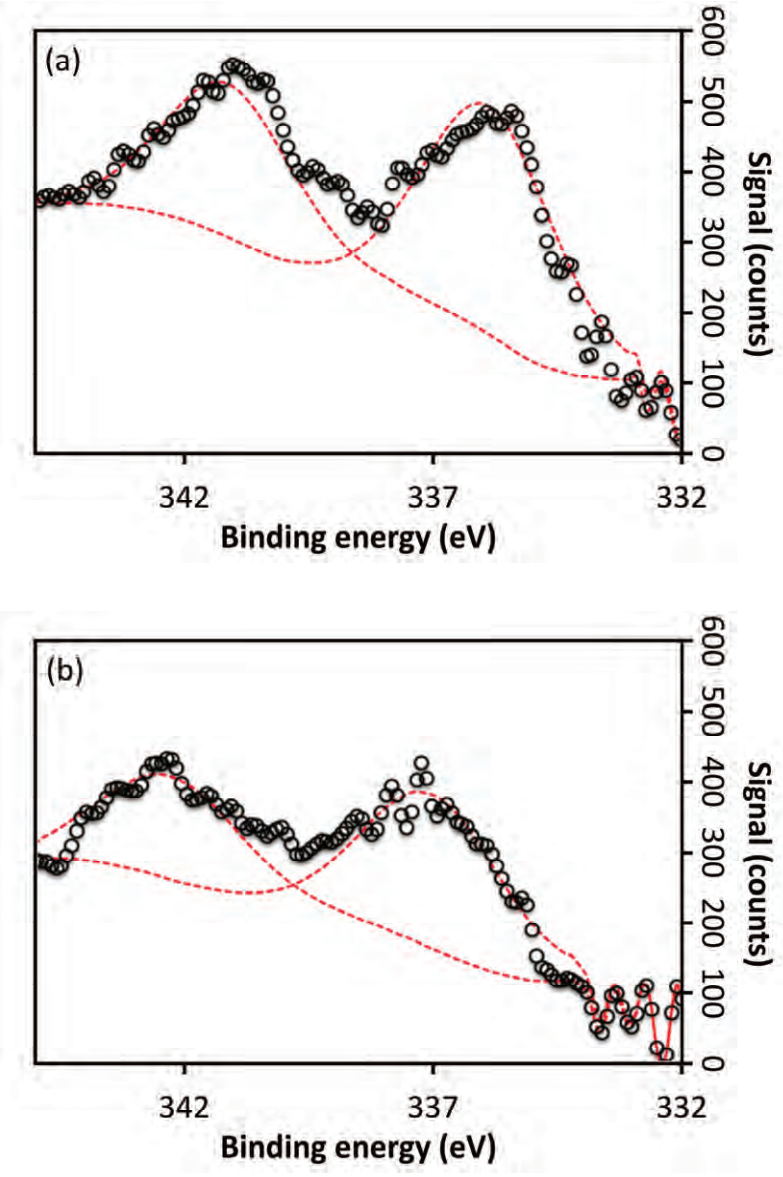

Figure 20. XPS of Pd/C: freshly activated (a) and after catalytic reaction (b).

5.1.3 Influence of pretreatment conditions on the catalytic activity of Ni/C in the hydrodechlorination of TCE in the aqueous phase

Although Pd catalysts show excellent activity in the HDC process [218], the high cost of this noble metal is the major drawback for its application in environmental protection. Hence, there is a strong need for readily available transition metals as catalysts, which could be used for effective purification of water from chloroorganic contaminants.

The current knowledge about catalytic HDC indicates several different less-expensive metals as suitable substitutes: Cu, Ni [218,219]. Among them, nickel seems to be the most promising due to its well-known and excellent activity in hydrodechlorination [144,220,221]. Nevertheless, the potential application of Ni catalysts in the water purification requires comprehensive studies on crucial for catalytic performance factors, like catalyst structure.

Catalytic hydrodechlorination proved to be a structural sensitive reaction [212,222,223]. It is well established that the kind of a metal precursor and pretreatment conditions affect the catalyst morphology (e.g. average particles size and their distribution), and in consequence – the catalytic performance [208,209,224,225].

Hence, to verify the impact of these parameters, a series of 2 wt.% Ni catalysts was synthesised by simple incipient wetness impregnation. As in the case of the palladium catalyst (**Chapter 5.1.2**), due to the highest sorption efficiency of trichloroethylene, CNR115/2173/26.54 was selected as a support material. The catalytic materials were prepared using two nickel salts as metal precursors – $Ni(NO_3)_2$ * $6H_2O$ and $NiCl_2$ * $6H_2O$, marked respectively with "(N)" and "(Cl)". In order to determine optimal parameters for the complete reduction of these precursors, temperature-

programmed reduction experiments, up to 1173 K, were performed for synthesised materials (**Figure 21**).

Using the Thermal Conductivity Detector's calibration curve in the TPR experiments, the full reduction of both Ni precursors during high-temperature treatment was confirmed. Both catalysts obtained in these conditions were marked with "H" suffix.

Analysis of the TPR profiles for Ni(Cl)/C and Ni(N)/C revealed some differences between these materials occurring during their activation. In the case of 2 wt.% Ni(N)/CNR115/2173/26.54, one dominant reduction peak is observed at 553 K and two significantly smaller at 634 K and 756 K (**Figure 21**). On the other hand, for 2 wt.% Ni(Cl)/CNR115/2173/26.54, two peaks were observed at 650 K and 731 K. The visible shift of the reduction peaks towards higher temperatures for chloride precursor results from the stronger interaction between the support and the metal precursor [226–228].

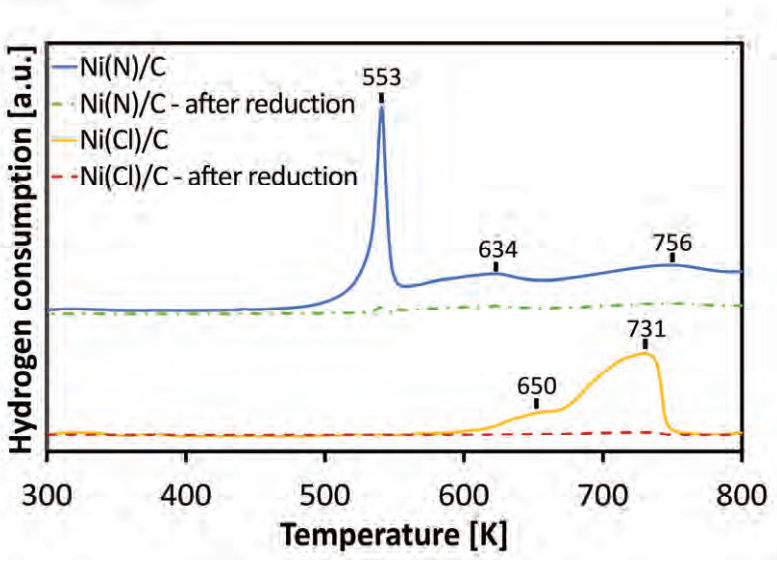

Figure 21. Temperature-programmed reduction of fresh 2 wt.% Ni/CNR115/2173/26 and activated catalyst (673 K, 3h, 25 ml/min 10 % H_2/Ar).

Based on the TPR results, the activation of carbon supported nickel materials was carried out for 3 h, at 673 K in the stream of 10 % H_2/Ar. The catalysts obtained by this procedure were marked with "L" suffix. Additionally, to verify the catalysts' reducibility at these conditions, TPR experiments for materials activated at 673 K were performed (**Figure 21**). The obtained profiles showed negligible changes with increasing temperature, which confirmed the total reduction of Ni precursor during the low-temperature treatment.

The nickel catalysts reduced at low and high temperature were investigated by TEM. These measurements allowed the visualisation of the structure of the catalysts an the average nickel particles sizes (**Table 5**, **Figure 22**).

Table 5. TEM determined average Ni nanoparticles size for 2 wt.% Ni/CNR115/2173/26.54 catalysts synthesised with different precursors and activated at different conditions.

Catalyst	Average particles size [nm]
Ni(N)/C-H	31
Ni(N)/C-L	3
Ni(Cl)/C-H	29
Ni(Cl)/C-L	28

H – reduction by heating up to 1173 K (10 K/min) in the 25 ml/min 10 % H_2/Ar

L – reduction at 673 K for 3 h in the 25 ml/min 10 % H_2/Ar

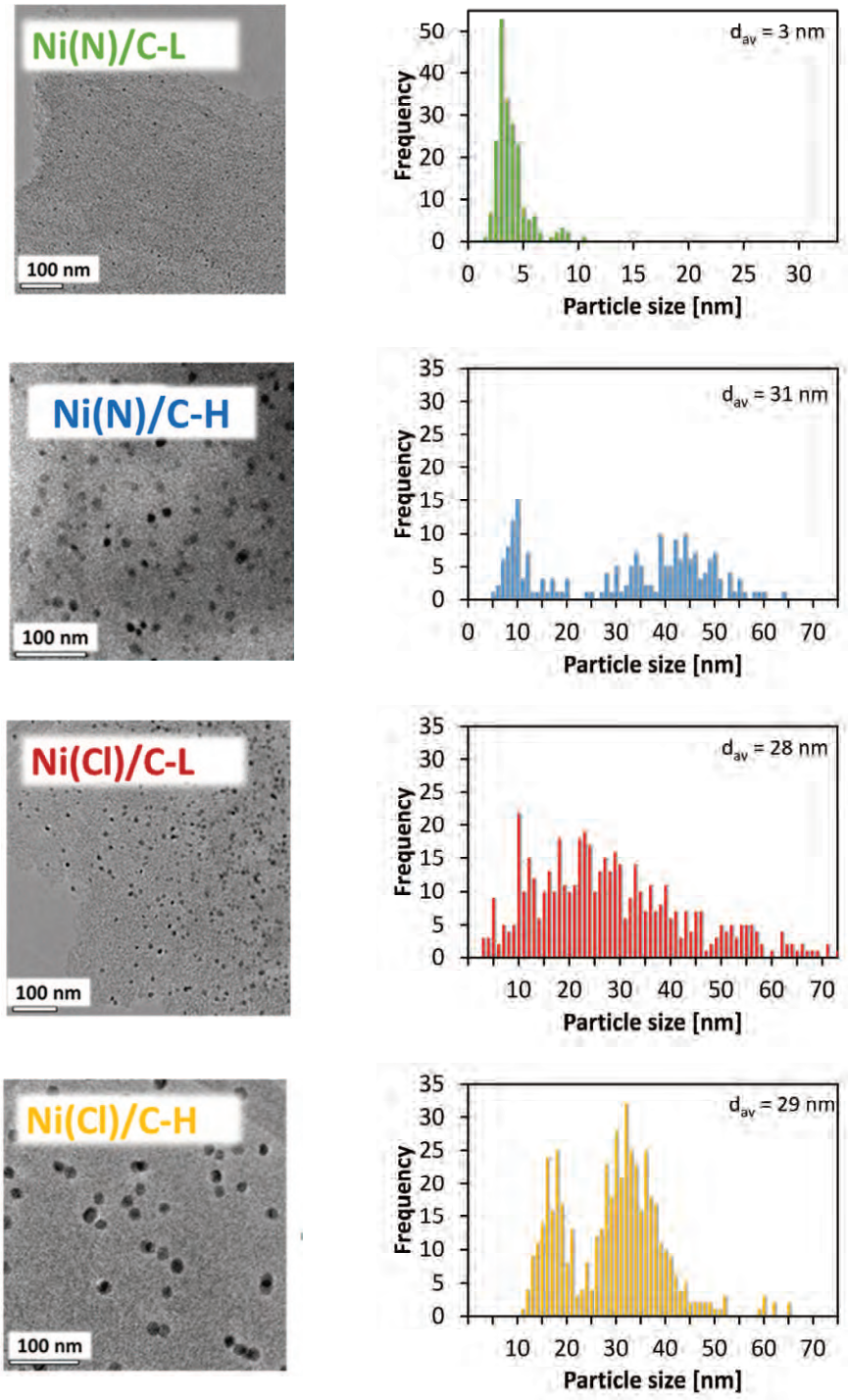

Figure 22. TEM images and particles size distribution for activated 2 wt.% Ni/CNRI15/2173/26.54 catalysts.

The smallest nanoparticles (~ 3 nm) with narrow size distribution were obtained for 2 wt.% Ni(N)/CNR115/2173/26.54 reduced at 673 K for 3 h (Ni(N)-L). Such small metal nanoparticles (>6 nm) are usually obtained for the catalysts synthesised from nickel nitrate precursor as opposed to other metal precursors [206–208]. Nevertheless, it is worth mentioning that the formation of Ni nanoparticles below 3 nm is rather unique in the case of simple incipient wetness impregnation of carbon support materials [229]. On the other hand, high-temperature treatment resulted in the formation of ~ 31 nm Ni nanoparticles, with bimodal distribution features (**Figure 22**).

A similar distribution was observed for the catalyst synthesised from nickel chloride and reduced at high temperature (**Figure 22**). In contrast, 2 wt.% Ni(Cl)/CNR115/2173/26.54 reduced at 673 K for 3 h did not show any bimodal character (**Figure 22**). These observations suggest that even short treatment above Tammann temperature (for Ni – 863 K [226]) results in nanoparticles sintering, especially the ones above 15 nm. This effect seems to be independent of the metal precursor type. However, it is more visible in the case of catalyst synthesised from nickel nitrate.

The catalysts reduced in different ways were used in the aqueous phase catalytic hydrodechlorination of trichloroethylene (**Figure 23**). In contrast to pure carbon materials (**Figure 10**), the analyses of the reaction samples showed the formation of ethane, ethene and hydrochloric acid as the reaction products.

Because the sorption properties of CNR115/2173/26.54 are essential in the aqueous phase trichloroethylene HDC, the kinetic parameters were calculated taking into account this phenomenon (**Table 6**).

The best results were obtained for the catalysts synthesised from nickel chloride (**Figure 23, Table 6**). The Ni(Cl) catalyst activated by high-temperature treatment revealed more rapid decomposition of TCE. Over 50 % of starting contamination was removed until 20 min by Ni(Cl)/C-H,

whereas the Ni(Cl)/C-L removed below 40 % of the initial concentration (**Figure 23**).

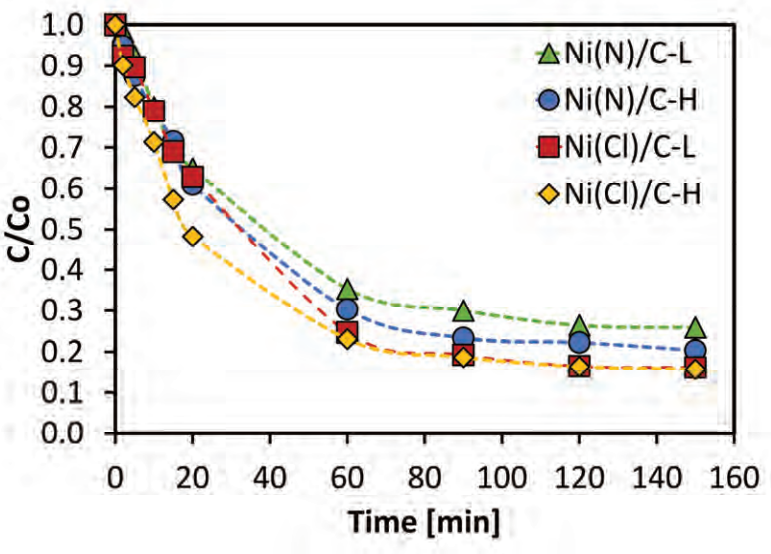

Figure 23. Catalytic hydrodechlorination of TCE in aqueous phase with 2 wt.% Ni/CNR115/2173/26.54; 303 K, 8 ppm TCE, 0.1 g of Ni catalyst.

Table 6. Kinetic parameters of TCE HDC in the aqueous phase calculated for 2 wt.% Ni/CNR115/2173/26.54.

Catalyst	Reaction rate constant k (0-60 min) s^{-1}	Initial reaction rate r_A (300 s) [mmol min^{-1} g_{Ni}^{-1}]
Ni(N)/C-H	0.015	0.15
Ni(N)/C -L	0.011	0.11
Ni(Cl)/C -H	0.016	0.26
Ni(Cl)/C -L	0.013	0.19

The lowest efficiency in removing TCE from water by hydrodechlorination was observed for the Ni catalyst synthesised from nickel nitrate, and reduced at low-temperature conditions – Ni(N)/C-L (**Figure 23**). Although this catalyst showed similar activity at the beginning of the process, the final conversion

achieved "only" 70 %. Slightly better results were obtained for the catalyst activated at a higher temperature – 75 % (Ni(N)-H) (**Figure 23**). The initial reaction rate decreased in order: Ni(Cl)/C-H → Ni(Cl)/C-L → Ni(N)/C-H → Ni(N)/C-L (**Table 6**), which clearly suggest that catalytic performance of carbon supported nickel catalysts depends on two factors: metal precursor and pretreatment conditions (**Figure 23**, **Table 6**).

In order to determine average particles size and investigate the impact of HDC conditions on catalysts structure, freshly activated and subjected to catalytic reaction catalysts (with TCE suffix) were characterised by XRD (**Figure 24** and **25**). Beside the Ni related reflections, all of the obtained profiles contain signals characteristic for the turbostratic structure of carbon support (~43.5° and~79°). This structure was not affected during the HDC for any of the tested catalysts.

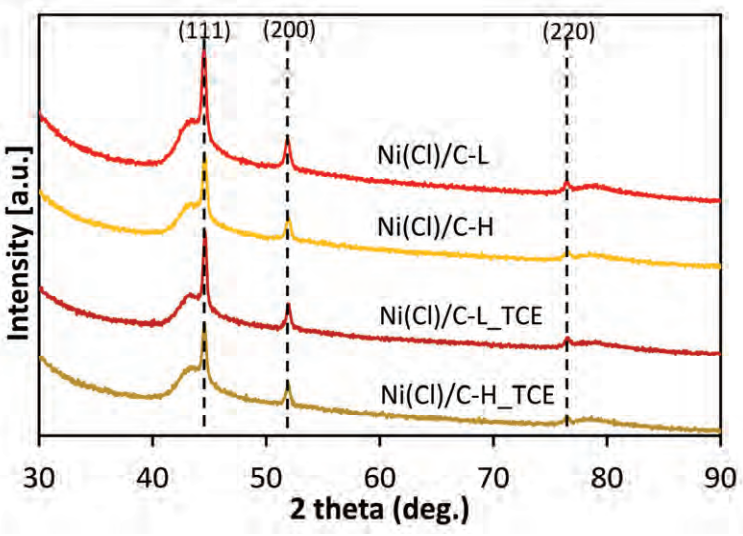

Figure 24. XRD profiles of 2 wt.% Ni(Cl)/CNRI15/2173/26.54 catalysts, before and after catalytic TCE hydrodechlorination in the aqueous phase.

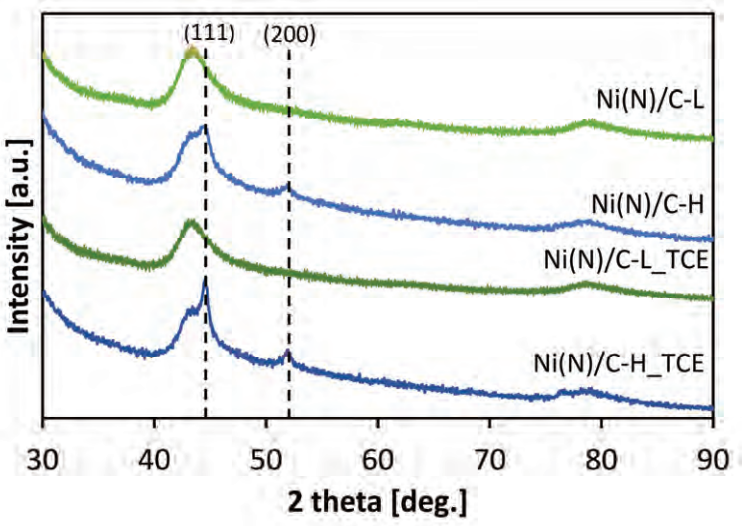

Figure 25. XRD profiles of 2 wt.% Ni(N)/CNR115/2173/26.54 catalysts, before and after catalytic hydrodechlorination in the aqueous phase.

The Ni crystallite sizes were calculated for fresh and spent catalysts with the Scherrer equation (**Table 7**). A high-temperature treatment (heating up to1173 K) applied to the reduction of nickel nitrate precursor resulted in the formation of significantly larger Ni nanoparticles (Ni(N)/C-H), than Ni(N)/C-L, where Ni (2 0 0) reflection was not even observed. It can indicated the presence of well-dispersed Ni nanoparticles with diameter below the detection threshold of the instrument (<3 nm). Interestingly, this phenomenon was not observed for the catalysts synthesised from nickel chloride, and independently from the applied treatment conditions, the average particles size was equal to 16 nm. The comparative analysis between Ni (2 0 0) reflections, used for determination of Ni nanoparticles size, revealed negligible differences for fresh and spent catalysts (**Table 7**). It confirms the stability of Ni catalysts under reaction conditions.

Table 7. An average Ni nanoparticles size for 2 wt.% Ni/CNR115/2173/26.54 catalysts synthesised with different precursors and activated at different conditions determined by XRD.

Catalyst	Average nanoparticles size [nm]
Ni(N)/C-H	9
Ni(N)-/C-H_TCE	11
Ni(N)/C-L	<3
Ni(N)-/C-L_TCE	<3
Ni(Cl)/C-H	16
Ni(Cl)/C-H_TCE	18
Ni(Cl)/C-L	16
Ni(Cl)/C-L_TCE	15

H – reduction by heating up to 1173 K (10 K/min) in the 25 ml/min 10 % H_2/Ar
L – reduction at 673 K for 3 h in the 25 ml/min 10 % H_2/Ar
TCE – catalyst after TCE HDC in the aqueous phase

Discrepancies between particles size obtained from and TEM and XRD are well visible for all investigated materials. However, the relations between particles sizes of tested catalysts were preserved. Literature investigation showed that high compliance between XRD and TEM results is achieved only for uniform particles, without the small ones' significant contribution [230].

After 120 min each of the tested catalysts achieved a plateau. It could suggest both their deactivation under reaction conditions or the not sufficient amounts of hydrogen solubilized in water. (**Figure 23**).

Temperature-programmed hydrogenation (TPH) of spent Ni(Cl)/C-L_TCE catalyst showed the presence of carbon containing-species on the metal active sites – methane and C_2H_X (m/z 15 and m/z 28) (**Figure 26**). The high temperature of desorption (~ 700 K) indicated a strong bond with the catalyst surface, which is the most probable reason for the catalyst deactivation. Additionally, chlorine-containing deposits were not observed

(m/z 36) during TPH, which suggest satisfying resistance of tested catalyst to chloride ions, considered as a catalysts poisons in the HDC [231,232].

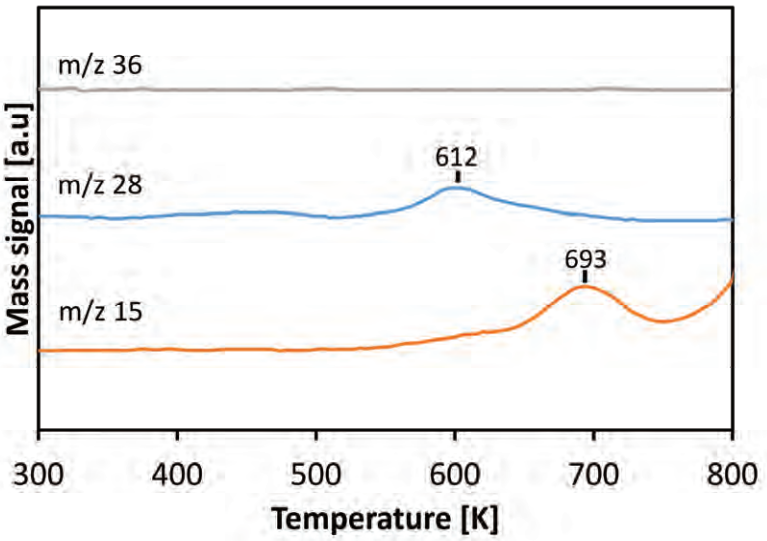

Figure 26. Temperature-programmed hydrogenation of 2 wt.% Ni(Cl)/CNRI15/2I73/26.54 after TCE hydrodechlorination in water.

In general, the relationship between Ni nanoparticles size and catalytic activity is quite well visible. The presence of larger Ni nanoparticles promotes higher effectiveness of the water purification process. Nevertheless, small metal species proved to be very active in the catalytic hydrodechlorination of chloroorganic compounds in the aqueous phase [233]. However, at the same time, these species tend to deactivate faster. The superior efficiency of larger metal nanoparticles was observed in earlier studies with the noble metal catalysts [222]. This phenomenon is usually explained by the higher resistance to deactivation of these species.

Nevertheless, the obtained results indicated that, in the studied conditions, the best efficiency in TCE removal is achieved with larger nickel species. The application of the chloride precursor allows formation of larger Ni nanoparticles, independently from the used pretreatment conditions. However, reduction above Tammann temperature may lead to the sintering

of Ni particles. Therefore, further studies with Ni nanoparticles supported on carbon materials were performed with catalysts synthesised from nickel chloride and reduced at 673 K for 3 h in the stream of 10 % H_2/Ar. These conditions allowed for obtaining catalysts with the optimal average nanoparticles size.

5.1.4 Influence of carbon support material structure on the catalytic activity of Ni/C in the hydrodechlorination of TCE in the aqueous phase

The results discussed in the **Chapter 5.1.3** proved that nickel nanoparticles are active in the catalytic hydrodechlorination of trichloroethylene in the aqueous phase. Moreover, conducted experiments showed that the size of metal nanoparticles affects the catalytic performance, and bigger nanoparticles are better than the smaller ones. However, all of the catalytic tests were performed with the Ni particles supported on the same active carbon with a partially ordered turbostratic structure, which had the best TCE sorption efficiency. However, considering the observations of Munoz et al. [126], high surface area and low ordered structure should lead to higher HDC rates. On the other hand, Baeza et al. [127] demonstrated higher activity of metal nanoparticles supported on highly ordered graphitised carbon. Such contradictory results allow for free interpretation, which is not desirable for the design of efficient catalysts.

In order to verify the influence of structure ordering on catalytic performance, a series of 2 wt.% Ni catalysts was prepared by incipient wetness impregnation with $NiCl_2$ as a metal precursor. Various carbon materials, previously tested in TCE sorption experiments (**Chapter 5.1.1**, **Figure 10** and **11**), were used as Ni nanoparticles supports: CNR115 – amorphous commercial activated carbon (1860 m^2/g, 1.1 cm^3/g), CNR 115/2173 – turbostratic carbon without porosity (1 m^2/g , 0 cm^3/g), CNR115/2173/0.62 – turbostratic

carbon with partially recovered specific surface area and porosity (825 m^2/g, 0.4 cm^3/g) and CNR115/2173/26.54 – turbostratic activated carbon with high surface area and large porosity (1610 m^2/g , 0.8 cm^3/g).

All of the synthesised materials were subjected to TPR experiments to verify the reducibility of $NiCl_2$ on the used carbon materials (**Figure 27**). The highest reduction temperature (maximum of the peak at 731 K) was observed for nickel precursor supported on the material with turbostratic structure and high specific surface area. The visible shift of the reduction temperature towards higher values indicates stronger interaction between metal active phase and support material. However, the other two turbostratic carbons show the reduction temperature (663 K and 667 K) lower than the amorphous CNR115 (682 K). These observations suggest that both high specific surface area and the structure ordering degree affect the metal-support interaction.

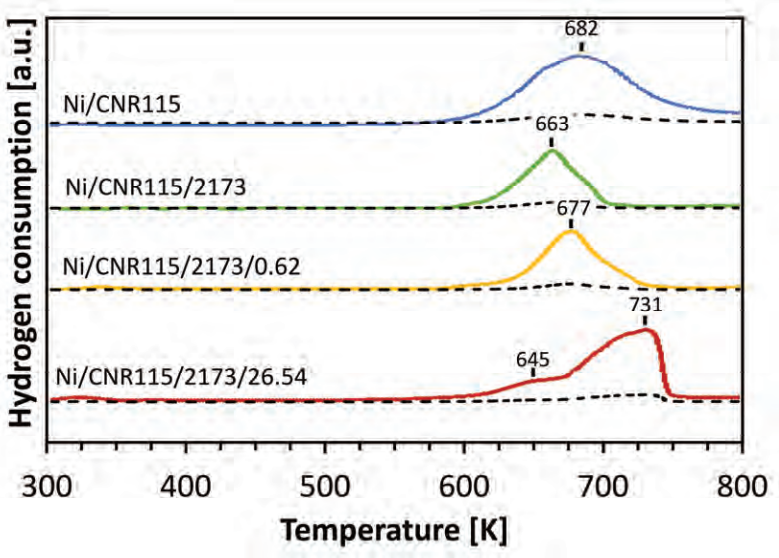

Figure 27. Temperature-programmed reduction of $NiCl_2$ precursor on different carbon materials and corresponding catalysts after activation at 673 K for 3 h in 10 % H_2/Ar (black dotted lines).

As it was determined in the previous experiments (**Chapter 5.1.3**), in order to obtain catalysts with optimal particles size, materials were activated at 673 K in the stream of 10 % H_2/Ar for 3 h. Additional TPR experiments for freshly activated catalysts were performed to verify the complete reduction of the metal precursor. Negligible changes in the TPR profiles confirmed that the applied conditions were sufficient for the full reduction of the Ni nanoparticles (**Figure 27**).

The average sizes of the obtained metal nanoparticles were initially determined by the XRD measurements. Analysis of the results showed that, independently from the support material, Ni nanoparticles' size was comparable and in line with the previously determined desired value (**Chapter 5.1.3**). A more detailed discussion related to this feature of the catalysts is placed later in this chapter in the context of changes in the catalyst structure induced by the reaction environment. Nevertheless, all of the turbostratic materials revealed reflections characteristic for partially ordered structure (marked with "*", **Figure 28**).

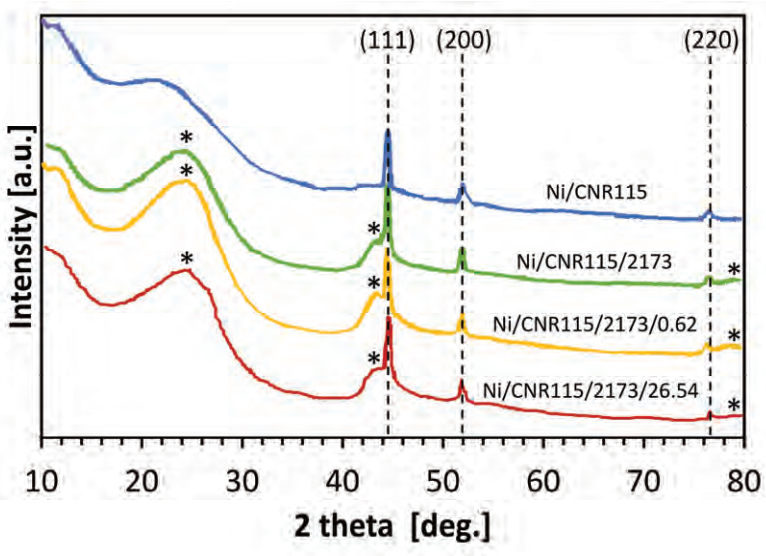

Figure 28. XRD of 2 wt.% Ni catalysts prepared with various activated carbons, activated at 673 K for 3 h in 10 % H_2/Ar. "*" - turbostratic structure.

Freshly activated materials were initially used in the hydrodechlorination of TCE in a batch reactor. The comparative analysis between four Ni/C catalysts revealed well-noticeable differences in the catalytic performance (**Figure 29**). Ni nanoparticles supported on the amorphous parent carbon material (CNR115) showed the greatest efficiency in the removal of TCE from water at the initial stage of the purification, 35 % in the 20th minute. However, later in the process, Ni/CNR115/2173/26.54 removed a higher amount of trichloroethylene, 85 % in the 150th minute. However, the turbostratic structure itself is not the most crucial factor because metal nanoparticles deposited on turbostratic carbon without porosity or with partially recovered surface demonstrated poor activity, 26 % and 35 %, respectively. These simple observations are in agreement with calculated kinetic parameters (**Table 8**).

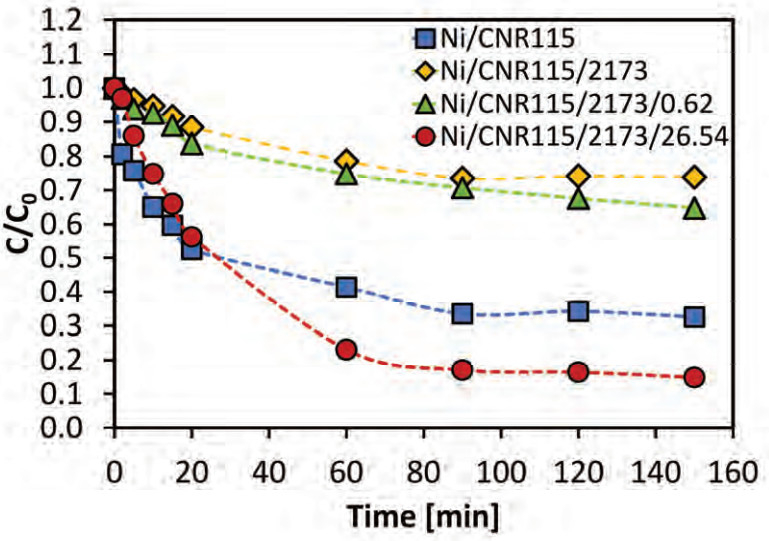

Figure 29. TCE HDC with 2 wt% Ni catalysts synthesised with various carbon materials, 1 atm, 303 K, 8 ppm TCE, 0.1 g of a catalyst.

Table 8. Catalytic hydrodechlorination of TCE in aqueous phase with 2 wt.% Ni on various carbons, 1 atm, 303 K, 8 ppm TCE, 0.1 g of catalyst.

Catalyst	Reaction rate constant k (0-150 min) s^{-1}	Initial reaction rate r_A (300 s) [mmol min^{-1} g_{Ni}^{-1}]
Ni/CNR115	0.028	0.38
Ni/CNR115/2173	0.004	0.06
Ni/CNR115/2173/0.62	0.005	0.08
Ni/CNR115/2173/26.54	0.024	0.28

Technological requirements indicate that the HDC catalyst should be reusable. In the case of batch reactors, it is associated with the necessity to filter, wash and dry the used catalyst. According to this procedure, the reusability tests were performed for the two best catalytic materials: Ni/CNR115 and Ni/CNR115/2173/26.54 (**Figure 30**). Three hydrodechlorination cycles for each catalyst showed progressive deactivation of the Ni/CNR115. On the other hand, Ni/CNR115/2173/26.54 demonstrated considerable stability during the purification process, with a minimal variation in the activity between cycles. Additional EDXRF experiments did not show any detectable amount of Ni in the reaction mixture. Hence, this effect could be explained by the mass loss during the filtration and drying processes. The metal leaching effect does not play a significant role in the catalyst deactivation, which is crucial from the application point of view.

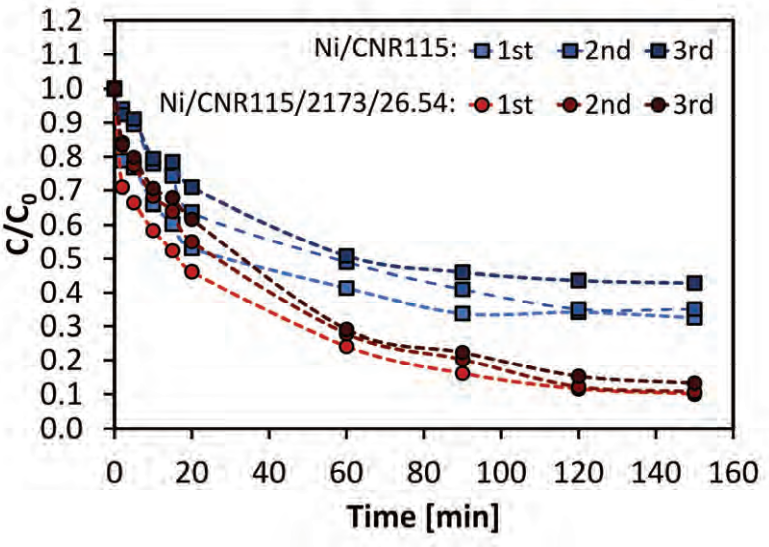

Figure 30. Stability test of Ni/CNR115 and Ni/CNR115/2173.26.54, 1 atm, 303 K, 8 ppm TCE, 0.1 g of a catalyst.

The experiments performed with Pd/C (**Chapter 5.1.2**) could suggested that the catalyst with limited activity in the batch operation might be very effective under flow conditions. Therefore, all of the Ni/C catalysts were also tested in the reactions conducted in a flow reactor under 10 bar at 303 K. In this case, the catalytic materials were subjected to even more challenging conditions - higher concentration of TCE – 83 ppm, which exceeded 8000 times the norm for tap water. Despite the much larger TCE quantity, most of the catalysts effectively purified water for 25 h without any signs of deactivation (**Figure 31**). Only for the catalyst without porosity – Ni/CNR115/2173, progressive deactivation was observed till the 600th minute of the process, after which conversion stabilised at approximately 10 %. However, this result should be regarded as satisfactory, given the catalyst's negligible activity in the batch reactor with lower TCE concentration (**Figure 29**). Even more spectacular efficiency was observed for Ni/CNR115/2173/0.62. The catalyst, which was almost inactive in the batch reactor, showed a stable 75 % conversion for 25 h. Similar to batch operation, the best efficiency in TCE removal was presented by nickel nanoparticles

supported on turbostratic active carbon with high specific surface area and large porosity – Ni/CNR115/2173/26.54. This catalytic material allowed for constant purification (~ 90 %) for 25 h, without any signs of deactivation (**Figure 31**). The additional catalytic experiment demonstrated that Ni/CNR115/2173/26.54 can effectively purify water even at atmospheric pressure at 303 K (**Figure 32**).

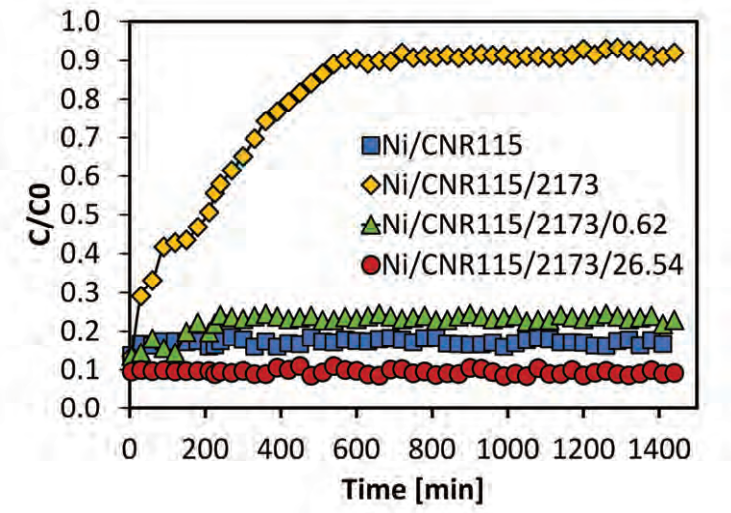

Figure 31. HDC of TCE in the aqueous phase in flow mode with 2 wt.% Ni on various carbons; 303 K, 10 bar, 83 ppm TCE, 0.15 g of catalyst.

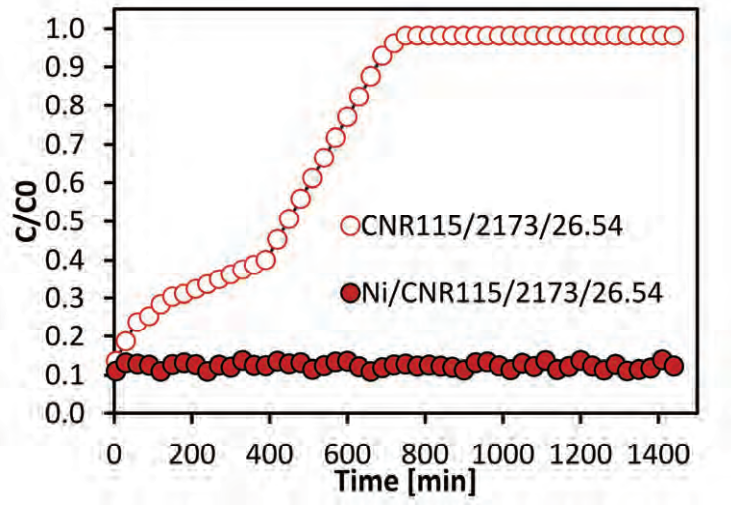

Figure 32. HDC of TCE in aqueous phase and TCE sorption test in flow mode with Ni/CNR115/2173/26.54; 303 K, 1 bar, 83 ppm TCE, 0.15 g of catalyst.

Such high efficiency of the tested catalysts should be discussed in the context of their structural parameters. Hence, all of the materials were subjected to XRD, TEM and XAS measurements, before and after catalytic tests.

The average particles sizes, calculated from XRD and TEM, are collected in **Table 9**. Discrepancies in the values obtained by these two different techniques could be explained similarly as for Ni nanoparticles synthesised from different precursors and subjected to different pretreatment conditions (**Chapter 5.1.3**). High compliance between XRD and TEM results is achieved only for uniform particles, without the small ones' significant contribution [230]. Based on the TEM results for Ni/CNR115, amorphous active carbon contributes to the formation of big Ni aggregates (~60 nm) and much smaller nanoparticles (~30 nm) (**Table 9**, **Figure 33**). Nevertheless, the relation between calculated values for all materials is preserved. For each catalyst, slight differences in particles size were observed between fresh and spend catalytic materials. It suggests that TCE HDC may affects to some extent Ni nanoparticles size. This effect is very-well visible in the case of Ni/CNR115/2173. Significant redispersion could be explained in the context of the structural properties of this carbon support (**Chapter 5.1.1**, **Table 4**). Small specific surface area and lack of porosity contribute to the formation of large nickel species, which are capable of migration on the carbon surface (**Table 9**, **Figure 34**). An almost indistinguishable change was noticed for Ni/CNR115/2173/26.54. The partially ordered turbostratic structure leads to the formation of well-dispersed and resistant to agglomeration and redispersion Ni nanoparticles (**Table 9**, **Figure 35**).

Table 9. Ni nanoparticles size estimated from XRD and TEM measurements for 2 wt.% Ni catalysts synthesised from $NiCl_2$.

Catalyst	Metal particles size [nm]		Dispersion [%
	XRD	TEM	
Ni/CNRI15	20	68	5.1
Ni/CNRI15_TCE	15	62	5.1
Ni/CNRI15/2I73	26	33	3.9
Ni/CNRI15/2I73_TCE	23	24	4.4
Ni/CNRI15/2I73/0.62	25	-	4.0
Ni/CNRI15/2I73/0.62_TCE	22	-	4.6
Ni/CNRI15/2I73/26.54	16	28	6.3
Ni/CNRI15/2I73/26.54_TCE	15	26	6.7

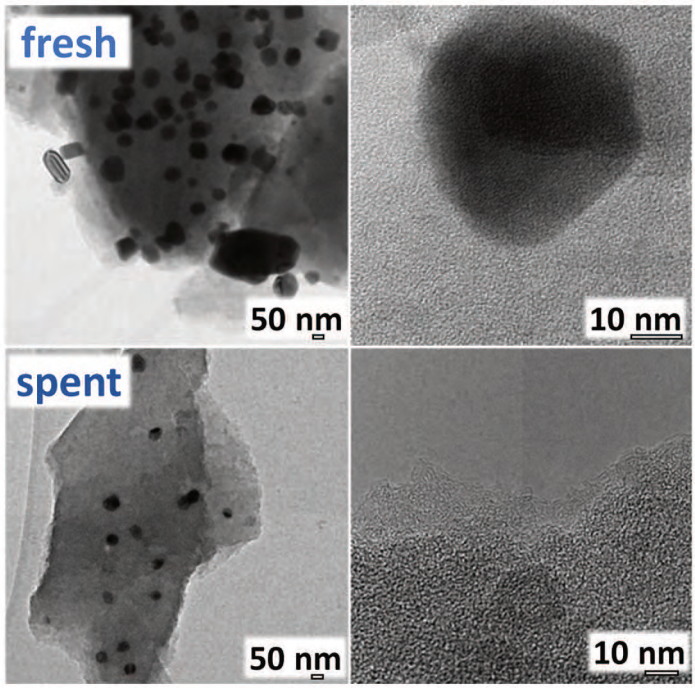

Figure 33. TEM images of Ni/CNRI15.

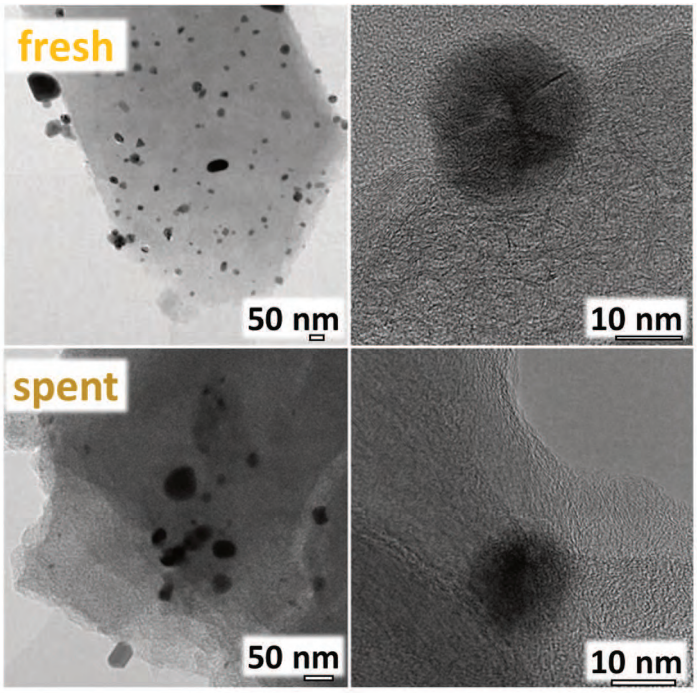

Figure 34. TEM images of Ni/CNR115/2173.

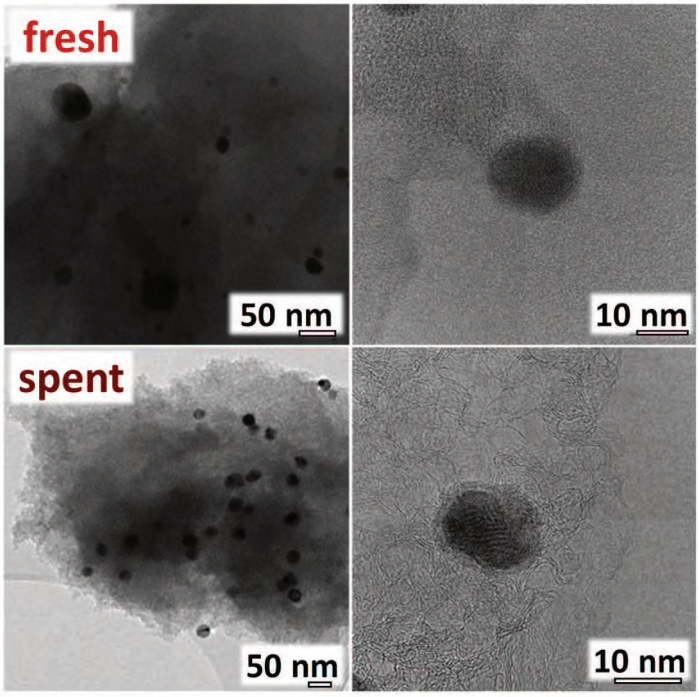

Figure 35. TEM images of Ni/CNR115/2173/26.54.

According to the literature, the highest activity of Ni/CNR115/2173/26.54 could be explained by the reducing ability of the graphitised carbon support, metal-support interactions (MSI) through electron transfer, which improves hydrogen spillover [234]. Moreover, Feng et al. [234] suggest the importance of the initial $M^0/M^{2+/3+}$ ratio for the catalytic performance of metal nanoparticles. Therefore, XAS around Ni K-edge measurements were performed for fresh and spent catalysts (**Table 10, Figure 36**). Activated Ni/CNR115/2173/0.62 and Ni/CNR115/2173 contained mainly Ni^0, with a small fraction of Ni^{2+}. On the other hand, for the other two catalysts, Ni^{3+} fraction was detected besides Ni^0. This phenomenon could be explained by the lower resistance of slightly smaller Ni nanoparticles to the influence of functional groups of the amorphous carbon support (CNR115) and electron deficiency of turbostratic carbon structure (CNR115/2173/26.54). Comparative analysis between fresh and spent catalysts showed that only for Ni/CNR115/2173, Ni oxidation state stayed almost unchanged. For other catalytic materials, the exposition to electron-deficient TCE resulted in the significant conversion of Ni^0 into Ni^{3+}, which may be the possible cause of the nanoparticles redispersion.

Table 10. The relative concentration of the Ni oxidation states estimated by XAS measurements.

Catalyst	Relative concentration of Ni oxidation states		
	Ni^0 [%]	Ni^{2+} [%]	Ni^{3+} [%]
Ni/CNR115	65	0	35
Ni/CNR115_TCE	18	0	82
Ni/CNR115/2173	97	3	0
Ni/CNR115/2173_TCE	95	0	5
Ni/CNR115/2173/0.62	98	2	0
Ni/CNR115/2173/0.62_TCE	62	0	38
Ni/CNR115/2173/26.54	87	0	13
Ni/CNR115/2173/26.54_TCE	60	0	40

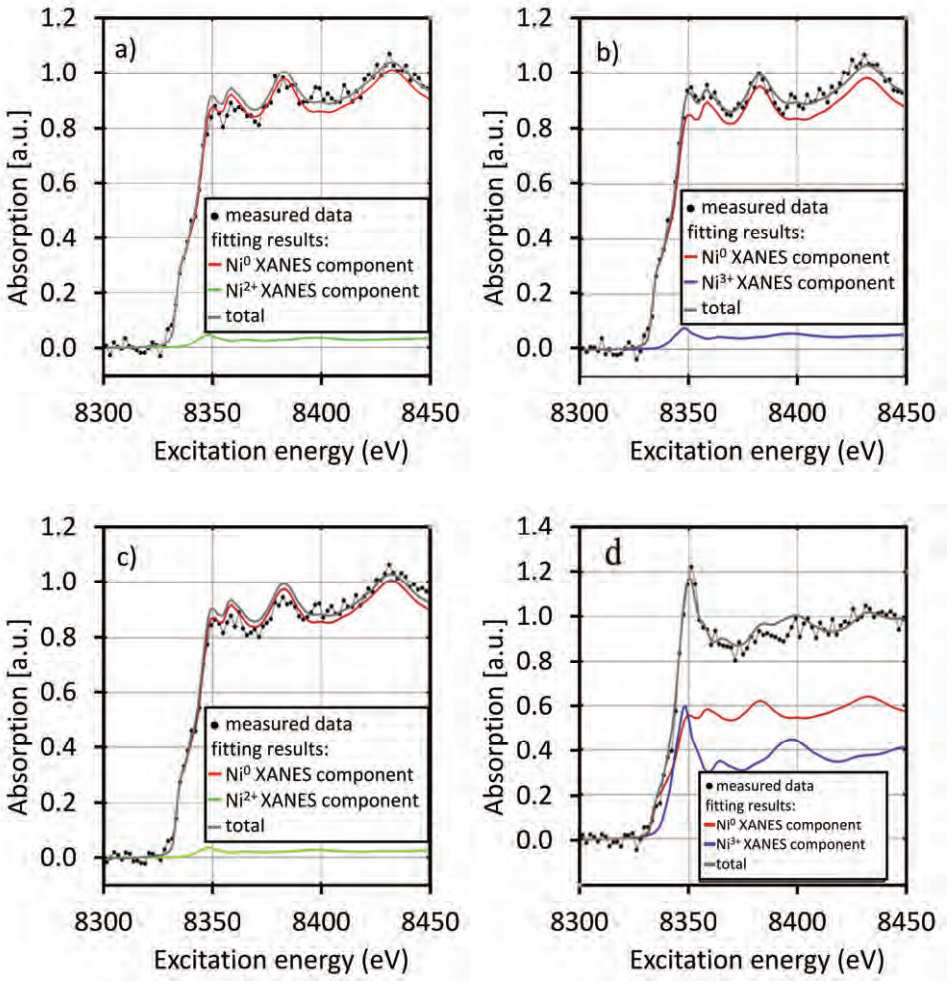

Figure 36. The Ni K-edge X-ray absorption spectrum for a) Ni/CNR115/2173, b) Ni/CNR115/2173_TCE, c) Ni/CNR115/2173/0.62 and Ni/CNR115/2173/0.62_TCE and fitted dominant spectral components.

Additional temperature-programmed hydrogenation experiments of spent samples showed the formation of carbonaceous deposits during catalytic hydrodechlorination, confirmed by the release of CH_4 (m/z = 15, **Figure 37**) and C_2H_X (m/z = 28, **Figure 38**). This phenomenon was the strongest for the most active catalyst – Ni/CNR115/2173/26.54. The carbon-containing species were strongly connected with Ni surface and desorbed at the temperature range of 580-750 K. The observed signal increase at higher temperatures indicated

the gasification of the carbon support material, which is typical for this kind of support.

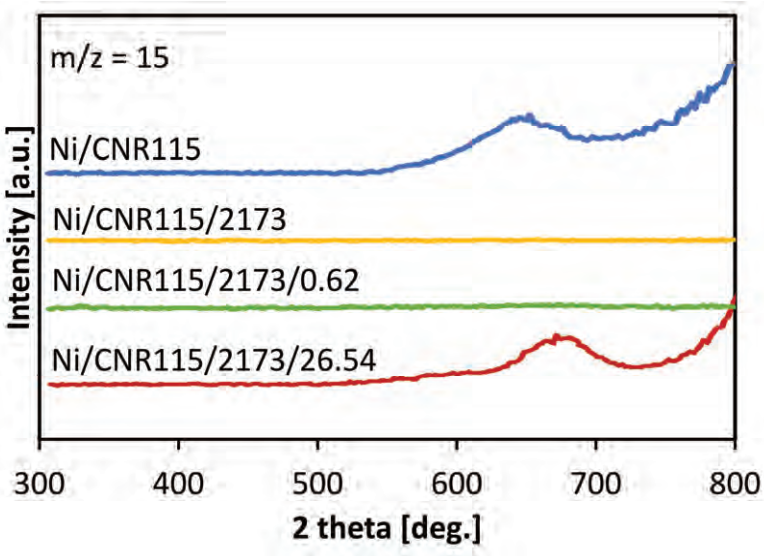

Figure 37. TPH profiles for the formation of methane after TCE HDC.

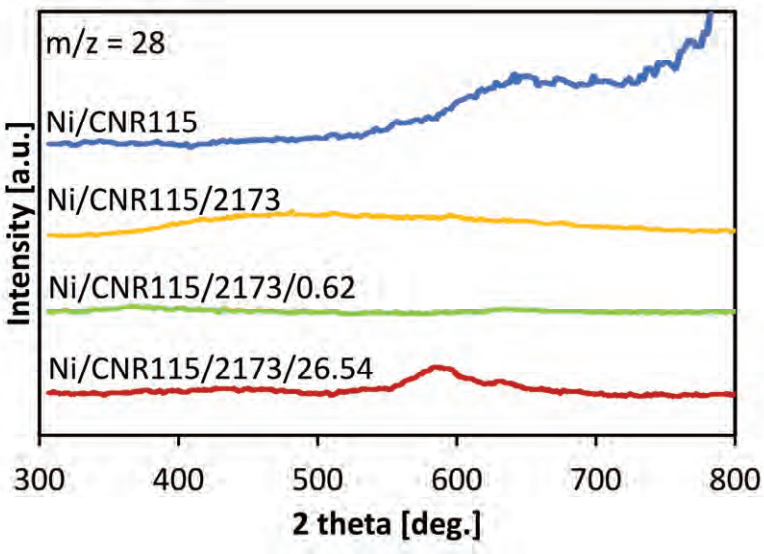

Figure 38. TPH profiles for the formation of C_2H_x species after TCE HDC.

All of the results obtained for Ni nanoparticles deposited on carbon materials proved their efficiency in the catalytic hydrodechlorination of trichloroethylene, both in batch and flow conditions. In general,

bigger Ni nanoparticles are more resistant to deactivation, and as a result, showed higher overall activity in the purification process. The optimal metal particles can be obtained by the application of the specific metal precursor and appropriate pretreatment conditions, like $NiCl_2$ and 673 K in the stream of 10 % H_2/Ar for 3 h, respectively.

Moreover, the properties of carbon materials are crucial for the catalyst morphology and catalytic performance. Hydrophobic character improves the resistance for ionic poisons in the aqueous phase. High surface area and porosity are necessary for satisfactory activity. Additionally, the electron deficiency character of the turbostratic structure increases the Ni nanoparticles activity.

Finally, extraordinary results obtained in continuous-flow conditions for the catalysts with negligible efficiency in the batch reactor opens completely new perspectives in water purification. Batch operations are still the most commonly applied in the aqueous phase hydrodechlorination and allow for removing higher amounts of trichloroethylene per unit of time [211]. However, flow mode offers: the possibility of performing long-term processes, reduces the time needed for scale-up, and eliminates the external separation of the catalyst and products. Hence, the application of the continuous-flow in catalytic water purification seems to be a promising alternative for the most common purification methods.

5.1.5 Hydrodechlorination of diclofenac in the aqueous phase with Pd nanoparticles supported on various support materials

Water pollution with trichloroethylene is a persistent and very well-known problem. However, raw freshwater may contain a lot of other anthropogenic chemicals. Sometimes the type of pollutant and contamination sources are not very obvious, and hence it is tough to identify and eliminate them. The presence of active pharmaceuticals in the aquatic systems is a relatively new recognized issue that has received enormous attention in the last few years.

Among detected pharmaceuticals, one of the most frequently observed in the environment is diclofenac, the very popular non-steroidal anti-inflammatory drug.

Due to the limited literature about catalytic hydrodechlorination of diclofenac in the aqueous phase, there was a rational need to start new research with catalysts showing well-known hydrogenolytic properties. Hence, a series of palladium-based catalysts was synthesised by various methods (**Chapter 4.1.3 - 4.1.5**). Independently from the used technique, all of them contained 1 wt.% of Pd. Metal precursors were selected based on the zeta-potential and the isoelectric point of a support surface [235,236]. Siliceous dealuminated BEA zeolite has a low isoelectric point (~2.0), similar to SiO_2 (~2.0). On the other hand, γ-Al_2O_3 has a lower charge and high isoelectric point (~6.0). Therefore Pd-loaded catalysts were prepared by the impregnation of two different zeolites (SiBEA with Si/Al = 1300 and HAlBEA with Si/Al = 19) with the aqueous solution of $PdCl_2$ (Pd@SiBEA and Pd@HAlBEA). The other two Pd-supported catalysts were synthesised by the ion exchange between the hydroxyl group of silica and $[Pd(NH_3)_4](NO_3)_2$ (Pd/SiO_2) and incipient wetness impregnation with $Pd(NO_3)_2$ (Pd/Al_2O_3). Each one of the 1 wt.% containing catalysts was calcined in the air flow at 773 K for 3 h and reduced in 10 % H_2/Ar for 3 h at 673 K. A more detailed description of the synthesis procedure is placed in the **Chapter 4.1.3 – 4.1.5**.

Physicochemical evaluation of the obtained materials revealed visible differences between the tested catalysts (**Table 11** and **12, Figure 39**). Pd-loaded zeolites showed a microporous structure and a significantly higher specific surface area than Pd supported catalysts (Pd/SiO_2 and Pd/Al_2O_3) with a mesoporous character. Pd@SiBEA and Pd@HAlBEA had similar and noticeably larger nanoparticles with a broad size distribution (**Figure 39a** and **39b**). In terms of the average size, comparable nanoparticles were obtained for Pd/Al_2O_3 (**Figure 39d**). However, their distribution was much more

concentrated. On the other hand, Pd/SiO_2 demonstrated only very small nanoparticles (**Figure 39c**).

Table 11. Surface parameters of 1 wt.% Pd containing catalysts.

Catalyst	Specific surface area [$m^2\ g^{-1}$]	Total pore volume [$cm^3\ g^{-1}$]	Micropores volume [$cm^3\ g^{-1}$]	Mesopores volume [$cm^3\ g^{-1}$]
Pd@SiBEA	390	0.16	0.13	0.03
Pd@HAlBEA	380	0.14	0.10	0.04
Pd/SiO_2	240	1.00	-	1.00
Pd/Al_2O_3	210	0.56	-	0.56

Table 12. The average particles size of 1 wt.% Pd containing catalysts.

Catalyst	The average Pd particles size [nm]	
	CO chemisorption*	TEM
Pd@SiBEA	11	8
Pd@HAlBEA	14	9
Pd/SiO_2	1	2
Pd/Al_2O_3	15	6

* Pd:CO stoichiometry = 1.5.

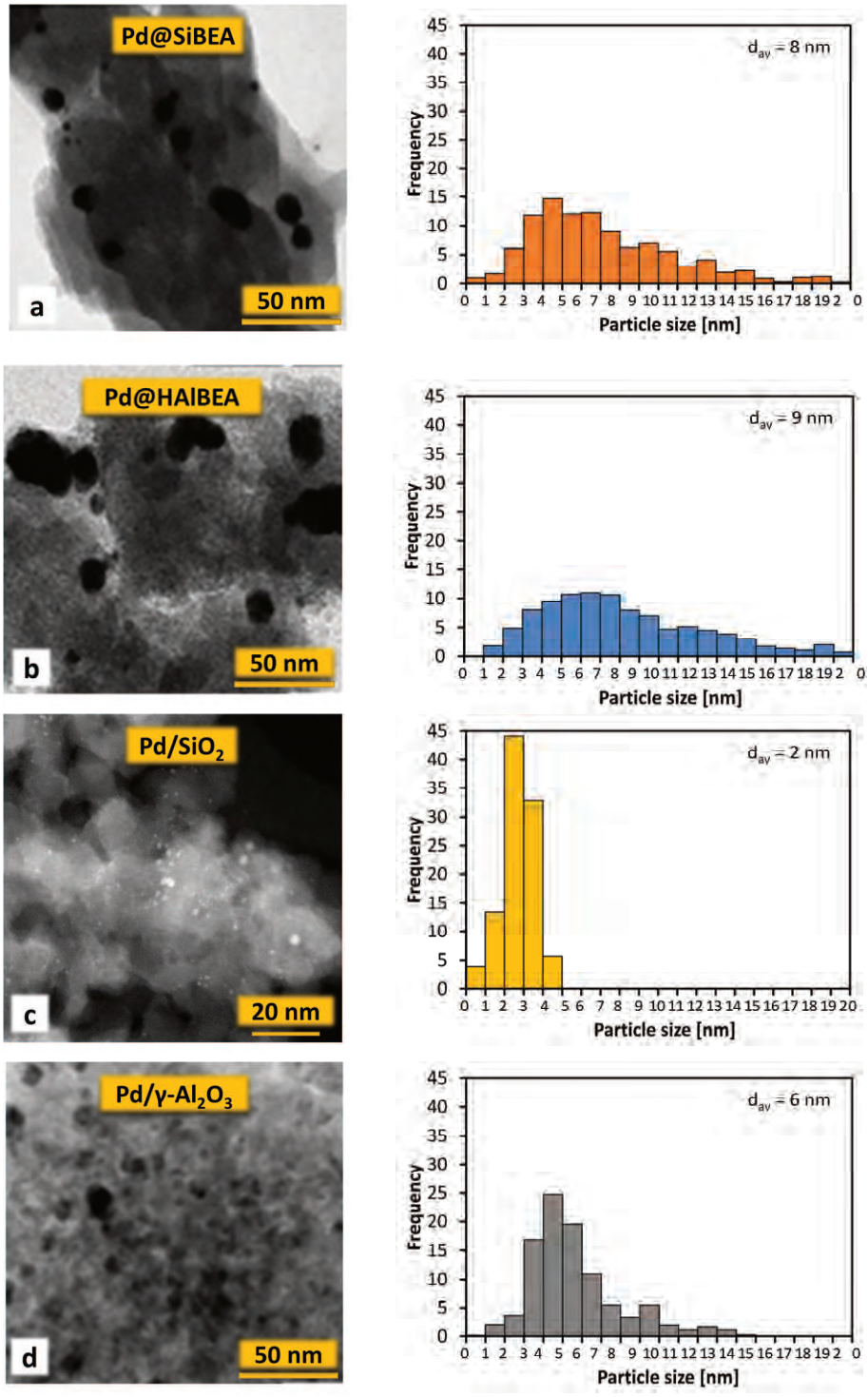

Figure 39. TEM images and Pd particles size distribution in 1 wt.% Pd containing catalysts.

Before catalytic measurements, all of the materials were tested for the sorption capacity of diclofenac. None of them showed any sorption properties in the tested conditions.

The activated forms of the Pd catalysts were used in the diclofenac hydrodechlorination in the aqueous phase (**Figure 40, Table 13**). In each experiment, 2-anilinophenylacetic acid was the only product confirmed by the HPLC-MS analysis. Independent studies performed by Nieto-Sandoval et al. [26] and Wu et al. [149] showed less ecotoxicity of this compound than the original diclofenac. Hence, hydrodechlorination with palladium catalysts proved its high applicability potential in water treatment plants.

Both Pd-loaded zeolites presented a similarly impressive activity in the hydrodechlorination of diclofenac in the aqueous phase (**Figure 40, Table 13**). After 20 minutes of the purification process, Pd@HAlBEA removed 88 % of the initial amount of DCF, while Pd@SiBEA removed 99 %. Despite the differences between those two catalysts, their overall activities were comparable. The final conversions were equal to 95 % and ~100 %, respectively. On the other hand, the Pd supported catalysts demonstrated entirely different results. Pd/Al_2O_3 showed the lowest activity at the beginning of the process, but at the same time, this catalyst constantly purified water for 150 minutes, with only slight signs of deactivation. Completely different behaviour was observed for Pd/SiO_2 with small nanoparticles. Its activity was comparable with Pd loaded zeolites, at least at the beginning of the process. However, Pd/SiO_2 deactivated rapidly after the first 10 minutes of the reaction and finally achieved the lowest overall conversion. All of the above mentioned observations were reflected in the kinetic parameters of the tested catalysts (**Table 13**). The activity of Pd@SiBEA and Pd@HAlBEA expressed in terms of TOF was approximately 6 times higher than the supported catalysts.

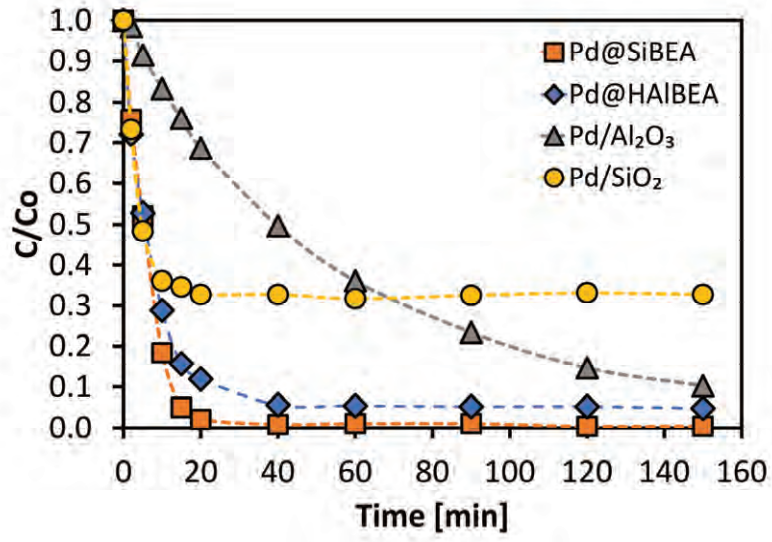

Figure 40. HDC of DCF in the aqueous phase with 1 wt.% Pd containing catalysts, 303 K, 1 atm, 240 μM DCF.

Table 13. Kinetic parameters of 1 wt.% Pd containing catalysts in DCF HDC.

Catalyst	Reaction rate constant k (0 – 150 min) [min^{-1}]	Initial reaction rate r_A (600 s) [mol L^{-1} s^{-1} g_{Pd}^{-1}] x 10^{-4}	TOF [s^{-1}] x 10^{-2}
Pd@SiBEA	0.19	3.43	26.1
Pd@HAlBEA	0.11	2.67	23.7
Pd/SiO_2	0.02	2.37	4.5
Pd/Al_2O_3	0.09	0.72	4.1

The superior activity of the Pd loaded zeolites could be explained in terms of structural parameters determined by the TEM measurements. The average particle size for Pd@SiBEA, PdHAlBEA and Pd/Al_2O_3 can be regarded as comparable. However, their distributions differ significantly (**Figure 39**). In the case of Pd/Al_2O_3, small and large nanoparticles were observed, with 60 % domination of the smaller ones (1-5 nm). Interestingly, in Pd-loaded zeolites, any specific particles fraction's dominance did not exceed 15 % and 11 % for Pd@SiBEA and Pd@HAlBEA, respectively. The catalytic hydrodechlorination of diclofenac in the aqueous phase proved to be a structure sensitive reaction.

This phenomenon could be explained by a different role of different nanoparticles. According to Wu et al. [149], TOF value initially decreased with the increasing metal particle size and then stabilised. It is connected with the fact that smaller nanoparticles contain more cationic species that promote the activation of the C-Cl bond. On the other hand, larger Pd nanoparticles contribute to the more effective activation of the H_2 [149,237]. The catalyst with only small Pd particles (Pd/SiO_2) deactivated more rapidly due to the formation of chlorine deposits [112,238] or the accumulation of organic species [239] under HDC conditions. A sufficient amount of the activated hydrogen may reduce catalyst deactivation. Hence, the catalysts with bigger nanoparticles (Pd/Al_2O_3, Pd@SiBEA and Pd@HAlBEA) demonstrated higher resistance to deactivation. Moreover, broader particle size distribution contributed to better overall catalytic performance (Pd@SiBEA and Pd@HAlBEA).

Above-mentioned conclusions may be the possible explanation for negligible activity of Pd/SiO_2 reported by Wu et al. [149]. However, the obtained at IPC PAS results for Pd/SiO_2 (**Figure 40**, **Table 13**) were much better than presented by Wu et al. [149]. Hence, in order to verify the structure's influence on the catalytic performance, an attempt to increase Pd/SiO_2 efficiency was made. Two different Pd/SiO_2 catalysts with various average nanoparticle size and distribution (Pd/SiO_2(bg) with big Pd nanoparticles and Pd/SiO_2(bim) with bimodal character) were synthesized and compared with already tested material – Pd/SiO_2(s) with small nanoparticles.

Initially performed temperature-hydride decomposition (TPHD) confirmed the achievement of the desired differences (**Figure 41**). Pd/SiO_2(s) and Pd/SiO_2(bg) profiles presented only one peak related to the Pd-hydride decomposition. The literature concerning the relationship between the palladium dispersion and the stability of the Pd-hydride phase indicate temperature shift towards higher temperatures for bigger Pd nanoparticles [215,240]. Such alteration in the peak's profile was observed for Pd/SiO_2(bg).

Simultaneously, the maximum of the peak detected for Pd/SiO_2 was located at a significantly lower temperature (**Figure 41**). Moreover, Pd/SiO_2(bim) contained precisely the same types of particles as for the unimodal catalysts – Pd/SiO_2(s) and Pd/SiO_2(bg). The bimodality was only observed for the material synthesised by incipient-wetness impregnation with the aqueous solution of $PdCl_2$. It was in agreement with the previous research, which showed the effect of chloride ion on the formation of mobile metallic chlorides at the specific activation conditions. These species can migrate on the surface of the support material and contribute to the formation of big aggregates [217,241,242].

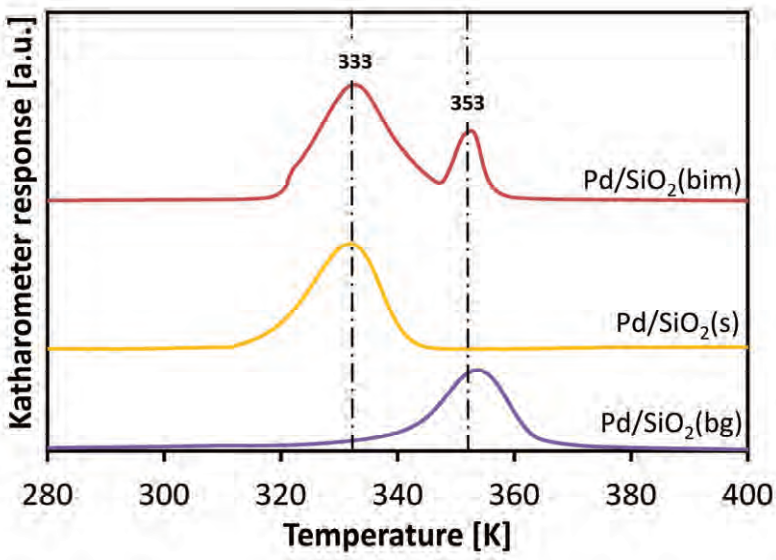

Figure 41. Temperature-programmed hydride decompositions for the series of Pd/SiO_2 catalysts with unimodal and bimodal character.

Physicochemical characterization of Pd/SiO_2 catalysts showed that the only differences between them were related to the average nanoparticle size and distribution (**Table 14, Figure 42**). Each catalyst showed well-developed porosity with a high specific surface area and a large pore volume. On the other hand, the clear and different maximum in the particles size distribution could be observed for all of the tested materials (**Figure 42**).

Table 14. Physicochemical characterization of Pd/SiO_2 catalysts with different particles average size and distribution.

Parameter	Pd/SiO_2		
	(s)	(bim)	(bg)
Surface area [$m^2\ g^{-1}$]	240	240	240
Pore volume [$cm^3\ g^{-1}$]	1.0	1.0	1.0
Average pore diameter [nm]	17	17	17
Average particles size [nm] TEM	1.6	2.9	3.4
Dispersion [%]	86	28	11

The results of the diclofenac hydrodechlorination in the aqueous phase are collected in **Figure 43**. Due to the different metal loading in the tested materials, the amount of the catalyst in each experiment was adjusted based on the dispersion values (**Table 14**). This correction allowed to ensure the same number of Pd active centres in every experiment.

The catalyst with the smallest nanoparticles (Pd/SiO_2(s)) showed the lowest efficiency (**Figure 43**). Only 40 % of the initial amount of DCF was removed till the 20^{th} minute of the process, and then the catalyst deactivated. Pd/SiO_2(bg) removed approximately 80 % of the contamination in the same time, but also deactivated after 20 minutes (**Figure 43**). Pd/SiO_2(bim) with a bimodal character of Pd particle size distribution showed greater efficiency – it completely purified water in 60 minutes. All of these results were in agreement with the previous observations. The smaller nanoparticles demonstrated a higher ability to activate diclofenac than H_2 but also had the tendencies to more rapid deactivation [149]. On the other hand, bigger Pd nanoparticles activated H_2 more efficiently. Nevertheless, only the specific combination of small and big nanoparticles, demonstrated in bimodal catalyst, resulted in satisfactory results (**Figure 43**).

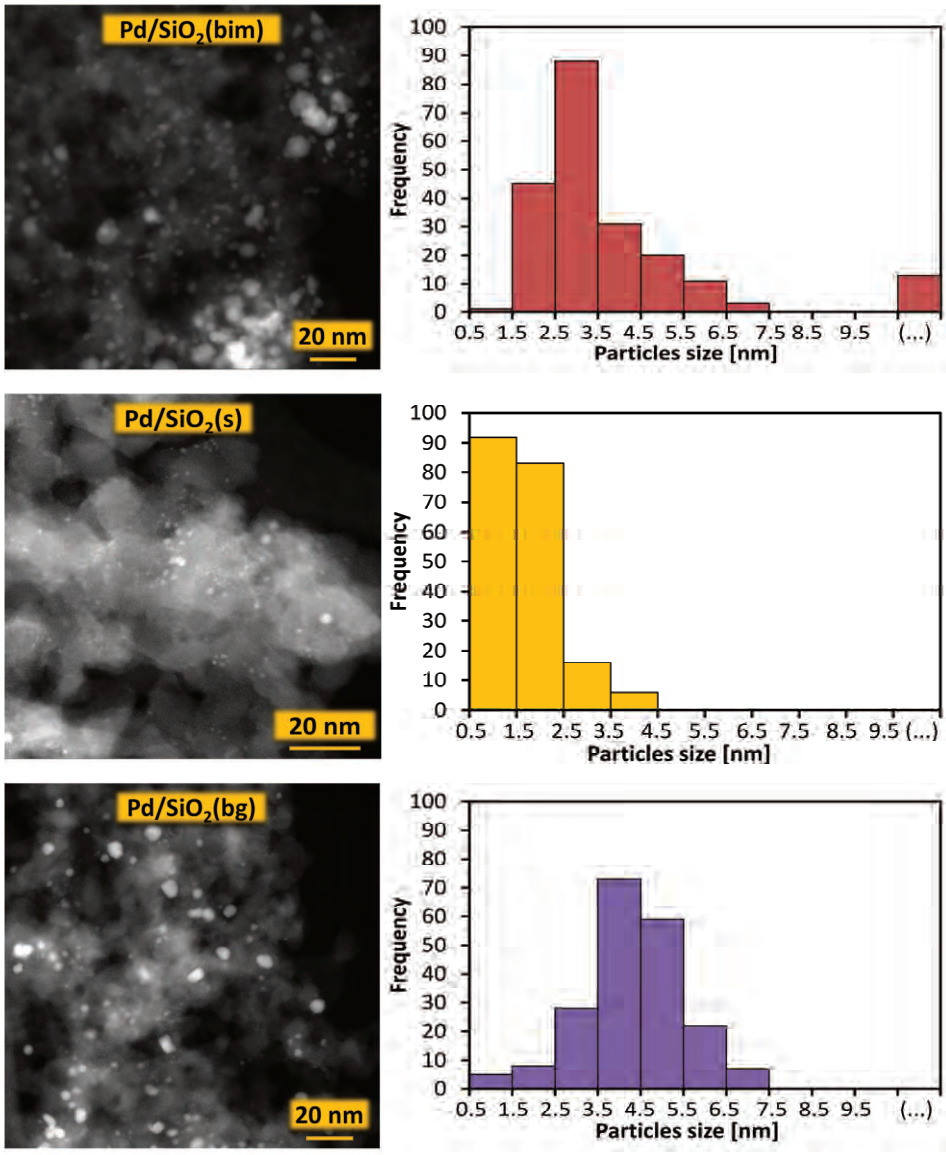

Figure 42. TEM images of Pd/SiO_2 with different average particles size and distribution.

In order to verify the positive impact of bimodal character on the catalytic performance, the physical mixture of unimodal catalysts was prepared. The amount of each catalyst was established based on the TPHD results (**Figure 41**). Although the physical mixture showed better efficiency than both unimodal catalysts, it was still slightly worse than Pd/SiO_2(bim) (**Figure 43**). Such a difference indicates that the Pd nanoparticles with a different size

should exist in close proximity in order to obtain the best catalytic performance. Moreover, only the specific ratio between small and large Pd nanoparticles guarantee adequately high catalytic activity.

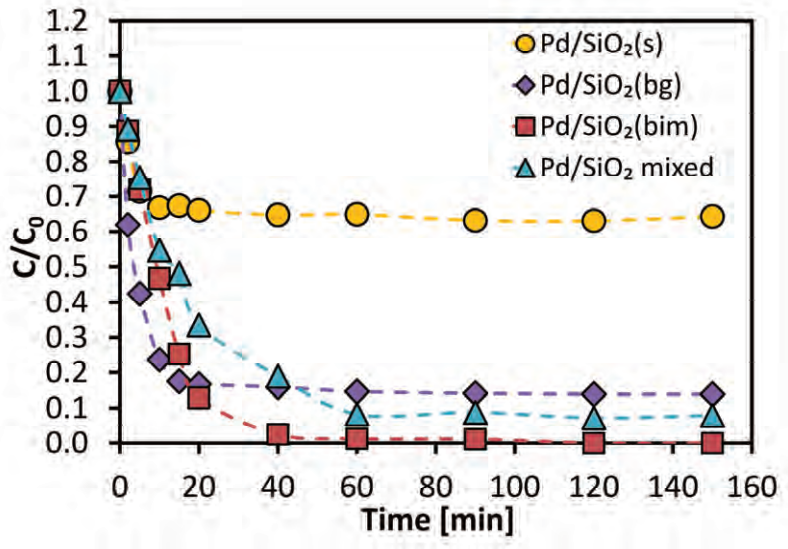

Figure 43. HDC of DCF in a batch reactor with Pd/SiO_2 catalysts with various average particles size and distribution, 240 μM DCF, 303 K, 1 atm.

Additionally, the best bimodal Pd/SiO_2(bim) was also tested in the flow reactor (**Figure 44**). As in the batch experiments, the sorption properties of SiO_2 did not play any role in the water purification from diclofenac. On the other hand, the same catalyst was able for constant removal of diclofenac for 10 h, and did not show any signs of deactivation.

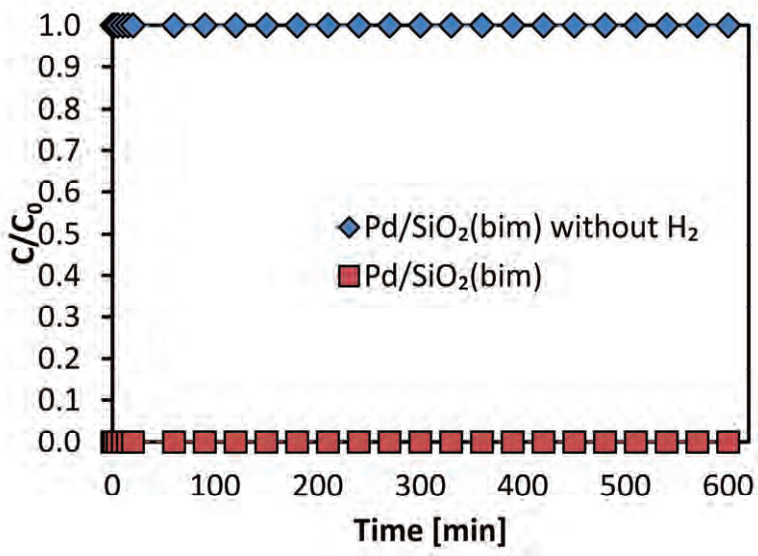

Figure 44. Sorption properties and catalytic performance of Pd/SiO_2 catalyst with bimodal character in HDC of DCF, 303 K, 10 atm, 0.24 μmol/min DCF.

There is limited literature data related to the catalytic removal of diclofenac from water. However, the comparison of the above-presented results with the experience of other research groups [26,145–149] clearly shows that our Pd catalysts proved to be very effective in this reaction. It should be stressed here that such high catalytic performance as obtained for Pd loaded zeolites has not been reported yet [26,145,146]. Moreover, the modification of the particles size distribution of Pd/SiO_2 catalysts allowed to achieve purification efficiency comparable with other catalysts [26,145,146], even despite the previously reported inactivity of Pd/SiO_2 [149].

The majority of the studies on the catalytic hydrodechlorination of chloroorganic compounds aim to synthesise catalysts with metal nanoparticles with the narrowest possible size distribution. However, the high activity of bimodal catalyst suggests a beneficial role of close proximity of nanoparticles of different size. The presented results suggest that striving for unifying nanoparticles may not be the only solution in the hydrodechlorination processes.

5.2. Catalytic hydrogenation for industrial applications

5.2.1 Catalytic hydrogenation of nitrocyclohexane with$PdTSNH_2$ catalyst

Most of the previous studies on the catalytic hydrogenation of nitrocyclohexane were performed in batch reactors at elevated pressure and temperature [189,190,192,193,196,197]. Only one research was done in the gas flow [199]. Hence, the initial experiments of nitrocyclohexane hydrogenation in the liquid flow reactor were performed with a catalyst showing well-known hydrogenolytic properties.

A palladium-based catalyst was selected for the preliminary studies on the nitrocyclohexane hydrogenation. $PdTSNH_2$ catalyst was synthesised by Pd nanoparticles grafting on the commercially available polymer terminated by amino group (TentaGel-S-NH_2), as was described in details in **Chapter 4.1.6.** Active form of the catalyst was characterized by elemental analysis (AAS and ICP-OES), XRD, XPS and miscroscopic techniques.

Elemental analysis of the obtained catalyst, performed by atomic absorption spectroscopy (AAS) and inductively coupled plasma-optical emission spectrometry (ICP-OES), revealed that the Pd loading in $Pd/TSNH_2$ was equal to 2.2 wt.%.

In the second step, $PdTSNH_2$ and parent polymer were subjected to XRD measurements (**Figure 45**). Both samples revealed reflections characteristic for polymeric resin, which were not affected by the Pd nanoparticles presence. The additional signal at $2\theta = 40.1°$ associated with Pd (1 1 1) was observed for $PdTSNH_2$. Based on the peak broadening, the average Pd nanoparticle size was estimated at 4 nm.

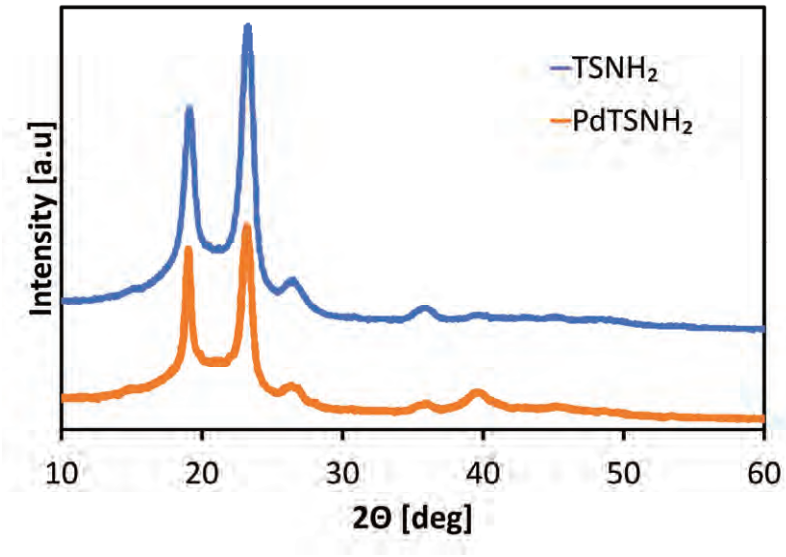

Figure 45. XRD results for pure polymer and $PdTSNH_2$.

The oxidation state of Pd nanoparticles was determined in further investigation with X-ray photoelectron spectroscopy. The obtained results are collected in **Table 15**. The Pd $3d_{5/2}$ peaks for Pd and PdO appeared at 334.38 eV and 335.56 eV [243,244], respectively. Compared to the reported bulk composition [8], the small shift towards lower energies and slight asymmetry of the peak implies the existence of Pd species in the nanoparticulated form [244]. Additionally, the total concentration of palladium on the catalyst surface was estimated at 1.54 at.%.

Table 15. Binding energies of the Pd $3d_{5/2}$ and Pd $3d_{3/2}$ of the $PdTSNH_2$ catalyst.

	BE [eV]	FWHM	Area [%]
3 $d_{5/2}$	334.38	1.36	48.11
3 $d_{5/2}$	339.64	1.36	32.04
3 $d_{5/2}$	335.65	1.36	8.29
3 $d_{5/2}$	340.91	1.36	5.52
3 $d_{5/2}$	336.95	1.36	3.63
3 $d_{3/2}$	342.21	1.36	2.41

TEM imaging confirmed the observations from XPS. SEM and TEM investigation showed that small nanoparticles were well dispersed

on the polymer surface. An average nanoparticle size was estimated at ~ 2 nm (**Figure 46**).

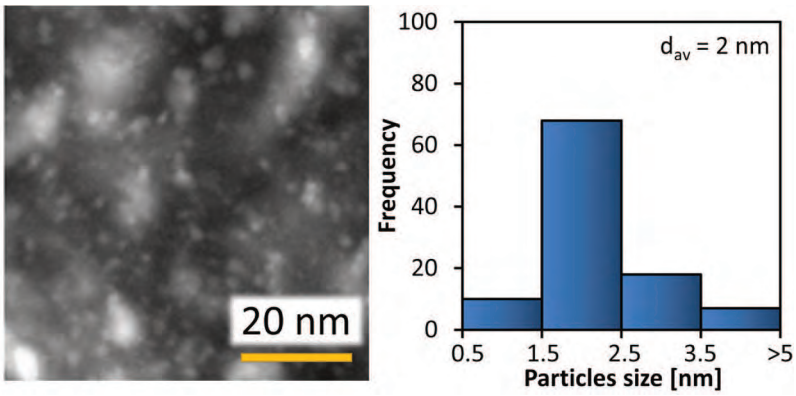

Figure 46. TEM results and particle size distribution for 2.2 wt.% $PdTSNH_2$.

The general assumption for the catalytic hydrogenation of nitrocyclohexane in the liquid flow reactor was to conduct the process at conditions comparable with batch hydrogenation studies [189,190,192,193,196,197]. Hence, all of the experiments were performed at a relatively low-pressure range (1 – 10 bar) and broad temperature range (298 – 303 K). Moreover, in the research mentioned above [189,190,192,193,196,197], on average 0.6 g of nitrocyclohexane (3.87 mol) and 0.1 g of a catalyst was used in batch experiments. Hence, the application of the same amount of a catalyst with a combination of 20.5 μmol_{NC} min^{-1} flow ensured the contact of a comparable amount of the substrate with a catalyst during a 3 h process (3.69 mol). This operation allowed for some comparison with the reported results [189,190,192,193,196,197].

The application of $PdTSNH_2$ in NC hydrogenation led to the formation of two different products: cyclohexanone oxime and cyclohexylamine (**Figure 47**). The influence of the reaction conditions on the catalyst's activity and selectivity was quite well visible (**Figure 47**). The formation of the cyclohexanone oxime did not depend as much on pressure as it depended on the reaction temperature. In general, a higher pressure requires a higher

temperature to achieve 100 % selectivity to cyclohexanone oxime (298 K for 5 bar, 313 K for 10 bar). On the other hand, with increasing temperature and pressure the selectivity to cyclohexylamine also increases. Its maximum value was achieved at 373 K under 2 bar (**Figure 47**).

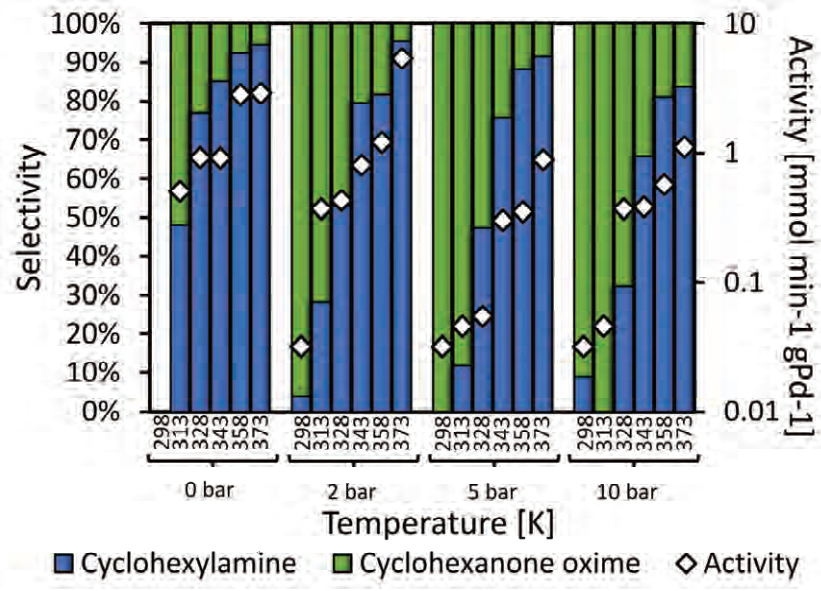

Figure 47. Impact of reaction conditions on the catalytic performance of 2.2 wt.% $PdTSNH_2$ in the hydrogenation of nitrocyclohexane in the liquid flow conditions, 20.5 μmol_{NC} min^{-1}, 60 ml min^{-1} H_2, 0.1 g of catalyst, residence time 2.7 min.

In comparison to the results reported in the literature [190,196,197], $PdTSNH_2$ gave lower conversion. For example, Liu et al. [197] achieved 96.4 % conversion combined with 96 % selectivity to cyclohexanone oxime in the process performed for 3 h at 3 bar and 323 K in ethylenediamine. However, considering that the proposed solution allows for a long-term process, inferior activity is reduced to some extent. Moreover, despite the lower overall activity of $PdTSNH_2$, its selectivity can be easily modified by changing the reaction temperature and pressure. Hence, the catalyst is more universal. Additionally, the application of environmental friendly solvent (ethanol)

increases the attractiveness of $PdTSNH_2$, but also the entire nitrocyclohexane hydrogenation.

5.2.2 Catalytic hydrogenation of nitrocyclohexane with CuZnAl hydrotalcites derived catalysts

The catalytic hydrogenation of nitrocyclohexane with the $PdTSNH_2$ was the first step in development of new catalysts with potential chemical industry applications. Following the international trend of increasing the economic efficiency of catalytic materials, it was decided to switch to low-cost transition metals. Inspired by the results obtained by Zhang et al. [192] for Cu catalysts and the successful application of hydrotalcite derived materials in hydrogenation reactions [245–249], a decision to use CuZnAl hydrotalcites derived catalysts was made.

Two catalysts with a different amount of Cu were prepared following the procedure described in details in Chapter **4.1.7.** Chemical compositions of raw hydrotalcites were determined by ICP-OES (**Table 16**). The obtained results showed slight differences between both materials. However, in each CuZnAl hydrotalcite, zinc and copper were detected at higher amounts than assumed theoretically.

Table 16. Theoretical and determined by ICP-OES Cu, Zn and Al composition.

Hydrotalcite	Molar ratio			
	Theoretical	Determined by ICP-OES		
	Cu:Zn:Al	Cu	Zn	Al
CuZnAl(0.5-1-1)	0.5-1-1	0.61	1.26	1
CuZnAl(1-1-1)	1-1-1	1.23	1.26	1

Before further temperature treatment of raw hydrotalcites, the thermal stability of these materials was determined by thermogravimetric analysis combined with monitoring of H_2O and CO_2 evolution by mass spectroscopy (**Figure 48**). The process of thermal decomposition was similar for both

materials. Each one demonstrated four main regions of mass loss, which were comparable in terms of temperature range value and percent mass loss (**Table 17**). The first two regions correspond to the process of dehydration and dihydroxylation, during which surface and interlayer water were released and the layered structure of hydrotalcites was collapsed. This was confirmed by changes in blue dotted lines with a peak maximum at 476 K for CuZnAl(0.5-1-1) and 466 K for CuZnAl(1-1-1). The observable peak broadening was caused by the water bound on metal in the form of hydroxyl groups. The third region (800 K – 1000 K) correspond to the release of CO_2 from the hydrotalcites interlayer region, where it was bounded as carbonate anions. This process allowed for the formation of new acid-base sites, previously blocked by carbonates, which are desired in the catalytic hydrogenation of nitrocyclohexane. However, at a temperature above 923 K, there is a possibility of spinels formation, which are inactive in hydrogenation processes. Hence, this temperature should not be exceeded in order to obtain the active form of CuZnAl materials. The last fourth region was also connected to the release of CO_2, with a maximum at 1094 K for CuZnAl(0.5-1-1-) and at 1023 K for CuZnAl(1-1-1).

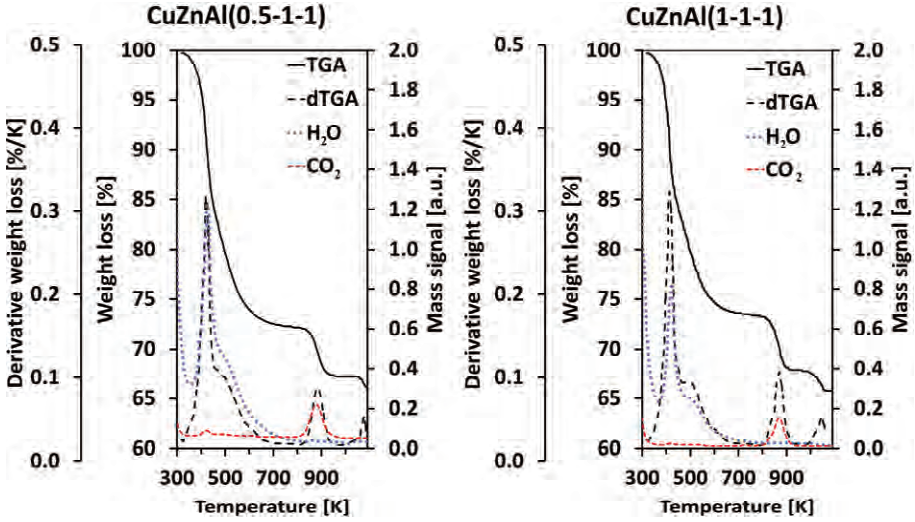

Figure 48. TGA and dTGA of CuZnAl(0.5-1-1) and CuZnAl(1-1-1).

Comparative analysis between tested hydrotalcites showed that CuZnAl(0.5-1-1) is more thermally stable, which can be the effect of lower amount of Cu in its structure. The obtained results allowed for the determination of safe temperature conditions for further treatment of the materials. Hence, both CuZnAl hydrotalcites were calcined at 773 K for 3 h in the air stream, which led to the formation of mixed oxides materials.

Table 17. Quantification of TGA experiments.

CuZnAl	I [wt.%]	T_{max} [K]	II [wt%]	T_{max} [K]	III [wt%]	T_{max} [K]	IV [wt%]	T_{max} [K]	Total [wt%]
0.5-1-1	18.56	433	9.23	499	5.04	916	1.25	1023	34.08
1-1-1	16.44	472	10.03	511	5.73	903	2.14	1094	34.34

The mixed oxides were subjected to temperature-programmed reduction measurements (TPR) (**Figure 49**). For both CuZnAl materials, two unseparated but distinguished peaks were observed, with a clear shift towards lower temperatures for CuZnAl(0.5-1-1). The presence of two peaks related to Cu reduction is usually explained in the literature by the existence of different copper species with a different availability for hydrogen [250–252]. For example, the reduction process of highly dispersed CuO occurs at a much lower temperature than for aggregated species. Moreover, CuO with a stronger interaction with a support material reduces at higher temperatures [253]. Considering the results of further characterisation tests, the reported effects [250–253] may be the reasonable explanation of results obtained for CuZnAl(0.5-1-1) and CuZnAl(1-1-1). However, the existence of two copper reduction peaks may also be the effect of a subsequent reduction of Cu^{2+} to Cu^{1+} and Cu^{1+} to the metallic form, in which Cu_2O appears as a stable intermediate form [254]. For samples activated at 673 K for 3 h in 10 % H_2/Ar, additional measurements showed relatively high reducibility of Cu species in CuZnAl materials (~ 98 %).

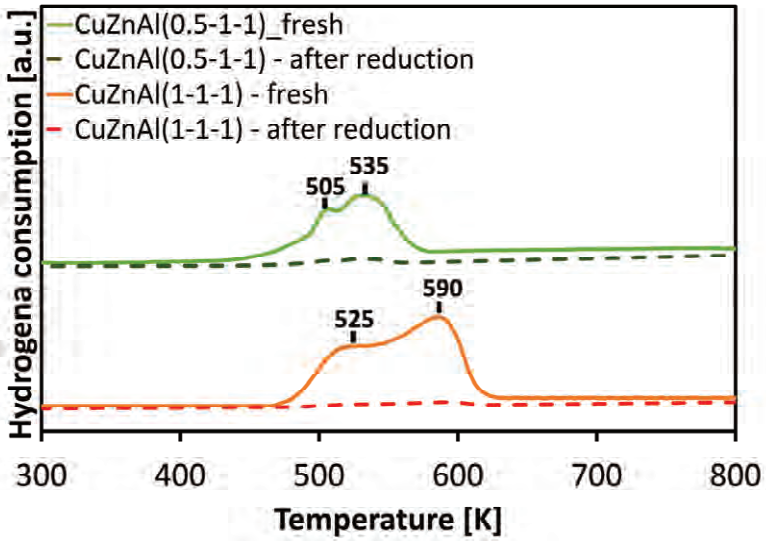

Figure 49. TPR of CuZnAl mixed oxides and CuZnAl catalysts after activation procedure performed at 673 K for 3 h in 10 % H_2/Ar.

The surface analysis of CuZnAl catalysts showed differences between those two materials (**Table 18**). CuZnAl(1-1-1) had a significantly lower specific surface area than CuZnAl(0.5-1-1). Nevertheless, both catalysts demonstrated similar pore volume. Additionally, the determined Cu surface area, in accordance with Witoon et al. [255], was relatively low for both CuZnAl catalysts (**Table 18**).

Table 18. Surface area, porosity and Cu surface area of activated CuZnAl catalysts.

Catalyst	Specific surface area [$m^2\ g^{-1}$]	Total pore volume [$cm^3\ g^{-1}$]	Mesopores pore volume [$cm^3\ g^{-1}$]	Cu surface area [$m^2\ g_{cat}^{-1}$]
CuZnAl(0.5-1-1)	115	0.24	0.16	7.4
CuZnAl(1-1-1)	60	0.18	0.13	10.7

Acid-base properties seem to be an essential parameter for nitrocyclohexane hydrogenation [189,190,192,193,196,197]. Hence, the amounts and strength of acid and basic sites in CuZnAl materials were determined in temperature-programmed desorption experiments with NH_3 and CO_2 (**Figure 50**).

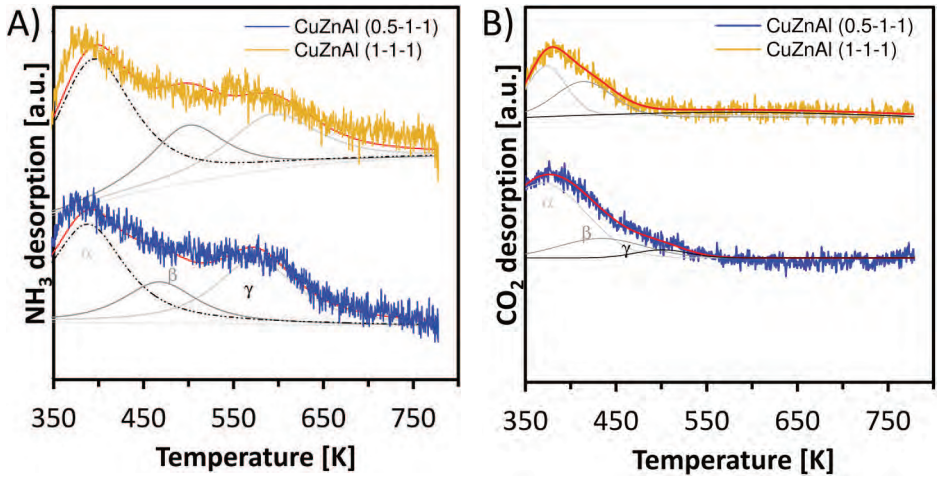

Figure 50. A) NH_3-TPD and B) CO_2-TPD profiles for CuZnAl(0.5-1-1) and CuZnAl(1-1-1) catalysts.

In agreement with the literature, NH_3-TPD profiles showed three desorption maxima (**Figure 50A**), which could be attributed to weak, strong, and moderate acidic sites (α, β and γ) [256]. However, for tested catalysts, there was a noticeable shift of desorption peaks towards higher temperatures (~ 20 K). The presence of the Lewis and Brønsted acid sites have been reported before for CuZnAl [256]. The Lewis acid sites proved to be generated by the deposition of alumina and zinc onto copper surface [257]. On the other hand, Brønsted acid sites' formation is the effect of substitution of $^{3+}$ cation into copper, which produce a labile proton (bonded to the surface by ionic forces) [258]. Moreover, strong Brønsted acid sites are produced by electronegative cations of alumina [256]. Both tested materials differed in the number of different acid centres. The catalyst with higher copper content contained

approximately 38 % more acidic sites, with significant domination in the number of weak acid sites (**Table 19**).

Table 19. Distribution of acidic sites on CuZnAl catalysts.

Catalyst	Acidic site distribution [$mmol_{NH3}$ g^{-1}]			
	Weak	Moderate	Strong	Total
CuZnAl(0.5-1-1)	1.4	0.6	1.1	3.1
CuZnAl(1-1-1)	2.3	0.8	1.2	4.3

On the other hand, temperature-programmed desorption of CO_2 allowed for the investigation of the Lewis and Brønsted basic sites in CuZnAl materials (**Table 20, Figure 50B**). As for acidic sites, both profiles were deconvoluted into three peaks related to weak, moderate and strong basic sites. The presence of weak type (α) was related to OH^- groups, medium (β) to metal-oxygen pairs (i.e. Zn–O, Al–O and Cu–O) and strong (γ) to low-coordination oxygen atoms [259]. The overall amount of basic centres was 25 % higher for CuZnAl(0.5-1-1), suggesting that basicity decreases with Cu content. However, it is only observed in the case of weak sites. The number of moderate and strong centres increased. Such observations could be explained in terms of alumina's weak basicity, which could be significantly influenced by Cu and Zn presence on the surface. Hajduk et al. [256] demonstrated that in multicomponent mixed oxide systems, the overall acidic-alkaline characteristics are often dominated by one cation-type component. Hence, the weak basicity of alumina was diminished with increasing Cu concentration in CuZnAl(1-1-1). Stronger basicity was related to unsaturated metal cations, which were able to act as Lewis basic sites [256]. Additionally, higher specific surface area combined with alumina weak basic sites could contribute to greater basicity of CuZnAl(0.5-1-1).

Table 20. Distribution of basic sites on CuZnAl catalysts.

Catalyst	Basic site distribution [$mmol_{CO2}$ g^{-1}]			
	Weak	Moderate	Strong	Total
CuZnAl(0.5-1-1)	83.7	9.6	4.1	97.4
CuZnAl(1-1-1)	35.3	29.7	8.5	73.5

Temperature treatment of CuZnAl hydrotalcites and then CuZnAl mixed oxide materials induced structural changes. XRD measurements performed for CuZnAl materials at each stage of their biography allowed for tracking and monitoring these effects (**Figure 51** and **52**).

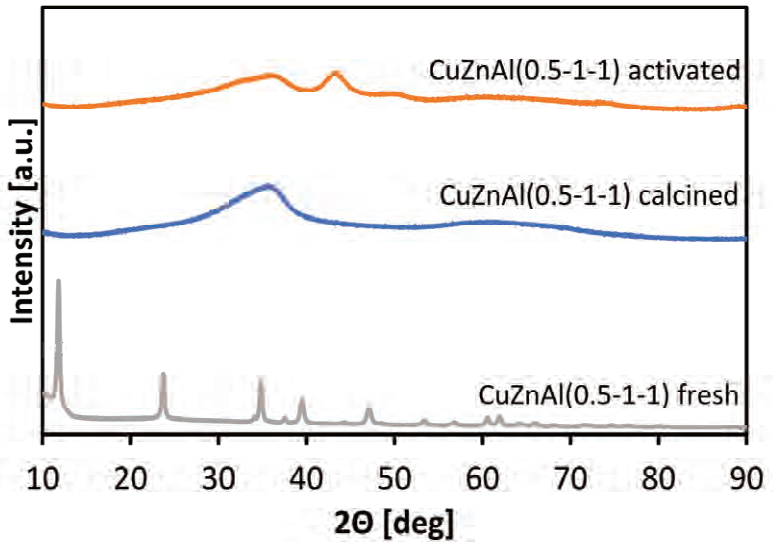

Figure 51. XRD profiles of CuZnAl(0.5-1-1) at different stages of its biography.

For both hydrotalcites, sharp and symmetric diffraction lines were observed at 2θ ~ 11.7°, 23.5°, 34.6°, 39.2°, 46.7°, 60.0° and 61.3°, which proved their high crystallinity and layered structure [260]. The calcination process led to the disappearance of these characteristic reflections and resulted in the appearance of one broad diffraction signal at 2θ ~ 35.6°. This reflection could be attributed to the formation of CuO (2θ ≈ 35.6°, 38.7°, 48.8° [261]) and ZnO (2θ ≈ 31.8°, 34.4°, 36.2°, 56.8° [262]). However, its indistinguishable shape

suggested the amorphous character of the mixed oxides and homogeneous dispersion of CuO and ZnO in Al_2O_3 lattice. Activation of both CuZnAl materials led to the appearance of reflections characteristic for the crystalline form of copper, probably in the form of metal nanoparticles on the surface of mixed oxide support material ($ZnO\text{-}Al_2O_3$).

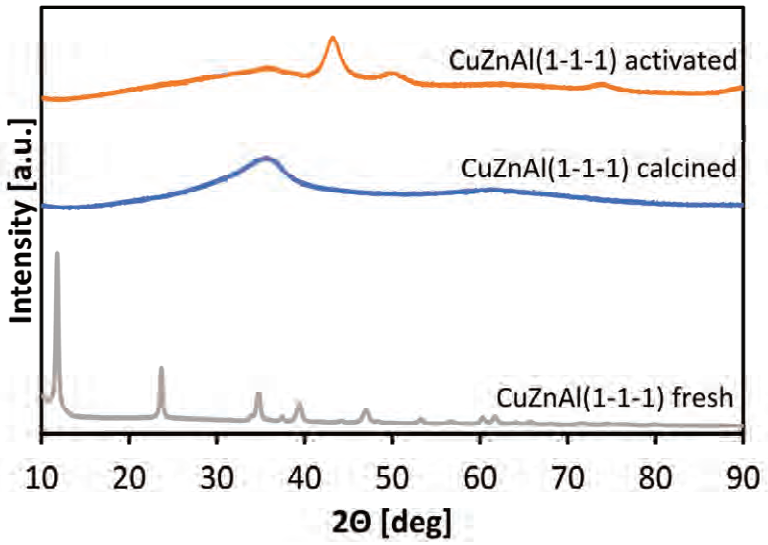

Figure 52. XRD profiles of CuZnAl(1-1-1) at different stages of its biography.

The above results were related to the changes induced in the bulk phase of tested materials. However, only the surface analysis could complement the information about CuZnAl catalysts. Hence, in the next step, the XPS measurements for calcined and activated materials were performed. The application of in-situ reduction allowed for the measurements of precisely the same area of the samples, which ensured a more accurate evaluation of structural differences.

The conducted experiments took into consideration the possible detrimental effects of irradiation for collected results. It is well known that the combined effect of exposure to X-rays and ultra-high vacuum can damage the sample [263]. Moreover, the detailed examination of Cu LMM

Auger lines as well as the Cu 2p XPS core level peak showed remarkable X-ray irradiation effects [264]. Hence, in order to verify the reproducibility of the obtained results, the Cu 2p, Cu LMM and Zn 2p spectra were repeatedly recorded for the activated CuZnAl(1-1-1) with a shorter time of acquisition (1h instead of 2.5 h). The comparative analysis did not show any differences, which confirmed that the chemical states of copper and zinc are relatively stable in the incident radiation.

The comparison of the surface compositions for the materials after calcination and after activation showed significant differences in elements concentration (**Table 21**). Enrichment of the surface with Cu was observed for both catalysts, 1.9 at.% for CuZnAl(0.5-1-1) and 8.5 at.% for CuZnAl(1-1-1). The analysis of copper chemical state indicated the presence of Cu^0, but also Cu^{1+} (Cu_2O) and Cu^{2+} (CuO) (**Table 21**).

Table 21. XPS results for CuZnAl materials after calcination and in-situ activation.

Element, oxidation state, form	CuZnAl(0.5-1-1)		CuZnAl(1-1-1)	
	Composition [at.%]			
	calc	act	calc	act
Cu: Cu^0, Cu^{1+}	8.9	10.8	11.3	19.8
Zn : Zn^{2+} ZnO, $Zn(OH)_2$, $ZnAl_2O_4$	24.8	25.3	17.9	20.2
Al : Al^{3+} Al_2O_3, $Al(OH)_3$, AlOOH, $ZnAl_2O_4$	38.4	40.1	46.9	38.3
O : CuO, Cu_2O, ZnO, Al_2O_3, CO_3^{2-}	24.4	21.1	19.5	18.4
C : C-C/C-H, HCO_3^-/CO_3^{2-}	3.5	2.7	4.1	3.1
Cu/Zn	0.36	0.43	0.63	0.98
Cu/Al	0.23	0.27	0.24	0.52
Zn/Al	0.65	0.63	0.38	0.53

High resolution Cu 2p XPS spectra for both catalysts showed the presence of Cu^0 and Cu^{1+} species, with a broad doublet contribution (main orbital peak located at 932.4 eV). Additionally, also Cu^{2+} species (933.3 eV) and typical poorly resolved and broad satellite features of Cu^{2+} were detected (**Figure 53**).

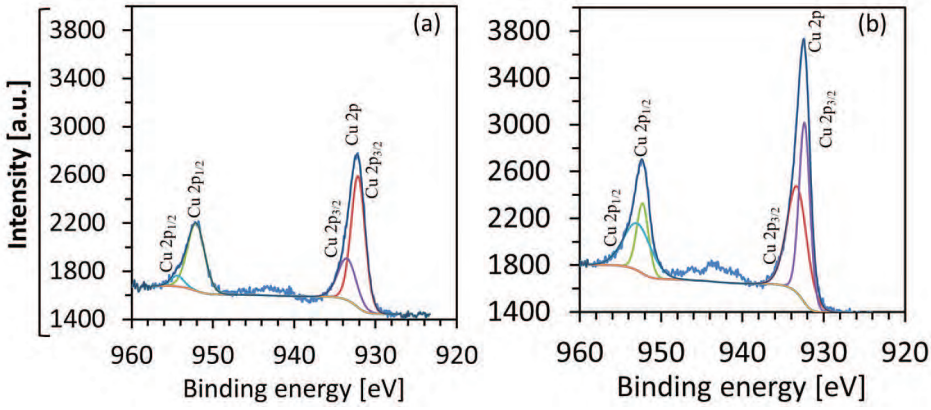

Figure 53. High resolution XPS Cu 2p signal for a) CuZnAl(0.5-1-1) and b) CuZnAl(1-1-1).

Analogous surface analysis for Zn showed a visible increase in zinc surface concentration after activation in the hydrogen stream. Its presence was associated with Zn^{2+} in the form of: ZnO, $Zn(OH)_2$ and/or $ZnAl_2O_4$ (**Table 21**). Additionally, high resolution Zn $2p_{3/2}$ spectra (**Figure 54**) demonstrated a single peak at 1021.7 eV, which indicated the presence of Zn^{2+} (Zn-O) surface species.

The position of the Zn $2p_{3/2}$ peak is slightly shifted towards higher energies in comparison to the reported values (1021.1 eV) [265] (**Figure 54**). It could be explained by a different chemical environment and was assigned to Zn-O-Cu bonds. Based on the electrostatic model, the larger electronegativity of Cu, compared to Zn, induces O → Cu electron transfer in Zn-O-Cu configuration. Such a phenomena led to a shift in electron density of the Zn-O bond toward the oxygen atoms, and in consequence, increased the electron deficiency of the Zn atoms [266]. Moreover, a dynamic SMSI effect in combination with a reduction of ZnO particles may lead to partial coverage of copper

nanoparticles with ZnO_x, which was reported by Behrens et al. [267] for the $Cu/ZnO/Al_2O_3$ catalyst used for methanol synthesis.

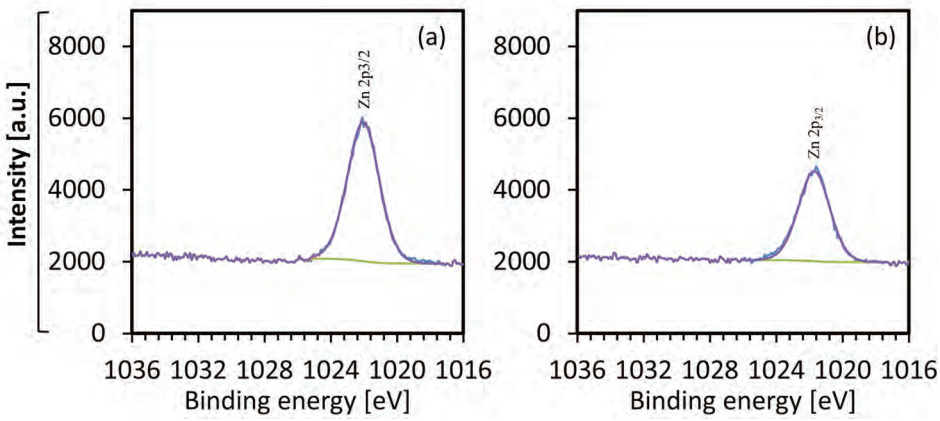

Figure 54. High resolution XPS Zn $2p_{3/2}$ signal for a) CuZnAl(0.5-1-1) and b) CuZnAl(1-1-1).

The surface analysis in terms of the Al concentrations demonstrated a completely different trend. The activation of the CuZnAl(0.5-1-1) increased the aluminium surface concentration by 1.7 at.%. On the other hand, the same process performed for CuZnAl(1-1-1) resulted in a decrease of 8.6 at%. For both catalysts, aluminium was present in the different forms of Al^{3+}: Al_2O_3, $Al(OH)_3$, AlOOH and/or $ZnAl_2O_4$ (**Table 21**). Despite the described results, Al analysis was only an estimation. It was related to the coincidence of Al 2p-Cu 3p and Al 2 s-Cu 3 s photoelectron signals and deconvolution of Al 2p and Al 2 s signals from common signals. Nevertheless, this analysis allowed for the determination of general trends.

The comparison of the XPS results for calcined and activated CuZnAl materials showed a marked increase in the concentration of zinc and copper in the surface layers after the activation step. The enrichment scale was different for tested catalysts. This phenomenon was much stronger for CuZnAl with higher copper concentration and took place at the expense of Al, which moved to the deeper layers (**Table 21**).

HRTEM and STEM-EDS measurements performed for both activated CuZnAl materials allowed for a more profound investigation of the surface of the catalysts (**Figure 55 - 58**). The analysis of average particle size and distribution for CuZnAl(0.5-1-1) showed the narrowly distributed metal nanoparticles (~ 3 nm), which have been identified as CuZn alloy surrounded by ZnO (**Figure 55** and **56**). It was confirmed by STEM-EDS, which revealed the presence of Cu and Zn in the same locations at EDS maps. On the other hand, the distribution of nanoparticles size for CuZnAl(1-1-1) was much broader (with two maxima at 10 and 16 nm), and the average size was equal to 16 nm (**Figure 57**). In this case, phase identification showed Cu-ZnO core-shell structure, where Cu was surrounded by ZnO (**Figure 58**).

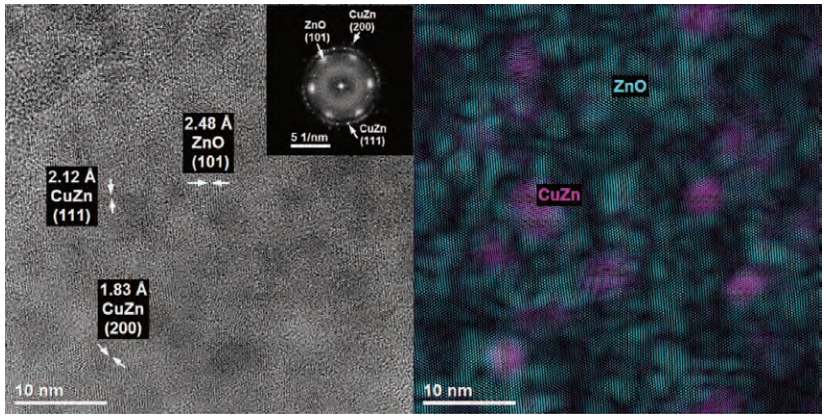

Figure 55. TEM and STEM-EDS results for CuZnAl(0.5-1-1) after activation in 10 % H_2/Ar at 673 K for 3 h.

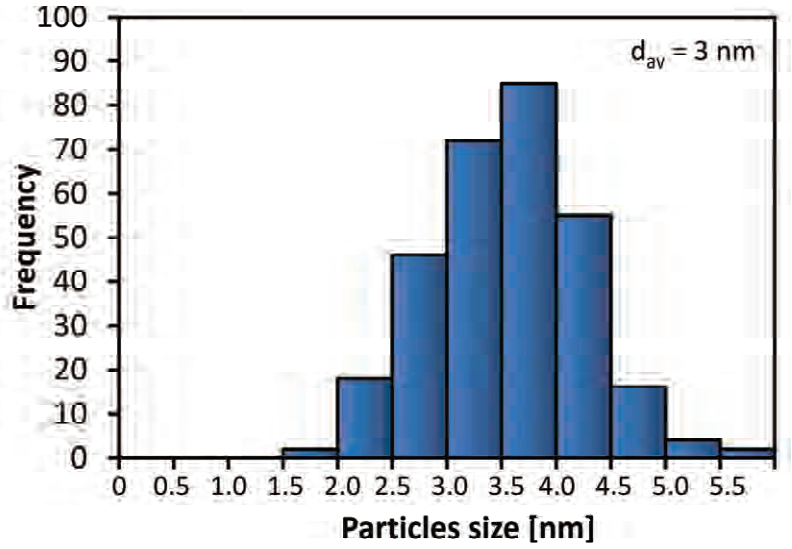

Figure 56. Particles size distribution for CuZnAl(0.5-1-1) after activation in 10 % H_2/Ar at 673 K for 3 h.

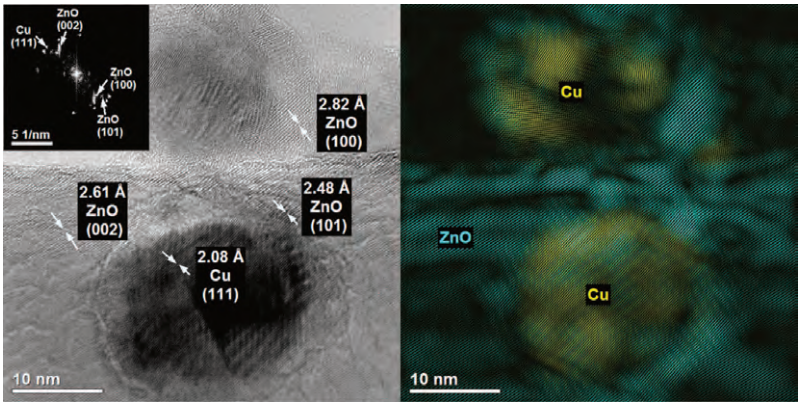

Figure 57. TEM and STEM-EDS results for CuZnAl(1-1-1) after activation in 10 % H_2/Ar at 673 K for 3 h.

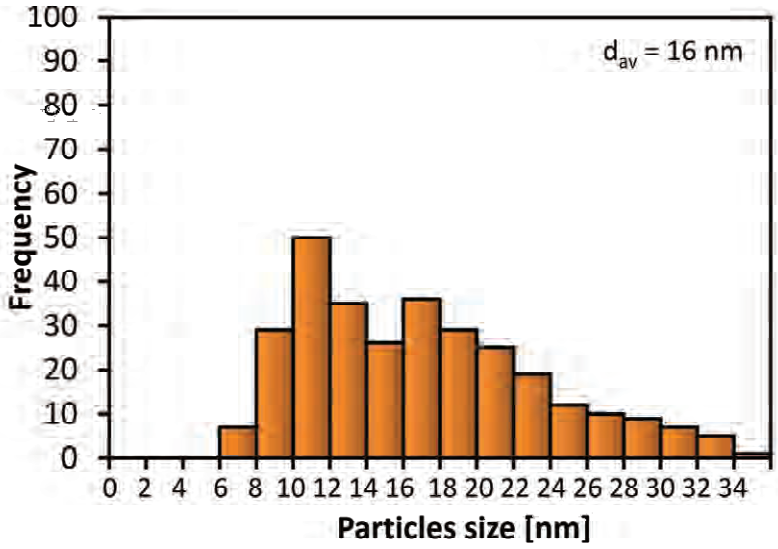

Figure 58. Particles size distribution for CuZnAl(1-1-1) after activation in 10 % H_2/Ar at 673 K for 3 h.

All of the characterisation measurements performed for CuZnAl materials at different stages of their biography revealed similarities and differences in their structure. Seemingly similar catalysts demonstrated substantial differences during TEM analyses, which proved to be essential in the nitrocyclohexane hydrogenation.

Before catalytic experiments, blank tests in all reaction conditions were performed. The obtained results showed negligible activity in all of the whole range of tested temperature and pressure.

On the other hand, both catalysts showed excellent activity and selectivity in nitrocyclohexane hydrogenation (**Figure 59 – 62, Table 22**).

The catalytic performance of CuZnAl(0.5-1-1) at 5 bar is presented in **Figure 59**. The catalyst activity increases remarkably with the increasing temperature. As a result of hydrogenation of nitrocyclohexane in the temperature range of 298-358 K, two products were obtained: cyclohexanone and cyclohexanone oxime. After exceeding the temperature 358 K, the formation of cyclohexanol was observed at the expense of the other

two compounds. Despite the slight fluctuation of selectivity, cyclohexanone was the dominant product in the whole temperature range. An increase in pressure to 10 bar resulted in significant growth of the overall activity, especially at higher temperatures (**Figure 60**). As with the experiments carried out at 5 bar, three reaction products were observed, and cyclohexanone was still the major. However, at higher temperatures, cyclohexanol was produced with a much higher yield. Nevertheless, it should be stressed that in the whole temperature and pressure range, cyclohexanone (necessary in the synthesis of cyclohexanone resins an essential in the production of adipic acid used in nylon production) was the dominant product of catalytic hydrogenation of nitrocyclohexane with CuZnAl(0.5-1-1).

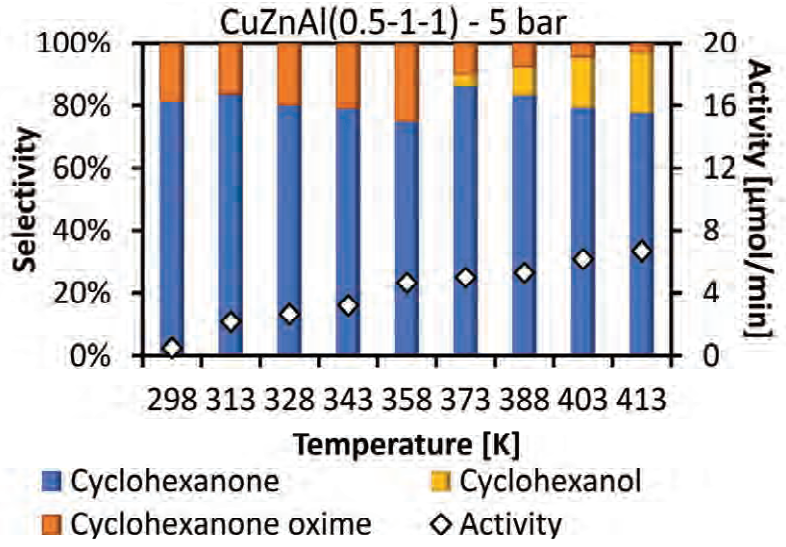

Figure 59. Results of catalytic hydrogenation of nitrocyclohexane with CuZnAl(0.5-1-1), 5 bar, 60 ml min^{-1} H_2, 20.5 μmol_{NC} min^{-1}, 0.1 g of the catalyst, contact time – 96.5 s.

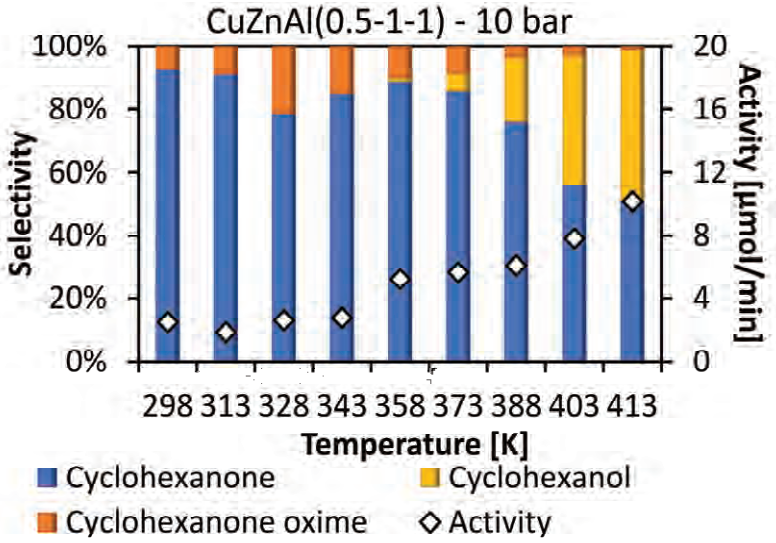

Figure 60. Results of catalytic hydrogenation of nitrocyclohexane with CuZnAl(0.5-1-1), 10 bar, 60 ml min^{-1} H_2, 20.5 μmol_{NC} min^{-1}, 0.1 g of the catalyst, contact time – 96.5 s.

On the other hand, the catalytic performance of CuZnAl(1-1-1) was completely different in the whole temperature and pressure range (**Figure 61** and **Figure 62**). The main product of nitrocyclohexane hydrogenation was cyclohexylamine – an essential building block for pharmaceuticals production. Surprisingly, despite the higher overall activity, this catalyst was completely inactive at temperatures below 358 K. An increase in catalytic activity with increasing temperature was also observed for this catalyst, with a marked maximum at 403 K. However, along with these changes, the catalyst's selectivity also changed. Catalytic hydrogenation of nitrocyclohexane under 5 bar with CuZnAl(1-1-1) resulted in cyclohexanone, cyclohexanol, cyclohexylamine and dicyclohexylamine. The first two substances were detected mainly in the lower temperature range, while the increase in temperature made dicyclohexylamine a major side product. Further application of higher pressure did not change the overall activity of CuZnAl(1-1-1) but affected the catalyst's selectivity (**Figure 62**). The highest efficiency

in cyclohexylamine production at 5 bar was preserved in the reaction conducted at 10 bar, but the selectivity to this compound increased to 100 %.

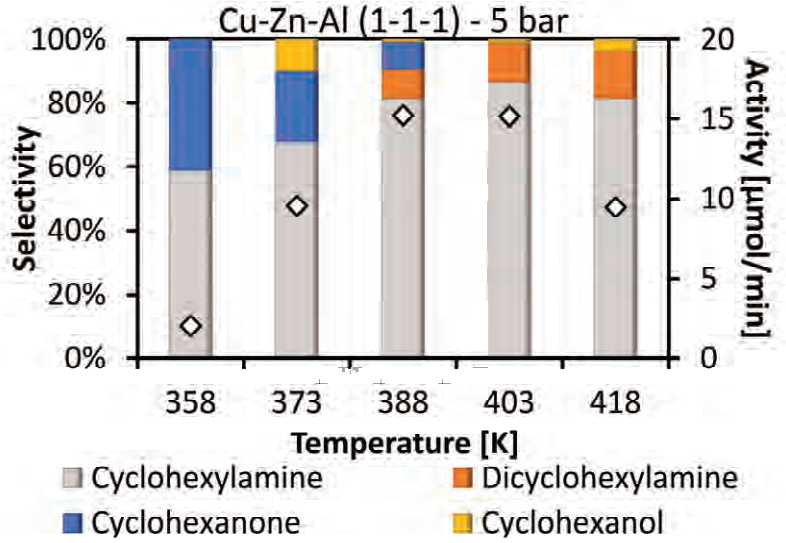

Figure 61. Results of catalytic hydrogenation of nitrocyclohexane with CuZnAl(1-1-1), 5 bar, 60 ml min^{-1} H_2, 20.5 μmol_{NC} min^{-1}, 0.1 g of the catalyst, contact time – 96.5 s.

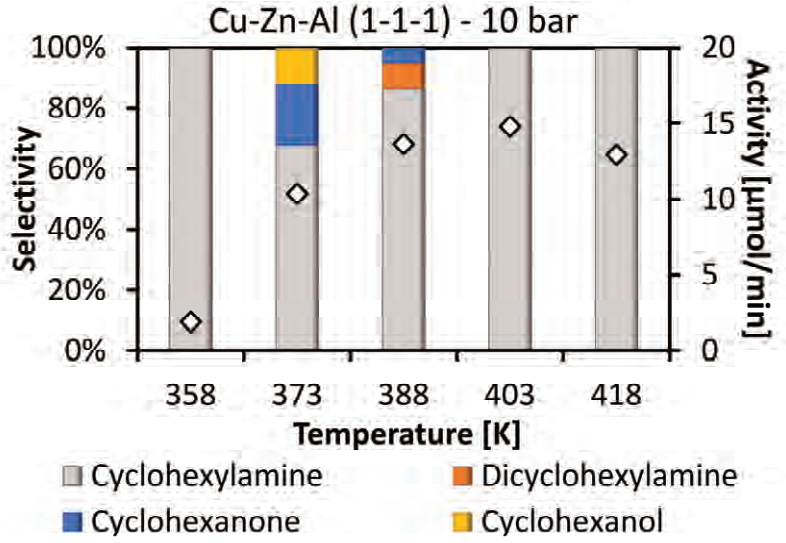

Figure 62. Results of catalytic hydrogenation of nitrocyclohexane with CuZnAl(1-1-1), 10 bar, 60 ml min^{-1} H_2, 20.5 μmol_{NC} min^{-1}, 0.1 g of the catalyst, contact time – 96.5 s.

Both CuZnAl catalysts proved to be active in nitrocyclohexane hydrogenation and selective to different products: CuZnAl(0.5-1-1) to cyclohexanone CuZnAl(1-1-1) to cyclohexylamine. Analysis of their efficiency in the formation of these products showed optimal parameters for their production (**Table 22**). The maximum cyclohexanone efficiency was determined for CuZnAl(0.5-1-1) at 5 bar and 413 K (3.12 mmol h^{-1} g_{cat}), and the maximum for cyclohexylamine was observed for CuZnAl(1-1-1) at 10 bar and 403 K (8.88 mmol h^{-1} g_{cat}).

Table 22. Effectivity of CuZnAl catalysts in the formation of selected products: (A) cyclohexanone and (B) cyclohexylamine.

p [bar]	T [K]	CuZnAl(0.5-1-1) yields to products [mmol h^{-1} g_{cat}]		CuZnAl(1-1-1) yields to products [mmol h^{-1} g_{cat}]	
		(A)	(B)	(A)	(B)
5	298	0.2	0	0	0
	313	1.1	0	0	0
	328	1.3	0	0	0
	343	1.5	0	0	0
	358	2.1	0	0.5	0.7
	373	2.6	0	1.3	3.9
	388	2.6	0	0.8	7.5
	403	2.9	0	0	7.9
	413	3.1	0	0	4.6
10	298	1.4	0	0	0.5
	313	1.0	0	0	0
	328	1.2	0	0	0
	343	1.4	0	0	0
	358	2.8	0	0	1.2
	373	2.9	0	1.2	4.2
	388	2.8	0	0.4	7.1
	403	2.6	0	0	7.9
	413	3.1	0	0	7.8

One of the advantages of conducting the catalytic reaction in continuous flow reactors is the possibility of carrying out the process for a long time. Hence, the stability of a catalyst is one of the most essential properties. Long term experiments with CuZnAl catalysts were performed at optimal conditions (**Figure 63** and **64**). The activity of both catalysts was relatively stable for 900 minutes, which means that hydrotalcite derived materials are relatively stable under reaction conditions. Although the selectivity to cyclohexanone fluctuated a little for the CuZnAl(0.5-1-1), the production of this compound was stable (~ 3 mmol h^{-1} g_{cat}) for 15 h without any signs of deactivation (**Figure 63**). A similar observation was performed for CuZnAl(1-1-1) in terms of cyclohexylamine formation (**Figure 64**). However, a tiny amount of cyclohexanone was detected in contrast to screening results.

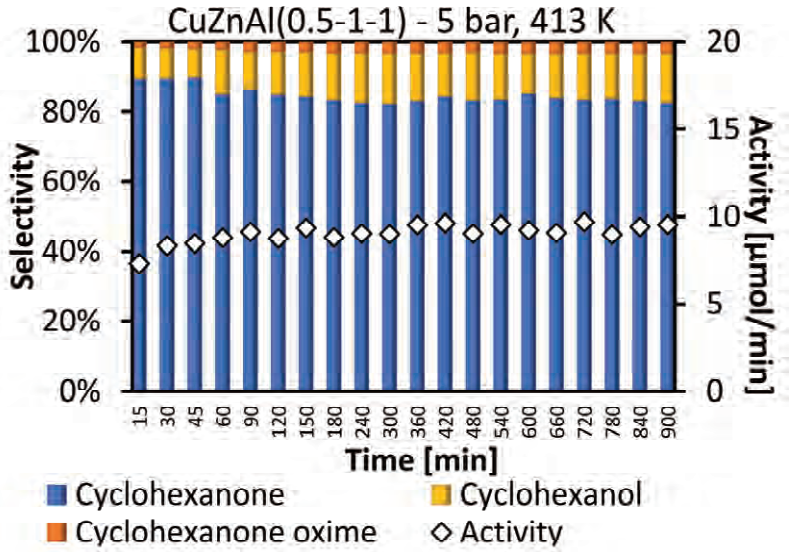

Figure 63. Results of catalytic hydrogenation of nitrocyclohexane with CuZnAl(0.5-1-1), 60 ml min^{-1} H_2, 20.5 μmol_{NC} min^{-1}, 0.1 g of the catalyst, contact time – 96.5 s.

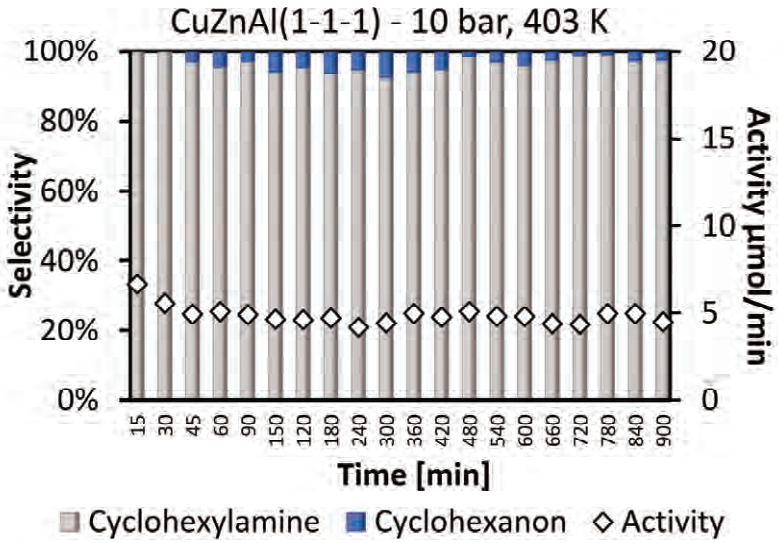

Figure 64. Results of catalytic hydrogenation of nitrocyclohexane with CuZnAl(1-1-1), 60 ml min^{-1} H_2, 20.5 μmol_{NC} min^{-1}, 0.1 g of the catalyst, contact time – 96.5 s.

Significant differences in the catalytic performance between CuZnAl hydrotalcite derived catalysts could be discussed in terms of various factors such as specific surface area of the active phase, the size of metal nanoparticles, the acidity and basicity of tested material and the copper-zinc interactions. The higher overall activity of CuZnAl(1-1-1) could be explained by the proportional correlation between copper specific surface area and catalytic activity [268]. However, due to the slight difference in the copper specific surface area between those two catalysts, it was an improbable cause of the different selectivity of CuZnAl. Nevertheless, both catalysts differed significantly in terms of average particle size. CuZnAl(0.5-1-1) demonstrated more than three times smaller metal nanoparticles (3 nm), which indicated the presence of a much larger number of open planes and defect/edge sites with coordinately unsaturated atoms [268]. Moreover, the presence of smaller copper nanoparticles means a larger interface area with the metal oxide, leading to synergistic interactions with the support material [269] and the formation of Cu-Zn alloy. On the other hand, larger nanoparticles

of CuZnAl(1-1-1) mainly contain low-index facets, with fewer defect or edgesites [270].

Additionally, Zhao et al. [271] proved the importance of the Cu/Zn ratio. The lower Cu/Zn ratio promotes the formation of Cu-ZnO_x species, which increase the amount of Cu^{2+} active sites. Similar observations were performed by Wang et al. [272]. ZnO promotes the dispersion of Cu species and affects the ratio of Cu^{+}/Cu^{0}. Interestingly, Behrens et al. [267] indicated the impact of $Zn^{\delta+}$ species at Cu defects/steps on decreasing reaction barriers and increasing the binding strength in methanol production.

Scientific reports indicate the impact of zinc species (CuZn, $CuZnO_x$) on catalytic performance in different processes [267,273–275]. Nevertheless, the interpretations of reported results are not consistent. Some of the reports explain the catalytic performance by the presence of CuZn, and some by the presence of Cu-ZnO_X [267,273,274]. Moreover, Liu et al. [275] proved the effect of the zinc source on catalytic behaviour. The electron transfer from Zn to Cu and Al can cause partial reduction of ZnO and the formation of oxygen deficiency species $Zn^{(2-\delta)}$. This phenomenon is inversely related to a number of weak acid centres and proved to be much stronger for zinc carbonate and zinc nitrate than for the CuZnAl with zinc oxide. Hence, a higher amount of weak basic sites and a lower number of weak acid sites for CuZnAl(0.5-1-1) could promote CuZn nanoparticles' formation. Despite the fact that ZnO may act as a reservoir for spillover hydrogen [276], which improves the hydrogenation process, metallic zinc in the CuZn alloy successfully blocked the Cu hydrogenolytic properties. As a consequence, this catalyst showed the selectivity to the products of partial hydrogenation of nitrocyclohexane: cyclohexanone and cyclohexanone oxime. On the other hand, Cu-ZnO core-shell structure surrounded by ZnO, observed for CuZnAl(1-1-1), allowed for efficient hydrogenation without restrains and the formation of cyclohexylamine and dicyclohexylamine – products of further hydrogenation.

The performed catalytic tests were unique due to the applied liquid flow conditions. Most of the studies were conducted in batch reactors [188–190,192,193,196], and only one in the gas flow reactor [176]. Hence, it is tough to perform a straight comparison of the obtained results with other research groups' achievements. However, as for the $PdTSNH_2$, the applied conditions allowed to perform comparative analysis.

As mentioned before, most of the studies were focused on applying noble metal catalysts in nitrocyclohexane hydrogenation. Although they showed superior hydrogenolytic properties(e.g. palladium [197]), the high cost of such metals encourages searching for alternatives based on cheaper transition metals, e.g. Cu, Co and Ni. The first attempts to use these metals in nitrocyclohexane hydrogenation were performed at the beginning of the 1950s [175]. Despite the high yield in cyclohexylamine production with Cu and Ni, these catalysts required harsh conditions: 100 bar 423 K and 30 bar 313 K, respectively. Recent works of Zhang et al. [192] proved that non-noble catalysts may be active at milder conditions. The application of 15 wt.% $CuSiO_2$ allowed to achieve 92 % selectivity to cyclohexanone oxime combined with 74 % conversion in the process performed for 3 h at 373 K under 10 bar. In the same conditions, Ni catalyst was selective to cyclohexanone oxime (59 %) and Co catalyst to cyclohexanone (88 %). The most recent studies of Yao et al. [193] proved that the combination of Ni with the addition of Cu (20%Ni-2%Cu/active carbon) gave 96 % conversion after an 8 h process performed in ethylenediamine at 353 K and 3 bar with 96.4 % selectivity to cyclohexanone oxime.

Comparing the above results [126,193,197] with those obtained for CuZnAl catalysts, it can be stated that CuZnAl materials demonstrated satisfactory activity per time unit. The catalytic performance of CuZnAl(1-1-1) is in line with the earlier study for monometallic copper catalysts [175] – 100 % selectivity to cyclohexylamine. However, CuZnAl(1-1-1) works effectively at 10 times lower pressure. On the other hand, equally efficient CuZnAl(0.5-1-1) was selective

to cyclohexanone, which could be explained by the modification of Cu performance by Zn. Moreover, both of the tested catalysts demonstrated stable performance for 15 h. Hence, the obtained results should certainly be regarded as satisfactory.

All of the obtained results suggest that hydrogenation of nitrocyclohexane in liquid flow conditions could be an excellent alternative source of various valuable chemicals. The application of the flow technique eliminates many problems of batch conditions but also facilitates the performance of the nitrocyclohexane hydrogenation. The presented research is a first step, perhaps a small, but extremely important one, to further investigation of catalytic hydrogenation of nitrocyclohexane in the liquid flow conditions with readily available transition metals as catalysts.

Conclusions

The uncontrolled development leads to progressive degradation of the environment, which markedly worsen the quality of life of all living organisms. The obtained results proved that catalytic hydrogenation is a versatile solution for such problems. It may be used to remove existing contaminants and prevent the formation of new ones. The application of effective catalysts in reactions of industrial importance, like nitrocyclohexane hydrogenation, lowers costs and increases efficiency. Moreover, the introduction of continuous flow operation mode into water purification from chloroorganic compounds and selective hydrogenation of nitrocyclohexane is a part of the international trend of making catalytic processes more effective and environmentally friendly.

Palladium nanoparticles supported on activated carbon with turbostratic structure proved to be very efficient in the removal of trichloroethylene from water, both in batch and flow conditions. Further experiments showed that adequate synthesis procedure allows for obtaining comparable active catalysts but based on cheaper Ni nanoparticles. In the case of Ni catalysts, bigger nanoparticles demonstrated higher activity and stability in hydrodechlorination of trichloroethylene in the aqueous phase. Moreover, the application of the continuous flow operation opens completely new perspectives for water purification from chloroorganic contaminants. Catalysts with poor activity in a batch reactor turned out to be very active in a flow reactor, which, among other things, was the effect of reducing the deactivation of the catalyst by removing the reaction products more efficiently.

The solutions obtained in water purification could be easily transferred into the removal of other chloroorganic contaminants. Diclofenac, recently recognized as severe pollution, could be neutralised by Pd-based catalysts. The results presented in this research for Pd-loaded zeolites surpass

all of the results reported so far for other catalysts used in water purification from diclofenac.

The outstanding performance was related to the broad distribution of Pd particle size. This phenomenon results from a different role of various nanoparticles, smaller ones promote the activation of the C-Cl bond, while bigger ones activate H_2 more efficiently. Pd/SiO_2 with a bimodal character of particle size distribution clearly outperformed monomodal catalysts. It suggests that striving for unifying nanoparticles may not be the only solution in hydrodechlorination processes.

As was mentioned before, catalytic hydrogenation is primarily used in industrial manufacturing processes. Selective hydrogenation of nitrocyclohexane could be an excellent source of various useful chemical compounds. Nevertheless, studies over this reaction have been performed mainly in the batch conditions, at elevated pressure and temperature. However, the obtained results showed high applicability of this transformation in the continuous liquid flow conditions. Pd nanoparticles grafted on the polymeric resin ($PdTSNH_2$) offered efficient production of cyclohexylamine and cyclohexanone. The selectivity of this catalyst could be easily changed by the modification of reaction conditions.

However, the most attractive results were obtained for CuZnAl hydrotalcite derived catalysts. The alteration of the copper content completely modified the selectivity of the used materials. It was caused by the modification of catalysts morphology and the formation of different Cu species: CuZn alloy or Cu-ZnO core-shell structure, which results in the formation of: cyclohexanone, cyclohexanone oxime, cyclohexylamine and dicyclohexylamine.

All of the tested catalysts demonstrated satisfactory catalytic performance. Thorough characterization of catalytic materials at different stages of their biography allowed drawing general conclusions about parameters

crucial for their performance. Therefore, I hope that the presented results and their analysis will fill some knowledge gaps about catalytic hydrogenation processes and contribute to the design of more effective catalysts.

List of scientific publications

1. **E. Kowalewski**, M. Krawczyk, G. Słowik, J. Kocik, I.S. Pięta, O. Chernyayeva, D. Lisovytskiy, K. Matus, A. Śrębowata,
   Continuous flow hydrogenation of nitrocyclohexane toward value-added products with CuZnAl hydrotalcite derived materials,
   Appl. Catal. A: General 618 (2021) 118.

2. **E. Kowalewski**, B. Zawadzki, K. Matus, K. Nikiforow, A. Śrębowata,
   Continuous-flow hydrogenation over resin supported palladium catalyst for the synthesis of industrially relevant chemicals,
   Reaction Kinetics Mechanisms and Catalysis 132 (2021) 717.

3. **E. Kowalewski**, M. Asztemborska, M. Bonarowska, K. Matus, A. Śrębowata,
   Effect of unimodality and bimodality of Pd nanoparticles on the catalytic activity of Pd/SiO_2 in the removal of diclofenac from water,
   Catal. Commun. 143 (2020) 106

4. **E. Kowalewski**, I.I. Kamińska, G. Słowik, D. Lisovytskiy, A. Śrębowata,
   Effect of metal precursor and pretreatment conditions on the catalytic activity of Ni/C in the aqueous phase hydrodechlorination of 1,1,2-trichloroethene,
   React. Kinet. Mech. Catal. 121 (2017) 3.

5. **E. Kowalewski**, M. Zienkiewicz-Machnik, D. Lisovytskiy, K. Nikiforov, K. Matus, A. Śrębowata, J. Sa,
   Turbostratic carbon supported palladium as an efficient catalyst for reductive purification of water from trichloroethylene,
   AIMS Mater. Sci. 4 (2017) 1276.

6. A.J. Fernandez-Ropero, B. Zawadzki, **E. Kowalewski**, I.S. Pięta, M. Krawczyk, K. Matus, D. Lisovytskiy, A. Śrębowata,
   Continuous 2-Methyl-3-Butyn-2-ol Selective Hydrogenation on Pd/γ-Al_2O_3 as a Greent Pathway of Vitamin a Precursor Synthesis,
   Catalysts 11 (2021) 501.

7. B. Zawadzki, **E. Kowalewski**, M. Asztemborska, K. Matus, S. Casale, S. Dźwigaj, A. Śrębowata,
   Palladium loaded BEA zeolites as efficient catalysts for aqueous-phase diclofenac hydrodechlorination,
   Catal. Commun. 145 (2020) 106.

8. I.I. Kamińska, **E. Kowalewski**, D. Lisovytskiy, W. Błachucki, W. Raróg-Pilecka, D. Łomot, A. Śrębowata,
   Batch and flow hydrotreatment of water contaminated by trichloroethylene on active carbon supported nickel catalyst,
   Appl. Catal. A: General 582 (2019) 117.

9. K. A. Tarach, A. Śrębowata, **E. Kowalewski**, K. Gołąbek, A. Kostuch, K. Kruczała, V. Girman, K. Góra-Marek,
   Nickel loaded zeolites FAU and MFI: Characterization and activity in water-phase hydrodehalogenation of TCE,
   Appl. Catal. A: General 568 (2018) 64.

10. E. Janiszewska, M. Zieliński, M. Kot, **E. Kowalewski**, A. Śrębowata, *Aqueous-phase hydrodechlorination of trichloroethylene on Ir Catalysts Supported on SBA-3 Materials,*
    ChemCatChem 10 (2018) 4109.

11. I. I. Kamińska, D. Lisovytskiy, L. Valentin, Ch. Calers, Y. Millot, **E. Kowalewski**, A. Śrębowata, S. Dźwigaj,
Influence of pretreatment and reaction conditions on the catalytic activity of HAlBEA and CoHAlBEA zeolites in vinyl chloride formation of1,2-dichloroethane,
Micropor. Mesopor. Mat. 266 (2018) 32.

12. J. M. Paszula**, E. Kowalewski,**
Badanie procesu rozwoju detonacji nieidealnych materiałów wybuchowych,
Materiały Wysokoenergetyczne 7 (2015) 95.

List of scientific presentations

The presented person is underlined.

Oral presentations

1. **E. Kowalewski**, M. Krawczyk, G. Słowik, D. Lisovytskiy, A. Śrębowata, *Catalytic hydrogenation of nitrocyclohexane into value-added products,* LII Ogólnopolskie Kolokwium Katalityczne, 25-27.11.20202, Kraków.
2. **E. Kowalewski**, j. Kocik, O. Chernyayeva, D. Lisovytskiy, K. Matus, A. Śrębowata, *Selective flow hydrogenation of nitrocyclohexane in flow conditions,* CzePoCat 9th, 7.02.2020, Ostrava, Czech Republic.
3. **E. Kowalewski**, *Water purification by catalytic hydrotreatment,* Annual Microsymposium of IPC PAS, 15-16.01.2020, Warszawa.
4. **E. Kowalewski**, D. Lisovytskiy, M. Asztemborska, A. Śrębowata, *Catalytic purification of water from chloroorganic contaminants,* 62 Zjazd Naukowy Polskiego Towarzystwa Chemicznego, 2-6.09.2019, Warszawa.
5. **E. Kowalewski**, O. Baka, M. Asztemborska, A. Śrębowata, *Katalityczne oczyszczanie wody ze związków chloroorganicznych,* Na pograniczu chemii i biologii, XVII Ogólnopolskie Seminarium dla doktorantów i studentów, 12-15.06.2019, Jastrzębia Góra.
6. **E. Kowalewski**, A. Śrębowata, *Selective flow hydrogenation of nitrocyclohexane,* LI Ogólnopolskie kolokwium katalityczne, 20-22.03.2019, Kraków.
7. **E. Kowalewski**, M.Zienkiewicz-Machnik, D. Lisovytskiy, K. Nikiforov, K. Matus, A. Śrębowata, J. Sa, *Catalytic hydrotreatment for removal of water contaminants,* CzePoCat 8th, 15.02.2019, Ostrava, Czech Republic.

8. **E. Kowalewski**, M. Zienkiewicz-Machnik, D. Lisovytskiy, K. Nikiforov, K. Matus, A. Śrębowata, J. Sa,
Catalytic purification of water from TCE in batch and flow mode,
14th Pannonian International Symposium on Catalysis, 3-7.09.2018, Stary Smokovec, Slovak Republic.
9. **E. Kowalewski**, M. Zienkiewicz-Machnik, D. Lisovytskiy, K. Nikiforov, K. Matus, A. Śrębowata, J. Sa,
Catalytic purification of water from TCE in two different modes: batch and flow,
International Conference on Catalysis and Surface Chemistry & 50 OKK, 18-23.03.2018, Kraków.
10. **E. Kowalewski**, I. I. Kamińska, D. Lisovytskiy, A. Śrębowata,
Catalytic purification of water from trichloroethylene (TCE) on active carbon supported catalysts
XLVIX Ogólnopolskie Kolokwium Katalityczne, 15-17.03.2017, Kraków.

Poster presentations

1. **E. Kowalewski**, D. Lisovytskiy, L. Valentin, Ch. Calers, Y. Millot, S. Dźwigaj, **A. Śrębowata**,
Zastosowanie katalizatorów na bazie zeolitu BEA w produkcji chlorku winylu,
62 Zjazd Naukowy Polskiego Towarzystwa Chemicznego, 2-6.09.2019, Warszawa.
2. **E. Kowalewski**, A. Śrębowata,
Selective catalytic flow hydrogenation of nitrocyclohexane,
14th International Symposium on Catalysis, 3-7.09.2018, Stary Smokovec, Republic of Slovakia.
3. **E. Janiszewska**, M. Zieliński, M. Kot, E. Kowalewski, A. Śrębowata,
Hydrodechlorination of trichloroethylene on Ir/SBA-3 catalysts,
International Conference on Catalysis and Surface Chemistry & 50 OKK, 18-23.03.2018, Kraków.

4. **K. A. Tarach**, E. Kowalewski, A. Śrębowata, K. Gołąbek, K. Góra-Marek, *Ni-loaded hierarchical zeolite Y as the catalyst in TCE and PCE removal from drinking water*
   Europacat 2017, 27-31.08.2017, Florence, Italy.
5. **E. Kowalewski**, I. I. Kamińska, G. Słowik, D. Lisovytskiy, A. Śrębowata, Catalytic purification of water from trichloroethylene on active carbon supported nickel catalysts,
   XIV Warszawskie Seminarium Doktorantów Chemików *ChemSession'17*, 9.06.2017, Warszawa.
6. **E. Kowalewski**, I. I. Kamińska, G. Słowik, D. Lisovytskiy, A. Śrębowata, *Catalytic purification of water from trichloroethylene on active carbon supported nickel catalyst,*
   XLIX Ogólnopolskie Kolokwium Katalityczne, 15-17.03.2017, Kraków.
7. **E. Kowalewski**, I. I. Kamińska, G. Słowik, D. Lisovytskiy, A. Śrębowata, *Effect of nickel precursor and pretreatment conditions on activity of Ni/C in aqueous phase hydrodechlorination of trichloroethylene,*
   13th Pannonian International Symposium on Catalysis, 19-23.09.2016 Siofok, Hungary.
8. **K. A. Tarach**, E. Kowalewski, A. Śrębowata, K. Góra-Marek, *Application of nickel loaded zeolites in tricholoroethylene removal from drinking water,*
   International Congress Green Chemistry and Sustainable Engineering, 20-22.07.2016, Rome, Italy.
9. **K. A. Tarach**, E. Kowalewski, A. Śrębowata, K. Góra-Marek, *Nickel loaded zeolites in trichloroethylene removal from drinking water,*
   XLVIII Ogólnopolskie Kolokwium Katalityczne, 16-18.04.2016, Kraków.
10. **E. Kowalewski**, I. I. Kamińska, D. Lisovytskiy, A. Śrębowata, *Catalytic purification of water from chloroorganic compounds on Ni-Mo catalysts,*
    XLVIII Ogólnopolskie Kolokwium Katalityczne, 16-18.04.2016, Kraków.

Bibliography

[1] W. Bonrath, J. Medlock, J. Schutz, B. Wustenberg, T. Netscher, Hydrogenation in the Vitamins and Fine Chemicals Industry – An Overview, in: Hydrogenation, InTech, 2012.

[2] D. Wang, D. Astruc, The Golden Age of Transfer Hydrogenation, Chem. Rev. 115 (2015) 6621–6686.

[3] J. Wisniak, The History of Catalysis. From the Beginning to Nobel Prizes, Educ. Química. 21 (2010) 60–69.

[4] M. Zhao, K. Yuan, Y. Wang, G. Li, J. Guo, L. Gu, W. Hu, H. Zhao, Z. Tang, Metal-organic frameworks as selectivity regulators for hydrogenation reactions, Nature. 539 (2016) 76–80.

[5] P.J. Chirik, Iron- and Cobalt-Catalyzed Alkene Hydrogenation: Catalysis with Both Redox-Active and Strong Field Ligands, Acc. Chem. Res. 48 (2015) 1687–1695.

[6] W. Bonrath, J. Medlock, J. Schutz, B. Wustenberg, T. Netscher, Hydrogenation in the Vitamins and Fine Chemicals Industry – An Overview, in: Hydrogenation, InTech, 2012.

[7] C.A. Busacca, D.R. Fandrick, J.J. Song, C.H. Senanayake, The growing impact of catalysis in the pharmaceutical industry, Adv. Synth. Catal. 353 (2011) 1825-1864.

[8] J.S. Anna Srebowata, B. Raton London New York, Hydrogenation with Low-Cost Transition Metals, CRC Press, 2018.

[9] S. Sharma, A. Bhattacharya, Drinking water contamination and treatment techniques, Appl. Water Sci. 7 (2017) 1043–1067.

[10] J.A. Mertens, Trichloroethylene, in: Kirk-Othmer Encycl. Chem. Technol., John Wiley & Sons, Inc., Hoboken, NJ, USA, 2000.

[11] Trichloroethylene (TRI) - Chlorinated Solvents, https://www.chlorinated-solvents.eu/products/trichloroethylene-tri/ (accessed October 12, 2020).

[12] U. EPA, Risk Evaluation for Trichloroethylene (TCE), 2020. https://www.epa.gov/assessing-and-managing-chemicals-under-tsca/risk-evaluation-trichloroethylene-tce-0 (accessed October 12, 2020).

[13] IHS Markit, C2 Chlorinated Solvents, (2020). https://ihsmarkit.com/products/c2-chlorinated-chemical-economics-handbook.html (accessed October 12, 2020).

[14] A.R. Sallmann, The history of diclofenac, Semin. Arthritis Rheum. 15 (1985) 57-60.

[15] The Top 300 Drugs of 2020, https://clincalc.com/DrugStats/Top300Drugs.aspx (accessed July , 2021).

[16] S. Schmidt, H. Hoffmann, L.A. Garbe, R.J. Schneider, Liquid chromatography–tandem mass spectrometry detection of diclofenac and related compounds in water samples, J. Chromatogr. A. 1538 (2018) 112–116.

[17] E.J. Tiedeken, A. Tahar, B. McHugh, N.J. Rowan, Monitoring, sources, receptors, and control measures for three European Union watch list substances of emerging concern in receiving waters – A 20 year systematic review, Sci. Total Environ. 574 (2017) 1140–1163.

[18] P. Sathishkumar, R.A.A. Meena, T. Palanisami, V. Ashokkumar, T. Palvannan, F.L. Gu, Occurrence, interactive effects and ecological risk of diclofenac in environmental compartments and biota - a review, Sci. Total Environ. 698 (2020) 134057.

[19] D. Dobrin, C. Bradu, M. Magureanu, N.B. Mandache, V.I. Parvulescu, Degradation of diclofenac in water using a pulsed corona discharge, Chem. Eng. J. 234 (2013) 389–396.

[20] L. Rizzo, S. Meric, D. Kassinos, M. Guida, F. Russo, V. Belgiorno, Degradation of diclofenac by TiO_2 photocatalysis: UV absorbance kinetics and process evaluation through a set of toxicity bioassays, Water Res. 43 (2009) 979–988.

[21] H. Ericson, G. Thorsén, L. Kumblad, Physiological effects of diclofenac, ibuprofen and propranolol on Baltic Sea blue mussels, Aquat. Toxicol. 99 (2010) 223–231.

[22] J. Schwaiger, H. Ferling, U. Mallow, H. Wintermayr, R.D. Negele, Toxic effects of the non-steroidal anti-inflammatory drug diclofenac: Part I: histopathological alterations and bioaccumulation in rainbow trout, Aquat. Toxicol. 68 (2004) 141-150.

[23] M.O. Barbosa, N.F.F. Moreira, A.R. Ribeiro, M.F.R. Pereira, A.M.T. Silva, Occurrence and removal of organic micropollutants: An overview of the watch list of EU Decision 2015/495, Water Res. 94 (2016) 257–279.

[24] I.Y. López-Pacheco, A. Silva-Núñez, C. Salinas-Salazar, A. Arévalo-Gallegos, L.A. Lizarazo-Holguin, D. Barceló, H.M.N. Iqbal, R. Parra-Saldívar, Anthropogenic contaminants of high concern: Existence in water resources and their adverse effects, Sci. Total Environ. 690 (2019) 1068–1088.

[25] J.L. Oaks, M. Gilbert, M.Z. Virani, R.T. Watson, C.U. Meteyer, B.A. Rideout, H.L. Shivaprasad, S. Ahmed, M. Jamshed, I. Chaudhry, M. Arshad, S. Mahmood, A. Ali, A.A. Khan, Diclofenac residues as the, Nature. 427 (2004) 630–633.

[26] J. Nieto-Sandoval, M. Munoz, Z.M. de Pedro, J.A. Casas, Fast degradation of diclofenac by catalytic hydrodechlorination, Chemosphere. 213 (2018) 141–148.

[27] S. Kutzer, H. Wintrich, A. Mersmann, Air stripping – a method for treatment of wastewater, Chem. Eng. Technol. 18 (1995) 149–155.

[28] B. Li, K. Lin, W. Zhang, S. Lu, Y. Liu, Effectiveness of air stripping, advanced oxidation, and activated carbon adsorption-coupled process in treating chlorinated solvent-contaminated groundwater, J. Environ. Eng. (United States). 138 (2012) 903–914.

[29] S.S. Ray, R. Gusain, N. Kumar, Adsorption in the context of water purification, in: Carbon Nanomater. Adsorbents Water Purif., Elsevier (2020) 67–100.

[30] V.K. Gupta, I. Ali, T.A. Saleh, A. Nayak, S. Agarwal, Chemical treatment technologies for waste-water recycling - An overview, RSC Adv. 2 (2012) 6380-6388.

[31] I. Ali, M. Asim, T.A. Khan, Low cost adsorbents for the removal of organic pollutants from wastewater, J. Environ. Manage. 113 (2012) 170–183.

[32] A. Karami, R. Sabouni, M. Ghommem, Experimental investigation of competitive co-adsorption of naproxen and diclofenac from water by an aluminum-based metal-organic framework, J. Mol. Liq. 305 (2020) 112808.

[33] B.Y.Z. Hiew, L.Y. Lee, K.C. Lai, S. Gan, S. Thangalazhy-Gopakumar, G.T. Pan, T.C.K. Yang, Adsorptive decontamination of diclofenac by three-dimensional graphene-based adsorbent: Response surface methodology, adsorption equilibrium, kinetic and thermodynamic studies, Environ. Res. 168 (2019) 241–253.

[34] Y. Miyake, A. Sakoda, H. Yamanashi, H. Kaneda, M. Suzuki, Activated carbon adsorption of trichloroethylene (TCE) vapor stripped from TCE-contaminated water, Water Res. 37 (2003) 1852–1858.

[35] C.B. Godiya, S. Kumar, Y. Xiao, Amine functionalized egg albumin hydrogel with enhanced adsorption potential for diclofenac sodium in water, J. Hazard. Mater. 393 (2020) 122417.

[36] B. Huang, C. Lei, C. Wei, G. Zeng, Chlorinated volatile organic compounds (Cl-VOCs) in environment — sources, potential human health impacts, and current remediation technologies, Environ. Int. 71 (2014) 118–138.

[37] E.M. Cuerda-correa, M.F. Alexandre-franco, C. Fern, Antibiotics from Water. An Overview, Water. 12 (2020) 1–50.

[38] R.J. Miltner, H.M. Shukairy, R.S. Summers, Disinfection by-product formation and control by ozonation and biotreatment, J. Am. Water Work. Assoc. 84 (1992) 53-62.

[39] Z. Qiu, J. Sun, D. Han, F. Wei, Q. Mei, B. Wei, X. Wang, Z. An, X. Bo, M. Li, J. Xie, M. He, Ozonation of diclofenac in the aqueous solution: Mechanism, kinetics and ecotoxicity assessment, Environ. Res. 188 (2020) 109713.

[40] P. Szabová, K. Hencelová, Z. Sameliaková, T. Marcová, A.V. Staňová, K. Grabicová, I. Bodík, Ozonation: effective way for removal of pharmaceuticals from wastewater, Monatshefte Für Chemie - Chem. Mon. 151 (2020) 685–691.

[41] K.H. Hama Aziz, H. Miessner, S. Mueller, D. Kalass, D. Moeller, I. Khorshid, M.A.M. Rashid, Degradation of pharmaceutical diclofenac and ibuprofen in aqueous solution, a direct comparison of ozonation, photocatalysis, and non-thermal plasma, Chem. Eng. J. 313 (2017) 1033–1041.

[42] M. Tammaro, A. Salluzzo, G. Romano, A. Lancia, Comparative evaluation of ozonation and stripping methods to treat contaminated groundwater by trichloroethylene. Assessment of effects on the other matrix components, J. Environ. Chem. Eng. 2 (2014) 943–951.

[43] D.S. Lee, S.J. Park, Water-mediated modulation of TiO_2 decorated with graphene for photocatalytic degradation of trichloroethylene, Curr. Appl. Phys. 15 (2015) 144–148.

[44] E. Mugunthan, M.B. Saidutta, P.E. Jagadeeshbabu, Photocatalytic degradation of diclofenac using TiO_2–SnO_2 mixed oxide catalysts, Environ. Technol. (United Kingdom). 40 (2019) 929–941.

[45] E. Mugunthan, M.B. Saidutta, P.E. Jagadeeshbabu, Photocatalytic activity of ZnO-WO3 for diclofenac degradation under visible light irradiation, J. Photochem. Photobiol. A Chem. 383 (2019) 111993.

[46] G. Vitiello, G. Iervolino, C. Imparato, I. Rea, F. Borbone, L. De Stefano, A. Aronne, V. Vaiano, F-doped ZnO nano- and meso-crystals with enhanced photocatalytic activity in diclofenac degradation, Sci. Total Environ. (2020) 143066.

[47] M. Farooq, I.A. Raja, A. Pervez, Photocatalytic degradation of TCE in water using TiO2 catalyst, Sol. Energy. 83 (2009) 1527–1533.

[48] A.N. Oliveros, J.A.I. Pimentel, M.D.G. de Luna, S. Garcia-Segura, R.R.M. Abarca, R.A. Doong, Visible-light photocatalytic diclofenac removal by tunable vanadium pentoxide/boron-doped graphitic carbon nitride composite, Chem. Eng. J. 403 (2021) 126213.

[49] D.X. Martínez Vargas, J. Rivera De la Rosa, C.J. Lucio-Ortiz, A. Hernández-Ramirez, G.A. Flores-Escamilla, C.D. Garcia, Photocatalytic degradation of trichloroethylene in a continuous annular reactor using Cu-doped TiO_2 catalysts by sol-gel synthesis, Appl. Catal. B Environ. 179 (2015) 249–261.

[50] S. Dobaradaran, H. Lutze, A.H. Mahvi, T.C. Schmidt, Transformation efficiency and formation of transformation products during photochemical degradation of TCE and PCE at micromolar concentrations, J. Environ. Heal. Sci. Eng. 12 (2014) 1-10.

[51] S. Salaeh, D. Juretic Perisic, M. Biosic, H. Kusic, S. Babic, U. Lavrencic Stangar, D.D. Dionysiou, A. Loncaric Bozic, Diclofenac removal by simulated solar assisted photocatalysis using TiO_2-based zeolite catalyst; mechanisms, pathways and environmental aspects, Chem. Eng. J. 304 (2016) 289–302.

[52] P. Calza, V.A. Sakkas, C. Medana, C. Baiocchi, A. Dimou, E. Pelizzetti, T. Albanis, Photocatalytic degradation study of diclofenac over aqueous TiO_2 suspensions, Appl. Catal. B Environ. 67 (2006) 197–205.

[53] M. Kitis, C.D. Adams, G.T. Daigger, The effects of Fenton's reagent pretreatement on the biodegradability of nonionic surfactants, Water Res. 33 (1999) 2561-2568.

[54] K. Choi, W. Lee, Enhanced degradation of trichloroethylene in nano-scale zero-valent iron Fenton system with Cu(II), J. Hazard. Mater. 211–212 (2012) 146–153.

[55] Y.F. Huang, Y.Y. Huang, P. Te Chiueh, S.L. Lo, Heterogeneous Fenton oxidation of trichloroethylene catalyzed by sewage sludge biochar: Experimental study and life cycle assessment, Chemosphere. 249 (2020) 126139.

[56] S. Ravi, L. Lonappan, I. Touahar, É. Fonteneau, V.K. Vaidyanathan, H. Cabana, Evaluation of bio-fenton oxidation approach for the remediation of trichloroethylene from aqueous solutions, J. Environ. Manage. 270 (2020) 110899.

[57] O. Oral, C. Kantar, Diclofenac removal by pyrite-Fenton process: Performance in batch and fixed-bed continuous flow systems, Sci. Total Environ. 664 (2019) 817-823.

[58] X. Wei, N. Zhu, X. Huang, N. Kang, P. Wu, Z. Dang, Efficient degradation of sodium diclofenac via heterogeneous Fenton reaction boosted by Pd/Fe@Fe_3O_4 nanoparticles derived from bio-recovered palladium, J. Environ. Manage. 260 (2020) 110072.

[59] M.C. Shin, H.D. Choi, D.H. Kim, K. Baek, Effect of surfactant on reductive dechlorination of trichloroethylene by zero-valent iron, Desalination. 223 (2008) 299–307.

[60] S. Bae, D. Kim, W. Lee, Degradation of diclofenac by pyrite catalyzed Fenton oxidation, Appl. Catal. B Environ. 134–135 (2013) 93–102.

[61] H. Che, S. Bae, W. Lee, Degradation of trichloroethylene by Fenton reaction in pyrite suspension, J. Hazard. Mater. 185 (2011) 1355–1361.

[62] K.H. Choo, D.I. Chang, K.W. Park, M.H. Kim, Use of an integrated photocatalysis/hollow fiber microfiltration system for the removal of trichloroethylene in water, J. Hazard. Mater. 152 (2008) 183–190.

[63] H. Bahrami, A. Eslami, R. Nabizadeh, A. Mohseni-Bandpi, A. Asadi, M. Sillanpää, Degradation of trichloroethylene by sonophotolytic-activated persulfate processes: Optimization using response surface methodology, J. Clean. Prod. 198 (2018) 1210–1218.

[64] Y. Huang, H. Liu, S. Liu, C. Li, S. Yuan, Glucose oxidase modified Fenton reactions for in-situ ROS generation and potential application in groundwater remediation, Chemosphere. 253 (2020) 126648.

[65] V. Naddeo, V. Belgiorno, D. Ricco, D. Kassinos, Degradation of diclofenac during sonolysis, ozonation and their simultaneous application, Ultrason. Sonochem. 16 (2009) 790–794.

[66] J. Diaz-Angulo, J. Porras, M. Mueses, R.A. Torres-Palma, A. Hernandez-Ramirez, F. Machuca-Martinez, Coupling of heterogeneous photocatalysis and photosensitized oxidation for diclofenac degradation: role of the oxidant species, J. Photochem. Photobiol. A Chem. 383 (2019) 112015.

[67] Z. Zhao, W. Zhang, W. Liu, Y. Li, J. Ye, J. Liang, M. Tong, Activation of sulfite by single-atom Fe deposited graphitic carbon nitride for diclofenac removal: the synergetic effect of transition metal and photocatalysis, Chem. Eng. J. 407 (2021) 127167.

[68] M. Hong, Y. Wang, G. Lu, UV-Fenton degradation of diclofenac, sulpiride, sulfamethoxazole and sulfisomidine: Degradation mechanisms, transformation products, toxicity evolution and effect of real water matrix, Chemosphere. 258 (2020) 127351.

[69] R.W. Gillham, J. Vogan, L. Gui, M. Duchene, J. Son, Iron Barrier Walls for Chlorinated Solvent Remediation, in: In situ remediation of Chlorinated Solvent Plumes, Springer, 2010.

[70] F. Fu, D.D. Dionysiou, H. Liu, The use of zero-valent iron for groundwater remediation and wastewater treatment: A review, J. Hazard. Mater. 267 (2014) 194–205.

[71] S.M. Wang, S. kung Tseng, Reductive dechlorination of trichloroethylene by combining autotrophic hydrogen-bacteria and zero-valent iron particles, Bioresour. Technol. 100 (2009) 111–117.

[72] M. Stefaniuk, P. Oleszczuk, Y.S. Ok, Review on nano zerovalent iron (nZVI): From synthesis to environmental applications, Chem. Eng. J. 287 (2016) 618–632.

[73] H. Kim, H.-J. Hong, Y.-J. Lee, H.-J. Shin, J.-W. Yang, Degradation of trichloroethylene by zero-valent iron immobilized in cationic exchange membrane, Desalination. 223 (2008) 212–220.

[74] L. Gong, N. Lv, J. Qi, X. Qiu, Y. Gu, F. He, Effects of non-reducible dissolved solutes on reductive dechlorination of trichloroethylene by ball milled zero valent irons, J. Hazard. Mater. 396 (2020) 122620.

[75] W. Yan, H.L. Lien, B.E. Koel, W.X. Zhang, Iron nanoparticles for environmental clean-up: Recent developments and future outlook, Environ. Sci. Process. Impacts. 15 (2013) 63–77.

[76] J. Prasad Rao, P. Gruenberg, K.E. Geckeler, Magnetic zero-valent metal polymer nanoparticles: Current trends, scope, and perspectives, Prog. Polym. Sci. 40 (2015) 138–147.

[77] N.D. Berge, C.A. Ramsburg, Oil-in-water emulsions for encapsulated delivery of reactive iron particles, Environ. Sci. Technol. 43 (2009) 5060–5066.

[78] W.F. Chen, L. Pan, L.F. Chen, Q. Wang, C.C. Yan, Dechlorination of hexachlorobenzene by nano zero-valent iron/activated carbon composite: Iron loading, kinetics and pathway, RSC Adv. 4 (2014) 46689–46696.

[79] L. Rajic, N. Fallahpour, A.N. Alshawabkeh, Impact of electrode sequence on electrochemical removal of trichloroethylene from aqueous solution, Appl. Catal. B Environ. 174–175 (2015) 427–434.

[80] L. Rajic, N. Fallahpour, E. Podlaha, A. Alshawabkeh, The influence of cathode material on electrochemical degradation of trichloroethylene in aqueous solution, Chemosphere. 147 (2016) 98–104.

[81] B.P. Chaplin, M. Reinhard, W.F. Schneider, C. Schüth, J.R. Shapley, T.J. Strathmann, C.J. Werth, Critical Review of Pd-Based Catalytic Treatment of Priority Contaminants in Water, Environ. Sci. Technol. 46 (2012) 3655–3670.

[82] Z. He, K. Lin, J. Sun, L. Wen, C. Gao, J. Chen, S. Song, Y. Qian, W. Liub, Kinetics of electrochemical dechlorination of 2-chlorobiphenyl on apalladium-modified nickel foam cathode in a basic medium:From batch to continuous reactor operation, Electrochim. Acta. 109 (2013) 502–511.

[83] Y. Zheng, Y. Jiao, M. Jaroniec, S.Z. Qiao, Advancing the electrochemistry of the hydrogen- Evolution reaction through combining experiment, Angew. Chemie - Int. Ed. 54 (2015) 52–65.

[84] M.A. Keane, Supported Transition Metal Catalysts for Hydrodechlorination Reactions, ChemCatChem. 3 (2011) 800–821.

[85] S. Kovenklioglu, Z. Cao, D. Shah, R.J. Farrauto, E.N. Balko, Direct Catalytic Hydrodechlorination of Toxic Organics in Wastewater, 38 (1992).

[86] Y. Mitoma, Y. Katayama, C. Simion, Mechanistic Considerations on the Hydrodechlorination Process of Polychloroarenes, in: Organochlorine, InTech, 2018.

[87] M. Cobo, J. Becerra, M. Castelblanco, B. Cifuentes, J.A. Conesa, Catalytic hydrodechlorination of trichloroethylene in a novel NaOH/2-propanol/methanol/water system on ceria-supported Pd and Rh catalysts, J. Environ. Manage. 158 (2015) 1–10.

[88] X. Yu, T. Wu, X.J. Yang, J. Xu, J. Auzam, R. Semiat, Y.F. Han, Degradation of trichloroethylene by hydrodechlorination using formic acid as hydrogen source over supported Pd catalysts, J. Hazard. Mater. 305 (2016) 178–189.

[89] F.J. Urbano, J.M. Marinas, Hydrogenolysis of organohalogen compounds over palladium supported catalysts, J. Mol. Catal. A Chem. 173 (2001) 329–345.

[90] E. Díaz, A. McCall, L. Faba, H. Sastre, S. Ordóñez, Trichloroethylene Hydrodechlorination in Water Using Formic Acid as Hydrogen Source: Selection of Catalyst and Operation Conditions, Environ. Prog. Sustain. Energy. 32 (2013) 1217–1222.

[91] F.D. Kopinke, K. Mackenzie, R. Koehler, A. Georgi, Alternative sources of hydrogen for hydrodechlorination of chlorinated organic compounds in water on Pd catalysts, Appl. Catal. A Gen. 271 (2004) 119–128.

[92] Y.L. Fang, K.N. Heck, P.J.J. Alvarez, M.S. Wong, Kinetics analysis of palladium/gold nanoparticles as colloidal hydrodechlorination catalysts, ACS Catal. 1 (2011) 128-138.

[93] S. Gómez-Quero, F. Cárdenas-Lizana, M.A. Keane, Liquid phase catalytic hydrodechlorination of 2,4-dichlorophenol over Pd/Al_2O_3: Batch vs. continuous operation, Chem. Eng. J. 166 (2011) 1044–1051.

[94] L.D. Mendes, G. Bernardi, W.C. Elias, D.C. de Oliveira, J.B. Domingos, E. Carasek, A green approach to DDT degradation and metabolite monitoring in water comparing the hydrodechlorination efficiency of Pd, Au-on-Pd and Cu-on-Pd nanoparticle catalysis, Sci. Total Environ. (2020) 143403.

[95] K. Meduri, C. Stauffer, W. Qian, O. Zietz, A. Barnum, G.O.B. Johnson, D. Fan, W. Ji, C. Zhang, P. Tratnyek, J. Jiao, Palladium and gold nanoparticles on carbon supports as highly efficient catalysts for effective removal of trichloroethylene, J. Mater. Res. 33 (2018) 2404–2413.

[96] J. Wei, Y. Qian, W. Liu, L. Wang, Y. Ge, J. Zhang, J. Yu, X. Ma, Effects of particle composition and environmental parameters on catalytic hydrodechlorination of trichloroethylene by nanoscale bimetallic Ni-Fe, J. Environ. Sci. (China). 26 (2014) 1162–1170.

[97] K.A. Tarach, A. Śrębowata, E. Kowalewski, K. Gołąbek, A. Kostuch, K. Kruczała, V. Girman, K. Góra-Marek, Nickel loaded zeolites FAU and MFI: Characterization and activity in water-phase hydrodehalogenation of TCE, Appl. Catal. A Gen. 568 (2018) 64–75.

[98] Q. Guo, L. Ren, Hydrodechlorination of trichloroethylene over MoP/γ-Al_2O_3 catalyst with high surface area, Catal. Today. 264 (2016) 158–162.

[99] A. Śrebowata, K. Tarach, V. Girman, K. Góra-Marek, Catalytic removal of trichloroethylene from water over palladium loaded microporous and hierarchical zeolites, Appl. Catal. B Environ. 181 (2016) 550–560.

[100] J. Nieto-Sandoval, M. Rodriguez, M. Munoz, Z.M. de Pedro, J.A. Casas, Catalyst deactivation in the hydrodechlorination of micropollutants. A case of study with neonicotinoid pesticides, J. Water Process Eng. 38 (2020) 101550.

[101] S. Ordóñez, B.P. Vivas, F. V. Díez, Minimization of the deactivation of palladium catalysts in the hydrodechlorination of trichloroethylene in wastewaters, Appl. Catal. B Environ. 95 (2010) 288–296.

[102] W. Sriwatanapongse, M. Reinhard, C.A. Klug, Reductive hydrodechlorination of trichloroethylene by palladium-on-alumina catalyst: 13C solid-state NMR study of surface reaction precursors, Langmuir. 22 (2006) 4158–4164.

[103] S.C. Fung, J.H. Sinfelt, Hydrogenolysis of methyl chloride on metals, J. Catal. 103 (1987) 220–223.

[104] P.P. Kulkarni, S.S. Deshmukh, V.I. Kovalchuk, J.L. d'Itri, Hydrodechlorination of dichlorodifluoromethane on carbon-supported group VIII noble metal catalysts, Catal. Letters. 61 (1999) 161–166.

[105] M. Zhang, D.B. Bacik, C.B. Roberts, D. Zhao, Catalytic hydrodechlorination of trichloroethylene in water with supported CMC-stabilized palladium nanoparticles, Water Res. 47 (2013) 3706–3715.

[106] W. Wu, J. Xu, R. Ohnishi, Complete hydrodechlorination of chlorobenzene and its derivatives over supported nickel catalysts under liquid phase conditions, Appl. Catal. B Environ. 60 (2005) 129–137.

[107] L. Calvo, M.A. Gilarranz, J.A. Casas, A.F. Mohedano, J.J. Rodríguez, Hydrodechlorination of alachlor in water using Pd, Ni and Cu catalysts supported on activated carbon, Appl. Catal. B Environ. 78 (2008) 259–266.

[108] A. V. Mekhaev, O.N. Chupakhin, M.A. Uimin, A.E. Ermakov, M.G. Pervova, T.I. Gorbunova, A.A. Mysik, V.I. Saloutin, Y.G. Yatlulk, Liquid-phase catalytic hydrodechlorination of aromatic chloro derivatives with metal nanopowders, Russ. Chem. Bull. 58 (2009) 1321–1324.

[109] T. Weidlich, B. Kamenická, K. Melánová, V. Čičmancová, A. Komersová, J. Čermák, Hydrodechlorination of different chloroaromatic compounds at room temperature and ambient pressure—differences in reactivity of Cu-and Ni-based Al alloys in an alkaline aqueous solution, Catalysts. 10 (2020) 1–21.

[110] M. Munoz, S. Ponce, G.R. Zhang, B.J.M. Etzold, Size-controlled PtNi nanoparticles as highly efficient catalyst for hydrodechlorination reactions, Appl. Catal. B Environ. 192 (2016) 1–7.

[111] M.D. Navalikhina, N.E. Kavalerskaya, E.S. Lokteva, A.A. Peristyi, E. V. Golubina, V. V. Lunin, Hydrodechlorination of chlorobenzene on Ni and Ni-Pd catalysts modified by heteropolycompounds of the keggin type, Russ. J. Phys. Chem. A. 86 (2012) 1669–1675.

[112] M.A. Aramendía, V. Boráu, I.M. García, C. Jiménez, F. Lafont, A. Marinas, J.M. Marinas, F.J. Urbano, Influence of the reaction conditions and catalytic properties on the liquid-phase hydrodechlorination of chlorobenzene over palladium-supported catalysts: Activity and deactivation, J. Catal. 187 (1999) 392–399.

[113] L.M. Gómez-Sainero, X.L. Seoane, J.L.G. Fierro, A. Arcoya, Liquid-phase hydrodechlorination of CCl_4 to $CHCl_3$ on Pd/carbon catalysts: Nature and role of Pd active species, J. Catal. 209 (2002) 279–288.

[114] T. Janiak, J. Okal, Effectiveness and stability of commercial Pd/C catalysts in the hydrodechlorination of meta-substituted chlorobenzenes, Appl. Catal. B Environ. 92 (2009) 384–392.

[115] K. Wu, X. Qian, L. Chen, Z. Xu, S. Zheng, D. Zhu, Effective liquid phase hydrodechlorination of diclofenac catalysed by Pd/CeO_2, RSC Adv. 5 (2015) 18702–18709.

[116] L. Calvo, M.A. Gilarranz, J.A. Casas, A.F. Mohedano, J.J. Rodríguez, Hydrodechlorination of 4-chlorophenol in water with formic acid using a Pd/activated carbon catalyst, J. Hazard. Mater. 161 (2009) 842–847.

[117] Z. Dong, C. Dong, Y. Liu, X. Le, Z. Jin, J. Ma, Hydrodechlorination and further hydrogenation of 4-chlorophenol to cyclohexanone in water over Pd nanoparticles modified N-doped mesoporous carbon microspheres, Chem. Eng. J. 270 (2015) 215–222.

[118] J.G. Mahy, L. Tasseroul, O. Tromme, B. Lavigne, S.D. Lambert, Hydrodechlorination and complete degradation of chlorinated compounds with the coupled action of Pd/SiO2 and Fe/SiO2 catalysts: Towards industrial catalyst synthesis conditions, J. Environ. Chem. Eng. 7 (2019) 103014.

[119] M.C. Liu, S.H. Chang, M.B. Chang, Catalytic hydrodechlorination of PCDD/Fs from condensed water with $Pd/\gamma\text{-}Al_2O_3$, Chemosphere. 154 (2016) 583–589..

[120] J. Nieto-Sandoval, M. Munoz, Z.M. de Pedro, J.A. Casas, Catalytic hydrodechlorination as polishing step in drinking water treatment for the removal of chlorinated micropollutants, Sep. Purif. Technol. 227 (2019) 115717.

[121] P. Paraskeva, D. Kalderis, E. Diamadopoulos, Production of activated carbon from agricultural by-products, J. Chem. Technol. Biotechnol. 83 (2008) 581–592.

[122] M. Munoz, V. Kolb, A. Lamolda, Z.M. de Pedro, A. Modrow, B.J.M. Etzold, J.J. Rodriguez, J.A. Casas, Polymer-based spherical activated carbon as catalytic support for hydrodechlorination reactions, Appl. Catal. B Environ. 218 (2017) 498–505.

[123] K. Kim, J. Han, J.S. Park, J. Lee, Preparation and evaluation of activated carbon supported catalysts derived waste materials for hybrid type Na-air battery, Mater. Lett. 245 (2019) 6–9.

[124] S. Akbayrak, Z. Özçifçi, A. Tabak, Activated carbon derived from tea waste: A promising supporting material for metal nanoparticles used as catalysts in hydrolysis of ammonia borane, Biomass and Bioenergy. 138 (2020) 105589.

[125] C. Ruiz-Garcia, F. Heras, L. Calvo, N. Alonso-Morales, J.J. Rodriguez, M.A. Gilarranz, Improving the activity in hydrodechlorination of Pd/C catalysts by nitrogen doping of activated carbon supports, J. Environ. Chem. Eng. 8 (2020) 103689.

[126] M. Munoz, G.R. Zhang, B.J.M. Etzold, Exploring the role of the catalytic support sorption capacity on the hydrodechlorination kinetics by the use of carbide-derived carbons, Appl. Catal. B Environ. 203 (2017) 591–598.

[127] J.A. Baeza, L. Calvo, N. Alonso-Morales, F. Heras, S. Eser, J.J. Rodriguez, M.A. Gilarranz, Effect of structural ordering of the carbon support on the behavior of Pd catalysts in aqueous-phase hydrodechlorination, Chem. Eng. Sci. 176 (2018) 400–408.

[128] G. Yuan, M.A. Keane, Liquid phase hydrodechlorination of chlorophenols over Pd/C and Pd/Al_2O_3: A consideration of HCl/catalyst interactions and solution pH effects, Appl. Catal. B Environ. 52 (2004) 301–314.

[129] M.A. Keane, A review of catalytic approaches to waste minimization: Case study - Liquid-phase catalytic treatment of chlorophenols, J. Chem. Technol. Biotechnol. 80 (2005) 1211–1222.

[130] E. López, S. Ordóñez, F. V. Díez, Deactivation of a Pd/Al_2O_3 catalyst used in hydrodechlorination reactions: Influence of the nature of organochlorinated compound and hydrogen chloride, Appl. Catal. B Environ. 62 (2006) 57–65.

[131] G. V. Lowry, M. Reinhard, Pd-catalyzed TCE dechlorination in groundwater: Solute effects, biological control, and oxidative catalyst regeneration, Environ. Sci. Technol. 34 (2000) 3217–3223.

[132] S. Gómez-Quero, F. Cárdenas-Lizana, M.A. Keane, Effect of metal dispersion on the liquid-phase hydrodechlorination of 2,4-dichlorophenol over Pd/Al_2O_3, Ind. Eng. Chem. Res. 47 (2008) 6841–6853.

[133] Z.M. de Pedro, E. Diaz, A.F. Mohedano, J.A. Casas, J.J. Rodriguez, Compared activity and stability of Pd/Al_2O_3 and Pd/AC catalysts in 4-chlorophenol hydrodechlorination in different pH media, Appl. Catal. B Environ. 103 (2011) 128–135.

[134] C. Xia, Y. Liu, S. Zhou, C. Yang, S. Liu, S. Guo, Q. Liu, J. Yu, J. Chen, The influence of ion effects on the Pd-catalyzed hydrodechlorination of 4-chlorophenol in aqueous solutions, Catal. Commun. 10 (2009) 1443–1445.

[135] L. Calvo, M.A. Gilarranz, J.A. Casas, A.F. Mohedano, J.J. Rodríguez, Hydrodechlorination of 4-chlorophenol in aqueous phase using Pd/AC catalysts prepared with modified active carbon supports, Appl. Catal. B Environ. 67 (2006) 68–76.

[136] E. Díaz, J.A. Casas, A.F. Mohedano, L. Calvo, M.A. Gilarranz, J.J. Rodríguez, Kinetics of 4-chlorophenol hydrodechlorination with alumina and activated carbon-supported Pd and Rh catalysts, Ind. Eng. Chem. Res. 48 (2009) 3351-3358.

[137] E. Díaz, J.A. Casas, Á.F. Mohedano, L. Calvo, M.A. Gilarranz, J.J. Rodríguez, Kinetics of the hydrodechlorination of 4-chlorophenol in water using Pd, Pt, and Rh/Al_2O_3 catalysts, Ind. Eng. Chem. Res. 47 (2008) 3840–3846.

[138] M. Zhang, D.B. Bacik, C.B. Roberts, D. Zhao, Catalytic hydrodechlorination of trichloroethylene in water with supported CMC-stabilized palladium nanoparticles, Water Res. 47 (2013) 3706–3715.

[139] G. Celik, S.A. Ailawar, H. Sohn, Y. Tang, F.F. Tao, J.T. Miller, P.L. Edmiston, U.S. Ozkan, Swellable Organically Modified Silica (SOMS) as a Catalyst Scaffold for Catalytic Treatment of Water Contaminated with Trichloroethylene, ACS Catal. 8 (2018) 6796–6809.

[140] G. Celik, S.A. Ailawar, S. Gunduz, P.L. Edmiston, U.S. Ozkan, Formation of carbonaceous deposits on Pd-based hydrodechlorination catalysts: Vibrational spectroscopy investigations over Pd/Al_2O_3 and Pd/SOMS, Catal. Today. 323 (2019) 129–140.

[141] G. Celik, S.A. Ailawar, S. Gunduz, J.T. Miller, P.L. Edmiston, U.S. Ozkan, Aqueous-Phase Hydrodechlorination of Trichloroethylene over Pd-Based Swellable Organically Modified Silica: Catalyst Deactivation Due to Sulfur Species, Ind. Eng. Chem. Res. 58 (2019) 4054–4064.

[142] C.H. Gammons, Experimental investigations of the hydrothermal geochemistry of platinum and palladium: V. Equilibria between platinum metal, Pt(II), and Pt(IV) chloride complexes at 25 to 300°C, Geochim. Cosmochim. Acta. 60 (1996) 1683–1694.

[143] A. Śrębowata, I.I. Kamińska, Turbostratic carbon supported Ni-Pd alloys inaqueous-phase hydrodechlorination of 1,1,2-trichloroethene, Recycl. Catal. 2 (2015) 17–22.

[144] A. Śrębowata, I.I. Kamińska, D. Giziński, D. Wideł, J. Oszczudłowski, Remarkable effect of soft-templating synthesis procedure on catalytic properties of mesoporous carbon supported Ni in hydrodechlorination of trichloroethylene in liquid phase, Catal. Today. 251 (2015) 60–65.

[145] S. De Corte, T. Hennebel, J.P. Fitts, T. Sabbe, V. Bliznuk, S. Verschuere, D. Van Der Lelie, W. Verstraete, N. Boon, Biosupported bimetallic Pd-Au nanocatalysts for dechlorination of environmental contaminants, Environ. Sci. Technol. 45 (2011) 8506–8513.

[146] S. De Corte, T. Sabbe, T. Hennebel, L. Vanhaecke, B. De Gusseme, W. Verstraete, N. Boon, Doping of biogenic Pd catalysts with Au enables dechlorination of diclofenac at environmental conditions, Water Res. 46 (2012) 2718–2726.

[147] X. Wang, J.R. Li, M.L. Fu, B. Yuan, H.J. Cui, Y.F. Wang, Fabrication and evaluation of Au-Pd core-shell nanocomposites for dechlorination of diclofenac in water, Environ. Technol. (United Kingdom). 36 (2015) 1510–1518.

[148] X. Quan, X. Wang, Y. Sun, W. Li, L. Chen, J. Zhao, Degradation of diclofenac using palladized anaerobic granular sludge: Effects of electron donor, reaction medium and deactivation factors, J. Hazard. Mater. 365 (2019) 155–163.

[149] K. Wu, X. Qian, L. Chen, Z. Xu, S. Zheng, D. Zhu, Effective liquid phase hydrodechlorination of diclofenac catalysed by Pd/CeO_2, RSC Adv. 5 (2015) 18702–18709.

[150] G. Yuan, M.A. Keane, Role of base addition in the liquid-phase hydrodechlorination of 2,4-dichlorophenol over Pd/Al_2O_3 and Pd/C, J. Catal. 225 (2004) 510–522.

[151] K. Masuda, T. Ichitsuka, N. Koumura, K. Sato, S. Kobayashi, Flow fine synthesis with heterogeneous catalysts, Tetrahedron. 74 (2018) 1705–1730.
[152] M. Trojanowicz, Flow chemistry in contemporary chemical sciences: A real variety of its applications, Molecules. 25 (2020).
[153] L. Vaccaro, D. Lanari, A. Marrocchi, G. Strappaveccia, Flow approaches towards sustainability, Green Chem. 16 (2014) 3680–3704.
[154] J. Wegner, S. Ceylan, A. Kirschning, Ten key issues in modern flow chemistry, Chem. Commun. 47 (2011) 4583–4592.
[155] J. Kobayashi, Y. Mori, K. Okamoto, R. Akiyama, M. Ueno, T. Kitamori, S. Kobayashi, A microfluidic device for conducting gas-liquid-solid hydrogenation reactions, Science 304 (2004) 1305–1308.
[156] Z. Amara, M. Poliakoff, R. Duque, D. Geier, G. Franciò, C.M. Gordon, R.E. Meadows, R. Woodward, W. Leitner, Enabling the Scale-Up of a Key Asymmetric Hydrogenation Step in the Synthesis of an API Using Continuous Flow Solid-Supported Catalysis, Org. Process Res. Dev. 20 (2016) 1321–1327.
[157] T. Yu, J. Jiao, P. Song, W. Nie, C. Yi, Q. Zhang, P. Li, Recent Progress in Continuous-Flow Hydrogenation, ChemSusChem. 13 (2020) 2876–2893.
[158] A.K. Rathi, M.B. Gawande, V. Ranc, J. Pechousek, M. Petr, K. Cepe, R.S. Varma, R. Zboril, Continuous flow hydrogenation of nitroarenes, azides and alkenes using maghemite-Pd nanocomposites, Catal. Sci. Technol. 6 (2016) 152–160.
[159] M. Irfan, T.N. Glasnov, C.O. Kappe, Heterogeneous catalytic hydrogenation reactions in continuous-flow reactors, ChemSusChem. 4 (2011) 300–316.
[160] L. Vaccaro, D. Lanari, A. Marrocchi, G. Strappaveccia, Flow approaches towards sustainability, Green Chem. 16 (2014) 3680–3704.
[161] P. Loos, H. Alex, J. Hassfeld, K. Lovis, J. Platzek, N. Steinfeldt, S. Hübner, Selective Hydrogenation of Halogenated Nitroaromatics to Haloanilines in Batch and Flow, Org. Process Res. Dev. 20 (2016) 452–464.
[162] T. Gustafsson, F. Pontén, P.H. Seeberger, Trimethylaluminium mediated amide bond formation in a continuous flow microreactor as key to the synthesis of rimonabant and efaproxiral, Chem. Commun. (2008) 1100–1102.
[163] D. Cantillo, M. Damm, D. Dallinger, M. Bauser, M. Berger, C.O. Kappe, Sequential nitration/hydrogenation protocol for the synthesis of triaminophloroglucinol: Safe generation and use of an explosive intermediate under continuous-flow conditions, Org. Process Res. Dev. 18 (2014) 1360–1366.
[164] E. Riva, S. Gagliardi, C. Mazzoni, D. Passarella, A. Rencurosi, D. Vigo, M. Martinelli, Efficient continuous flow synthesis of hydroxamic acids and suberoylanilide hydroxamic acid preparation, J. Org. Chem. 74 (2009) 3540–3543.
[165] Z. Yu, Y. Lv, C. Yu, W. Su, A high-output, continuous selective and heterogeneous nitration of p -difluorobenzene, Org. Process Res. Dev. 17 (2013) 438–442.
[166] J.P. Mcmullen, K.F. Jensen, An Automated Microfluidic System for Online Optimization in Chemical Synthesis Abstract : An automated , continuous flow system for the online , multivariable optimization of a chemical reaction is presented. Time and material required for an optimizatio, Org. Process Res. Dev. 14 (2010) 1169–1176.
[167] OpenFlowChem – a platform for quick , robust and flexible automation and self-optimisation of flow chemistry, React. Chem. Eng. 3 (2018) 769-780.

[168] C. V. Rode, A.A. Ghalwadkar, R.B. Mane, A.M. Hengne, S.T. Jadkar, N.S. Biradar, Selective hydrogenolysis of glycerol to 1,2-propanediol: Comparison of batch and continuous process operations, Org. Process Res. Dev. 14 (2010) 1385–1392.

[169] Y. Shen, A. Maamor, J. Abu-Dharieh, J.M. Thompson, B. Kalirai, E.H. Stitt, D.W. Rooney, Moving from batch to continuous operation for the liquid phase dehydrogenation of tetrahydrocarbazole, Org. Process Res. Dev. 18 (2014) 392-401.

[170] A.D.M. Mendonça, A.V.B. De Oliveira, J. Cajaiba, A Comparison between Continuous and Batch Processes to Capture Aldehydes and Ketones by Using a Scavenger Resin, Org. Process Res. Dev. 21 (2017) 1794–1800.

[171] J.G. Costandy, T.F. Edgar, M. Baldea, Switching from Batch to Continuous Reactors Is a Trajectory Optimization Problem, Ind. Eng. Chem. Res. 58 (2019) 13718–13736.

[172] Y. Wang, P. Prinsen, K.S. Triantafyllidis, S.A. Karakoulia, A. Yepez, C. Len, R. Luque, Batch versus Continuous Flow Performance of Supported Mono- and Bimetallic Nickel Catalysts for Catalytic Transfer Hydrogenation of Furfural in Isopropanol, ChemCatChem. 10 (2018) 3459–3468.

[173] G.S. Calabrese, S. Pissavini, From batch to continuous flow processing in chemicals manufacturing, AIChE J. 57 (2011) 828–834.

[174] S.K. Teoh, C. Rathi, P. Sharratt, Practical Assessment Methodology for Converting Fine Chemicals Processes from Batch to Continuous, (2016).

[175] C. Grundmann, Über die partielle Reduktion von Nitro-cyclohexan, Angew. Chemie. 62 (1950) 558–560.

[176] X. Wang, N. Perret, M.A. Keane, Gas phase hydrogenation of nitrocyclohexane over supported gold catalysts, Appl. Catal. A Gen. 467 (2013) 575–584.

[177] J. Wen, K. You, X. Liu, J. Jian, F. Zhao, P. Liu, Q. Ai, H. Luo, Highly selective one-step catalytic amination of cyclohexene to cyclohexylamine over HZSM-5, Catal. Commun. 127 (2019) 64–68.

[178] S. Araki, K. Nakanishi, A. Tanaka, H. Kominami, A ruthenium and palladium bimetallic system superior to a rhodium co-catalyst for TiO_2-photocatalyzed ring hydrogenation of aniline to cyclohexylamine, J. Catal. 389 (2020) 212–217.

[179] J. Becker, J.P.M. Niederer, M. Keller, W.F. Hölderich, Amination of cyclohexanone and cyclohexanol/cyclohexanone in the presence of ammonia and hydrogen using copper or a group VIII metal supported on a carrier as the catalyst, Appl. Catal. A Gen. 197 (2000) 229–238.

[180] M. Chatterjee, M. Sato, H. Kawanami, T. Ishizaka, T. Yokoyama, T. Suzuki, Hydrogenation of aniline to cyclohexylamine in supercritical carbon dioxide: Significance of phase behaviour, Appl. Catal. A Gen. 396 (2011) 186–193.

[181] J. Wen, K. You, F. Zhao, J. Jian, P. Liu, Q. Ai, H. Luo, AlCl3 immobilized on silicic acid as efficient Lewis acid catalyst for highly selective preparation of dicyclohexylamine from the vapor phase hydroamination of cyclohexene with cyclohexylamine, Catal. Commun. 145 (2020) 106112.

[182] G. Darsow, R. Langer, Method for producing variable mixtures of cyclohexylamine and dicyclohexylamine , US 6335 470 (2002).

[183] M.T. Musser, Cyclohexanol and Cyclohexanone, in: Ullmann's Encycl. Ind. Chem., Wiley-VCH Verlag GmbH & Co. KGaA, Weinheim (2011).

[184] D. Contreras, V. Melin, K. Márquez, G. Pérez-González, H.D. Mansilla, G. Pecchi, A. Henríquez, Selective oxidation of cyclohexane to cyclohexanol by BiOI under visible light: Role of the ratio (1 1 0)/(0 0 1) facet, Appl. Catal. B Environ. 251 (2019) 17–24.

[185] J.F. Van Peppen, V. Chester, Process for production of cyclohexanol, US5015787, (1991).

[186] D.C. Thomas, J.T. Adams, Chromium amine complex catalyzed oxidation of cycloc hydrocarbons to ketones, US3404185A, (1964).

[187] R.L. Purgason, Process for the preparation of cyclohexanone oxime, US3991115A, (1975).

[188] P. Serna, M. López-Haro, J.J. Calvino, A. Corma, Selective hydrogenation of nitrocyclohexane to cyclohexanone oxime with H_2 on decorated Pt nanoparticles, J. Catal. 263 (2009) 328–334.

[189] K.I. Shimizu, T. Yamamoto, Y. Tai, A. Satsuma, Selective hydrogenation of nitrocyclohexane to cyclohexanone oxime by alumina-supported gold cluster catalysts, J. Mol. Catal. A Chem. 345 (2011) 54–59.

[190] H.G. Liao, Y.J. Xiao, H.K. Zhang, P. Le Liu, K.Y. You, C. Wei, H. Luo, Hydrogenation of nitrocyclohexane to cyclohexanone oxime over Pd/CNT catalyst under mild conditions, Catal. Commun. 19 (2012) 80–84.

[191] Y. Yan, S. Liu, F. Hao, P. Liu, H. Luo, Nitrocyclohexane hydrogenation to cyclohexanone oxime over mesoporous carbon supported Pd catalyst, Catal. Commun. 50 (2014) 9–12.

[192] Q.Q. Zhang, J. Dong, Y.M. Liu, Y. Cao, H.Y. He, Y.D. Wang, An efficient noble-metal-free supported copper catalyst for selective nitrocyclohexane hydrogenation to cyclohexanone oxime, Chem. Commun. 53 (2017) 2930–2933.

[193] F. Yao, S. Liu, H. Cui, Y. Lv, Y. Zhang, P. Liu, F. Hao, W. Xiong, H. Luo, Activated Carbon Supported Non-noble Bimetallic Ni-Based Catalysts for Nitrocyclohexane Hydrogenation to Cyclohexanone Oxime under Mild Conditions, ACS Sustain. Chem. Eng. (2021).

[194] DuPont, Improvement in the production of oximes, GB857902, (1961).

[195] DuPont, A process fo the perparation of Ketoximes, GB86340, (1961).

[196] P. Le Liu, H.K. Zhang, S.H. Liu, Z.J. Yao, F. Hao, H.G. Liao, K.Y. You, H.A. Luo, Palladium supported catalysts for nitrocyclohexane hydrogenation to cyclohexanone oxime with high selectivity, ChemCatChem. 5 (2013) 2932-2938.

[197] S. Liu, F. Hao, P. Liu, H. Luo, The influences of preparation methods on the structure and catalytic performance of single-wall carbon nanotubes supported palladium catalysts in nitrocyclohexane hydrogenation, RSC Adv. 5 (2015) 22863–22868.

[198] S. Jun, Sang Hoon Joo, R. Ryoo, M. Kruk, M. Jaroniec, Z. Liu, T. Ohsuna, O. Terasaki, Synthesis of new, nanoporous carbon with hexagonally ordered mesostructure [5], J. Am. Chem. Soc. 122 (2000) 10712–10713.

[199] X. Wang, N. Perret, M.A. Keane, Gas phase hydrogenation of nitrocyclohexane over supported gold catalysts, Appl. Catal. A Gen. 467 (2013) 575–584.

[200] R. V. Jones, L. Godorhazy, N. Varga, D. Szalay, L. Urge, F. Darvas, Continuous-flow high pressure hydrogenation reactor for optimization and high-throughput synthesis, J. Comb. Chem. 8 (2006) 110–116.

[201] R. Javaid, S.I. Kawasaki, A. Suzuki, T.M. Suzuki, Simple and rapid hydrogenation of p-nitrophenol with aqueous formic acid in catalytic flow reactors, Beilstein J. Org. Chem. 9 (2013) 1156–1163.

[202] S.S. Yakushkin, A.L. Nuzhdin, E.A. Artiukha, P.E. Plyusnin, G.A. Bukhtiyarova, O.N. Martyanov, In situ EPR study of chemoselective hydrogenation of nitroarenes on Au/Al_2O_3 catalyst, Mendeleev Commun. 28 (2018) 536–537.

[203] V.G. Dorokhov, G.F. Dorokhova, V.I. Savchenko, Study of the products of platinum-catalyzed hydrogenation of chlorinated nitro and amino aromatic compounds at high degree of dehalogenation, Russ. Chem. Bull. 67 (2018) 1412-1418.

[204] A.L. Nuzhdin, G.A. Bukhtiyarova, T. Lin, E.Y. Gerasimov, V.I. Bukhtiyarov, Chemoselective hydrogenation of 3-nitrostyrene over Ag/TiO_2-SiO_2 catalyst in a flow reactor, Mendeleev Commun. 29 (2019) 553–555.

[205] I.I. Kamińska, D. Lisovytskiy, S. Casale, A. Śrębowata, S. Dzwigaj, Influence of preparation procedure on catalytic activity of PdBEA zeolites in aqueous phase hydrodechlorination of 1,1,2-trichloroethene, Microporous Mesoporous Mater. 237 (2017) 65–73.

[206] W. Wu, J. Xu, Liquid-phase hydrodechlorination of chlorinated benzenes over active carbon supported nickel catalysts under mild conditions, Catal. Commun. 5 (2004) 591–595.

[207] J. Wang, G. Fan, F. Li, Carbon-supported Ni catalysts with enhanced metal dispersion and catalytic performance for hydrodechlorination of chlorobenzene, RSC Adv. 2 (2012) 9976–9985.

[208] A. Śrebowata, W. Juszczyk, Z. Kaszkur, J.W. Sobczak, L. Kepiński, Z. Karpiński, Hydrodechlorination of 1,2-dichloroethane and dichlorodifluoromethane over Ni/C catalysts: The effect of catalyst carbiding, Appl. Catal. A Gen. 319 (2007) 181–192.

[209] P. Kim, H. Kim, J.B. Joo, W. Kim, I.K. Song, J. Yi, Effect of nickel precursor on the catalytic performance of Ni/Al_2O_3 catalysts in the hydrodechlorination of 1,1,2-trichloroethane, J. Mol. Catal. A Chem. 256 (2006) 178–183.

[210] H. Sohn, G. Celik, S. Gunduz, S.L. Dean, E. Painting, P.L. Edmiston, U.S. Ozkan, Hydrodechlorination of trichloroethylene over Pd supported on swellable organically-modified silica (SOMS), Appl. Catal. B Environ. 203 (2017) 641–653.

[211] J. Xiong, Y. Ma, W. Yang, L. Zhong, Rapid, highly efficient and stable catalytic hydrodechlorination of chlorophenols over novel Pd/CNTs-Ni foam composite catalyst in continuous-flow, J. Hazard. Mater. 355 (2018) 89–95.

[212] J.A. Baeza, L. Calvo, M.A. Gilarranz, A.F. Mohedano, J.A. Casas, J.J. Rodriguez, Catalytic behavior of size-controlled palladium nanoparticles in the hydrodechlorination of 4-chlorophenol in aqueous phase, J. Catal. 293 (2012) 85–93.

[213] M. Bonarowska, Z. Karpiński, R. Kosydar, T. Szumełda, A. Drelinkiewicz, Hydrodechlorination of CCl_4 over carbon-supported palladium-gold catalysts prepared by the reverse “water-in-oil” microemulsion method, Comptes Rendus Chim. 18 (2015) 1143–1151.

[214] C. Amorim, M.A. Keane, Palladium supported on structured and nonstructured carbon: A consideration of Pd particle size and the nature of reactive hydrogen, J. Colloid Interface Sci. 322 (2008) 196–208.

[215] M. Bonarowska, J. Pielaszek, V.A. Semikolenov, Z. Karpiński, Pd-Au/sibunit carbon catalysts: Characterization and catalytic activity in hydrodechlorination of dichlorodifluoromethane (CFC-12), J. Catal. 209 (2002) 528–538.

[216] F. Letellier, J. Blanchard, K. Fajerwerg, C. Louis, M. Breysse, D. Guillaume, D. Uzio, Search for confinement effects in mesoporous supports: Hydrogenation of o-xylene on Pt°/MCM-41, Catal. Letters. 110 (2006) 115–124.

[217] S. Ordóez, F. V. Díez, H. Sastre, Characterisation of the deactivation of platinum and palladium supported on activated carbon used as hydrodechlorination catalysts, Appl. Catal. B Environ. 31 (2001) 113–122.

[218] M. Hu, Y. Liu, Z. Yao, L. Ma, X. Wang, Catalytic reduction for water treatment, Front. Environ. Sci. Eng. 12 (2018) 1–18.

[219] M.R. Flid, L.M. Kartashov, Y.A. Treger, Theoretical and Applied Aspects of Hydrodechlorination Processes — Catalysts and Technologies, Catalysts. 10 (2020) 216.

[220] A. Śrebowata, R. Baran, D. Łomot, D. Lisovytskiy, T. Onfroy, S. Dzwigaj, Remarkable effect of postsynthesis preparation procedures on catalytic properties of Ni-loaded BEA zeolites in hydrodechlorination of 1,2-dichloroethane, Appl. Catal. B Environ. 147 (2014) 208–220.

[221] Y. Wang, J. Wang, G. Fan, F. Li, Synthesis of a novel Ni/C catalyst derived from a composite precursor for hydrodechlorination, Catal. Commun. 19 (2012) 56–60.

[222] E. Díaz, L. Faba, S. Ordóñez, Effect of carbonaceous supports on the Pd-catalyzed aqueous-phase trichloroethylene hydrodechlorination, Appl. Catal. B Environ. 104 (2011) 415–417.

[223] E. Diaz, A.F. Mohedano, J.A. Casas, L. Calvo, M.A. Gilarranz, J.J. Rodriguez, Comparison of activated carbon-supported Pd and Rh catalysts for aqueous-phase hydrodechlorination, Appl. Catal. B Environ. 106 (2011) 469-475.

[224] M. Bonarowska, Z. Kaszkur, L. Kepiński, Z. Karpiński, Hydrodechlorination of tetrachloromethane on alumina- and silica-supported platinum catalysts, Appl. Catal. B Environ. 99 (2010) 248–256.

[225] M. Martin-Martinez, L.M. Gómez-Sainero, J. Palomar, S. Omar, J.J. Rodriguez, Dechlorination of Dichloromethane by Hydrotreatment with Bimetallic Pd-Pt/C Catalyst, Catal. Letters. 146 (2016) 2614–2621.

[226] Z. Yaakob, A. Bshish, A. Ebshish, S.M. Tasirin, F.H. Alhasan, Hydrogen production by steam reforming of ethanol over nickel catalysts supported on sol gel made alumina: Influence of calcination temperature on supports, Materials (Basel). 6 (2013) 2229–2239.

[227] W. Wang, W. Chu, N. Wang, W. Yang, C. Jiang, Mesoporous nickel catalyst supported on multi-walled carbon nanotubes for carbon dioxide methanation, Int. J. Hydrogen Energy. 41 (2016) 967–975.

[228] M.A. Nieva, M.M. Villaverde, A. Monzón, T.F. Garetto, A.J. Marchi, Steam-methane reforming at low temperature on nickel-based catalysts, Chem. Eng. J. 235 (2014) 158–166.

[229] B. Fidalgo, L. Zubizarreta, J.M. Bermúdez, A. Arenillas, J.A. Menéndez, Synthesis of carbon-supported nickel catalysts for the dry reforming of CH_4, Fuel Process. Technol. 91 (2010) 765–769.

[230] G. Słowik, A. Gawryszuk-Rżysko, M. Greluk, A. Machocki, Estimation of Average Crystallites Size of Active Phase in Ceria-Supported Cobalt-Based Catalysts by Hydrogen Chemisorption vs TEM and XRD Methods, Catal. Letters. 146 (2016) 2173–2184.

[231] F. Sakina, C. Fernandez-Ruiz, J. Bedia, L. Gomez-Sainero, R.T. Baker, Ordered mesoporous carbon as a support for palladium-based hydrodechlorination catalysts, Catalysts. 11 (2021) 1–16.

[232] S. Ordóñez, B.P. Vivas, F. V. Díez, Minimization of the deactivation of palladium catalysts in the hydrodechlorination of trichloroethylene in wastewaters, Appl. Catal. B Environ. 95 (2010) 288–296.

[233] J. Zhou, K. Wu, W. Wang, Z. Xu, H. Wan, S. Zheng, Pd supported on boron-doped mesoporous carbon as highly active catalyst for liquid phase catalytic hydrodechlorination of 2,4-dichlorophenol, Appl. Catal. A Gen. 470 (2014) 336-343.

[234] J. Feng, Y. He, Y. Liu, Y. Du, D. Li, Supported catalysts based on layered double hydroxides for catalytic oxidation and hydrogenation: general functionality and promising application prospects, Chem. Soc. Rev. 44 (2015) 5291–5319.

[235] S. Soled, W. Wachter, H. Wo, Use of zeta potential measurements in catalyst preparation, in: Stud. Surf. Sci. Catal., Elsevier Inc., 2010: pp. 101–107.

[236] G.A. Parks, P.L. De Bruyn, The zero point of charge of oxides, J. Phys. Chem. 66 (1962) 967–973.

[237] Z. Jin, C. Yu, X. Wang, Y. Wan, D. Li, G. Lu, Liquid phase hydrodechlorination of chlorophenols at lower temperature on a novel Pd catalyst, J. Hazard. Mater. 186 (2011) 1726–1732.

[238] Z. Wu, T. Pan, Y. Chai, S. Ge, Y. Ju, T. Li, K. Liu, L. Lan, A.C.K. Yip, M. Zhang, Synthesis of palladium phosphides for aqueous phase hydrodechlorination: Kinetic study and deactivation resistance, J. Catal. 366 (2018) 80–90.

[239] E. Diaz, A.F. Mohedano, J.A. Casas, J.J. Rodriguez, Analysis of the deactivation of Pd, Pt and Rh on activated carbon catalysts in the hydrodechlorination of the MCPA herbicide, Appl. Catal. B Environ. 181 (2016) 429–435.

[240] M. Bonarowska, M. Zieliński, K. Matus, J. Sá, A. Śrębowata, Influence of microwave activation on the catalytic behavior of Pd-Au/C catalysts employed in the hydrodechlorination of tetrachloromethane, React. Kinet. Mech. Catal. 124 (2018) 375–388.

[241] M.A. Álvarez-Montero, L.M. Gómez-Sainero, A. Mayoral, I. Diaz, R.T. Baker, J.J. Rodriguez, Hydrodechlorination of chloromethanes with a highly stable Pt on activated carbon catalyst, J. Catal. 279 (2011) 389–396.

[242] Z. Karpiński, M. Bonarowska, W. Juszczyk, Hydrodechlorination of tetrachloromethane over silica-supported palladium-gold alloys, Polish J. Chem. Technol. 16 (2014) 101–105.

[243] M. Brun, A. Berthet, J.C. Bertolini, XPS, AES and Auger parameter of Pd and PdO, J. Electron Spectros. Relat. Phenomena. 104 (1999) 55–60.

[244] E.H. Voogt, A.J.M. Mens, O.L.J. Gijzeman, J.W. Geus, XPS analysis of palladium oxide layers and particles, Surf. Sci. 350 (1996) 21–31.

[245] M.M. Villaverde, N.M. Bertero, T.F. Garetto, A.J. Marchi, Selective liquid-phase hydrogenation of furfural to furfuryl alcohol over Cu-based catalysts, in: Catal. Today, Elsevier, 2013: pp. 87–92.

[246] J.M. Beiramar, A. Griboval-Constant, A.Y. Khodakov, Effects of Metal Promotion on the Performance of CuZnAl Catalysts for Alcohol Synthesis, ChemCatChem. 6 (2014) 1788–1793.

[247] C. Wen, F. Li, Y. Cui, W.L. Dai, K. Fan, Investigation of the structural evolution and catalytic performance of the CuZnAl catalysts in the hydrogenation of dimethyl oxalate to ethylene glycol, Catal. Today. 233 (2014) 117–126.

[248] H. Niu, J. Luo, C. Li, B. Wang, C. Liang, Transfer Hydrogenation of Biomass-Derived Furfural to 2-Methylfuran over CuZnAl Catalysts, Ind. Eng. Chem. Res. 58 (2019) 6298–6308.

[249] C. Gan, Y. Wang, C. Ye, C. Guo, Effect of Aging Methods on CuZnAl Catalysts for Methyl Acetate Hydrogenation, Aust. J. Chem. 72 (2019) 417.

[250] S.Y. Cheng, J.W. Kou, Z.H. Gao, W. Huang, Preparation of complexant-modified $Cu/ZnO/Al_2O_3$ catalysts via hydrotalcite-like precursors and its highly efficient application in direct synthesis of isobutanol and ethanol from syngas, Appl. Catal. A Gen. 556 (2018) 113–120.

[251] Y. Liu, Y. Pan, H. Wang, Y. Liu, C. Liu, Ordered mesoporous $Cu\text{-}ZnO\text{-}Al_2O_3$ adsorbents for reactive adsorption desulfurization with enhanced sulfur saturation capacity, Cuihua Xuebao/Chinese J. Catal. 39 (2018) 1543–1551.

[252] C. Zhang, Z. Huo, D. Ren, Z. Song, Y. Liu, F. Jin, W. Zhou, Catalytic transfer hydrogenation of levulinate ester into γ-valerolactone over ternary $Cu/ZnO/Al_2O_3$ catalyst, J. Energy Chem. 32 (2019) 189–197.

[253] J.F. Moulder, J. Chastain, R.C. King, Handbook of x-ray photoelectron spectroscopy : a reference book of standard spectra for identification and interpretation of XPS data, Physical Electronics, Eden Prairie Minn., 1995.

[254] S. Kühl, A. Tarasov, S. Zander, I. Kasatkin, M. Behrens, Cu-Based Catalyst Resulting from a Cu,Zn,Al Hydrotalcite-Like Compound: A Microstructural, Thermoanalytical, and In Situ XAS Study, Chem. - A Eur. J. 20 (2014) 3782–3792.

[255] T. Witoon, N. Kachaban, W. Donphai, P. Kidkhunthod, Tuning of catalytic CO_2 hydrogenation by changing composition of $CuO – ZnO – ZrO_2$ catalysts, Energ. Convers. Manage.118 (2016) 21–31.

[256] Š. Hajduk, V.D.B.C. Dasireddy, B. Likozar, G. Dražić, Z.C. Orel, CO_x-free hydrogen production via decomposition of ammonia over Cu–Zn-based heterogeneous catalysts and their activity/stability, Appl. Catal. B Environ. 211 (2017) 57–67.

[257] H. Lei, R. Nie, G. Wu, Z. Hou, Hydrogenation of CO2 to CH3OH over Cu/ZnO catalysts with different ZnO morphology, Fuel. 154 (2015) 161–166.

[258] T. Shishido, M. Yamamoto, D. Li, Y. Tian, H. Morioka, M. Honda, T. Sano, K. Takehira, Water-gas shift reaction over Cu/ZnO and $Cu/ZnO/Al_2O_3$ catalysts prepared by homogeneous precipitation, Appl. Catal. A Gen. 303 (2006) 62–71.

[259] P. Gao, F. Li, H. Zhan, N. Zhao, F. Xiao, W. Wei, L. Zhong, H. Wang, Y. Sun, Influence of Zr on the performance of Cu/Zn/Al/Zr catalysts via hydrotalcite-like precursors for CO2 hydrogenation to methanol, J. Catal. 298 (2013) 51–60.

[260] J. Kolena, L. Soukupová, J. Kocík, J. Lederer, Modified hydrotalcites as precursors for catalysts effective in the hydrogenolysis of glycerol to 1,2-propanediol, React. Kinet. Mech. Catal. 122 (2017) 803–816.

[261] R. Etefagh, E. Azhir, N. Shahtahmasebi, Synthesis of CuO nanoparticles and fabrication of nanostructural layer biosensors for detecting Aspergillus niger fungi, Sci. Iran. 20 (2013) 1055–1058.

[262] A.C. Mohan, B. Renjanadevi, Preparation of Zinc Oxide Nanoparticles and its Characterization Using Scanning Electron Microscopy (SEM) and X-Ray Diffraction(XRD), Procedia Technol. 24 (2016) 761–766.

[263] D.R. Baer, K. Artyushkova, C. Richard Brundle, J.E. Castle, M.H. Engelhard, K.J. Gaskell, J.T. Grant, R.T. Haasch, M.R. Linford, C.J. Powell, A.G. Shard, P.M.A. Sherwood, V.S. Smentkowski, Practical guides for x-ray photoelectron spectroscopy: First steps in planning, conducting, and reporting XPS measurements, J. Vac. Sci. Technol. A. 37 (2019) 031401.

[264] S. Poulston, P.M. Parlett, P. Stone, M. Bowker, Surface Oxidation and Reduction of CuO and Cu_2O Studied Using XPS and XAES, Surf. Interface Anal. 24 (1996) 811–820.

[265] M. Wang, L. Jiang, E.J. Kim, S.H. Hahn, Electronic structure and optical properties of $Zn(OH)_2$: LDA+U calculations and intense yellow luminescence, RSC Adv. 5 (2015) 87496–87503.

[266] M. Brzezińska, N. Keller, A.M. Ruppert, Self-tuned properties of CuZnO catalysts for hydroxymethylfurfural hydrodeoxygenation towards dimethylfuran production, Catal. Sci. Technol. 10 (2020) 658–670.

[267] M. Behrens, F. Studt, I. Kasatkin, S. Kühl, M. Hävecker, F. Abild-Pedersen, S. Zander, F. Girgsdies, P. Kurr, B.L. Kniep, M. Tovar, R.W. Fischer, J.K. Nørskov, R. Schlögl, The active site of methanol synthesis over $Cu/ZnO/Al_2O_3$ industrial catalysts, Science 336 (2012) 893–897.

[268] C. Baltes, S. Vukojević, F. Schüth, Correlations between synthesis, precursor, and catalyst structure and activity of a large set of $CuO/ZnO/Al_2O_3$ catalysts for methanol synthesis, J. Catal. 258 (2008) 334–344.

[269] M. Kurtz, N. Bauer, C. Büscher, H. Wilmer, O. Hinrichsen, R. Becker, S. Rabe, K. Merz, M. Driess, R.A. Fischer, M. Muhler, New synthetic routes to more active Cu/ZnO catalysts used for methanol synthesis, Catal. Letters. 92 (2004) 49–52.

[270] R.M. Rioux, H. Song, J.D. Hoefelmeyer, P. Yang, G.A. Somorjai, High-surface-area catalyst design: Synthesis, characterization, and reaction studies of platinum nanoparticles in mesoporous SBA-15 silica, J. Phys. Chem. B. 109 (2005) 2192-2202.

[271] Y. Zhao, B. Shan, Y. Wang, J. Zhou, S. Wang, X. Ma, An Effective $CuZn\text{-}SiO_2$ Bimetallic Catalyst Prepared by Hydrolysis Precipitation Method for the Hydrogenation of Methyl Acetate to Ethanol, Ind. Eng. Chem. Res. 57 (2018) 4526–4534.

[272] Y. Wang, J. Liao, J. Zhang, S. Wang, Y. Zhao, X. Ma, Hydrogenation of methyl acetate to ethanol by Cu/ZnO catalyst encapsulated in SBA-15, AIChE J. 63 (2017) 2839–2849.

[273] I. Kasatkin, P. Kurr, B. Kniep, A. Trunschke, R. Schlögl, Role of Lattice Strain and Defects in Copper Particles on the Activity of $Cu/ZnO/Al_2O_3$ Catalysts for Methanol Synthesis, Angew. Chemie Int. Ed. 46 (2007) 7324–7327.

[274] T. Fujitani, J. Nakamura, The chemical modification seen in the Cu/ZnO methanol synthesis catalysts, Appl. Catal. A Gen. 191 (2000) 111–129.

[275] J. Liu, Y. Liu, W. Yan, D. Yang, J. Fan, W. Huang, Effect of zinc source on the ethanol synthesis from syngas over a slurry CuZnAl catalyst, Int. J. Hydrogen Energy. 45 (2020) 22469–22479.

[276] R. Burch, S.E. Golunski, M.S. Spencer, The role of copper and zinc oxide in methanol synthesis catalysts, J. Chem. Soc. Faraday Trans. 86 (1990) 2683-2691.

Institute of Physical Chemistry

Kasprzaka 44/52
01-224 Warsaw
Poland

www.ichf.edu.pl